

Cheap Design and Behavioral Diversity for Autonomous Adaptive Robots

Dissertation
zur
Erlangung der naturwissenschaftlichen Doktorwürde
(Dr. sc. nat.)
vorgelegt der
Mathematisch-naturwissenschaftlichen Fakultät
der
Universität Zürich
von
Fumiya Iida
aus
Japan

Promotionskomitee
Prof. Dr. Rolf Pfeifer
Prof. Dr. Hiroshi Yokoi

Zürich, 2005

The following paper was accepted as a dissertation by the University of Zurich, Faculty of Science in winter semester 2005/2006.

Doctorate Committee: Prof. Dr. Rolf Pfeifer (Chair)
Prof. Dr. Hiroshi Yokoi (Dissertation Supervisor)
Prof. Dr. Rodney Douglas

Abstract

Adaptive autonomous systems in the real world continuously encounter new demanding situations derived from the physical constraints of their own body and the environment. They have to acquire the information about the environment through their own sensory systems, and adaptive behaviors have to be achieved by using a highly restricted amount of resources such as limited number of sensors and motors. It turns out that the physical constraints derived from the body and the environment can also be exploited to achieve behavior. This idea was previously formulated as the principle of “cheap design”, and a number of case studies have demonstrated its biological plausibility. The underlying problem of cheap design, however, is that it leads to a strong dependency of the behaviors on the environment, which results in limited adaptivity. In order to realize an adaptive system, behavioral diversity is required.

This thesis explores cheap design and behavioral diversity in relation to body dynamics, morphological properties, and sensory-motor coordination. By considering dynamic interactions between real-world robots and their environment as the central issue of interest, underlying mechanisms of behavioral diversity are identified. Moreover, it is also shown how these dynamic interactions are related to perception and cognitive processes. Through a number of case studies of biologically inspired autonomous robots, these mechanisms are conceptualized as a set of design principles. These principles can not only be used for building robots but also capture important insights of biological systems.

Zusammenfassung

Adaptive autonome Systeme werden in der realen Welt ständig mit neuen Situationen konfrontiert, die aufgrund der physikalischen Gegebenheiten ihres eigenen Körpers und der Umwelt zustandekommen. Insbesondere müssen sie alle Informationen über die Umwelt mit ihren körpereigenen Sensoren sammeln und adaptives Verhalten trotz stark limitierter Ressourcen (z.B. beschränkte Anzahl Sensoren und Motoren) erreichen. Es stellt sich aber heraus, dass diese physikalischen Einschränkungen ausgenützt werden können, um Verhalten zu erzeugen. Diese Idee wurde unter dem Namen “Cheap Design” bekannt, und mehrere Fallstudien konnten ihre biologische Plausibilität demonstrieren. Das diesem Ansatz inhärente Problem ist jedoch, dass es zu einer starken Abhängigkeit des Verhaltens von der Umwelt führt und somit zu einer limitierten Adaptivität. Für ein adaptives System ist eine grosse Verhaltensvielfalt notwendig.

Die vorliegende Dissertation untersucht “Cheap Design” und Verhaltensvielfalt im Kontext von “Body Dynamics”, morphologischen Eigenschaften und sensor-motorischer Koordination. Dynamische Interaktion zwischen Robotern und ihrer Umwelt wird als zentrales Thema betrachtet, um die zugrundeliegenden Mechanismen von Verhaltensvielfalt zu identifizieren. Es wird ausserdem gezeigt, wie dynamische Interaktionen mit Wahrnehmung und kognitiven Prozessen zusammenhängen. Schliesslich dienen Fallstudien von biologisch inspirierten autonomen Robotern dazu, diese Mechanismen als eine Sammlung von Design-Prinzipien zu konzeptualisieren. Diese Prinzipien können nicht nur für die Konstruktion von Robotern verwendet werden, sondern enthalten auch wichtige Erkenntnisse von biologischen Systemen.

Acknowledgments

I would like to thank all my colleagues of the AI Lab, University of Zurich for many productive discussions and collaborations. Especially, Rolf Pfeifer provided me all the resources and support during the whole time I worked for the research projects. In addition, special thanks go to Dimitrios Lambrinos, Raja Dravid, Max Lungarella, Chandana Paul, Josh Bongard, Gabriel Gomez, and all the other students who worked together with me in the stimulating projects. A part of the work is also considerably supported by the Locomotion Lab, University of Jena, and I would like to thank Andre Seyfarth and Hartmut Geyer for the fruitful discussions. I wish to give special thanks to Hiroshi Yokoi not only for the exceptional experiences to work together, but also for a number of constructive and thoughtful suggestions as a reviewer of this thesis. Finally, I would like to thank my family for their continuous support and understanding of my study in Zurich.

Contents

1	Introduction	1
1.1	Background	1
1.2	Motivation	2
1.3	Methodology	3
1.4	Design Principles	4
1.4.1	Design Principles of Body Dynamics for Behavioral Diversity	5
1.4.2	Design Principles of Body Dynamics for Sensing	6
1.4.3	Design Principles of Control for Behavioral Diversity	8
1.5	Overview of the thesis	10
2	A biologically inspired visual odometer for flying robot navigation	11
2.1	Introduction	12
2.2	Elementary Motion Detectors and the Visual Odometer	14
2.2.1	Basic EMD Circuit	14
2.2.2	Initial Experiments Using a Panoramic Camera	15
2.2.3	3-D Navigation with EMDs and the Visual Odometer	18
2.3	Simulation Experiments	20
2.3.1	Method	20
2.3.2	Result and Discussion	21
2.4	Discussion and Further Work	22
3	Biologically Inspired Goal-Directed Navigation of a Flying Robot	26
3.1	Introduction	26
3.2	Experimental Platform	27
3.3	Course Stabilization and Visual Odometer	28
3.3.1	Model	28
3.3.2	Course Stabilization Model	29
3.3.3	Visual Odometer Model	30
3.3.4	Experiments	31
3.3.5	Method	31
3.3.6	Results	31
3.4	Discussion	35
3.5	Summary	36

4	Design and Control of a Pendulum Driven Hopping Robot	37
4.1	Introduction	37
4.2	Robot Mechanical Structure	39
4.3	Modelling and Analysis	39
4.4	Control	42
4.4.1	Tuning the Hopping Height	43
4.4.2	Straight Walking	43
4.4.3	Control of Turning Rate	44
4.5	Discussion	45
4.6	Summary	46
5	Exploiting Friction for the Locomotion of a Hopping Robot	47
5.1	Introduction	47
5.2	Design Principle to Exploit Friction for the Locomotion	48
5.2.1	Increasing the Stability of Locomotion	49
5.2.2	Locomotion by Controlling the Friction	49
5.3	Robotic Platform	50
5.3.1	Mechanical Design of the Stumpy Robot	50
5.3.2	Control of the Robot	51
5.3.3	Friction	51
5.4	Stability and Gait Analysis	52
5.4.1	Method of the Experiment and Observed Gaits	52
5.4.2	Stability Analysis	54
5.5	Lateral Bounding	55
5.5.1	Experiments of the Lateral Bounding and the Observed Gait	56
5.5.2	Gait Analysis	57
5.6	Controlling the Turning Rate	58
5.7	Discussion	58
5.8	Summary	59
6	Cheap Rapid Locomotion of a Quadruped Robot	63
6.1	Introduction	63
6.2	Design and Control of a Quadruped Robot	65
6.2.1	Morphological Design	65
6.2.2	Controller	66
6.3	Experiments	67
6.3.1	Experimental Method	68
6.3.2	Stability Analysis	68
6.3.3	Forward Speed Control	71
6.4	Discussion	72
7	Sensing through Body Dynamics	74
7.1	Introduction	74
7.2	Body Dynamics of a Quadruped Robot	76
7.2.1	Morphological Design	76

7.2.2	Motor Control	77
7.2.3	Intrinsic Stability	78
7.2.4	Simulation Model	80
7.3	Behavior and Sensory Information	80
7.4	Situated Sensing of Body Dynamics	82
7.5	Sensing Physical Properties	84
7.5.1	Effect of Body Mass	85
7.5.2	Effect of Ground Friction	86
7.6	Discussion	87
7.7	Summary	88
8	Final Discussion	89
8.1	Summary of Results	89
8.2	Evaluation and Perspectives	90
8.3	Body Dynamics in Nature	91
8.3.1	Cheap Design for Speed and Precision	91
8.3.2	Body Dynamics of Artificial and Biological Systems	92
8.4	From Locomotion to Cognition	93
8.5	Embodied Incremental Development	94
8.5.1	Simulation and the Real World	95
8.5.2	Design Principles for Incremental Development	96
8.6	Conclusion	97
	Bibliography	101
	Publications	
	Curriculum Vitae	

List of Figures

1-1	Classification of behavior.	4
1-2	Design principles and their relation to the topics described in this thesis.	9
2-1	Left: the Reichardt model of elementary motion detection. Photoreceptors, high-pass filters, low-pass filters, multipliers, and the subtraction module are wired in series. The output of the last step (subtraction) is an estimate of image speed (see text for details). Right: the visual odometer based on a wide field motion detector. The integrated response of an array of EMDs, each tuned to a different part of the visual field, is used to implement a wide field motion detector. Its outputs are then integrated over time to provide an estimate of the distance traveled (for explanations, see text).	14
2-2	Vision system and initial experiment setup. Left: The panoramic vision system we developed for this experiment consists of CCD camera, panoramic mirror, and housing components, which weighs 90 g in total so that it can be embedded in the flying robot. The visual field covers 360 degrees on the horizontal plane, and 260 degrees vertically. Middle and right: This vision system is equipped with the caster-frame on a pair of rails, and an external motor drives the vision system along a straight route at a constant speed. Initially walls with black and white stripes were installed along the rails (20cm width period of black and white, 60cm distance from vision system).	16
2-3	Typical responses of the EMD and the visual odometer. Upper: Photoreceptor activity is calculated directly from the image captured by CCD camera. This graph shows the time-series of photoreceptor activity. Fluctuations on the signal correspond to the stripe pattern of the walls when the vision system moves horizontally along the corridor. Middle: The outputs of High-pass and low-pass filters. Fluctuations on these signals correspond to the edges in the image. Bottom: Responses of the wide field motion detectors and the accumulated visual odometer response.	17

2-4	Visual odometer responses at 3 different speeds. Time series of photoreceptor activity for 3 different speeds: 15cm/sec (Upper Left), 28cm/sec (Upper Right), and 40cm/sec (Bottom Left). Bottom Right: Visual odometer response. Because the outputs of the EMDs depend on temporal frequency, the odometer produces different distance estimates at different speeds.	18
2-5	The response of the visual odometer in an experiment performed in a natural office environment. Left: Typical output values of four photoreceptors. Their output profile depends on the structure of environment and the light conditions. Right: Visual odometer response. The vision system moved along the same route 5 times at the same constant speed. This graph shows that the proposed odometer mechanism provides a robust distance estimate as long as it moves along the same route.	19
2-6	(a) Panoramic view of an office environment acquired through the omni-directional camera, and (b) distribution of two dimensional EMD array in the panoramic image.	20
2-7	Left: Two-dimensional EMDs. Filled ellipses denote photoreceptors, filters and operators are represented by the boxes, and their outputs provide independent estimates of vertical and horizontal image motion. Right: Typical responses of vertical and horizontal EMDs when the vision system moves horizontally straight in the natural environment. This graph indicates that the EMDs could also be used to detect vertical motion with very small errors.	21
2-8	Top: The simulation setup. Bottom: The typical patterns used on the wall. (Noise 0, 20, 50 and 100 % from top to bottom.)	22
2-9	Sensory-motor control circuit. Outputs of left and right EMD networks provide the vertical (EMD-V-L, EMD-V-R) and horizontal (EMD-H-L, EMD-H-R) image motion values of each side. The horizontally, vertically tuned EMDs are connected to a motor neuron that controls the robot's rotation, elevation, respectively. The outputs of the horizontally tuned EMDs are also used by visual odometer. The thrust motor neuron has a connection to bias neuron that implements the default move-forward behavior.	23
2-10	Trajectories of the simulated agent. Each graph contains the results from 20 trials with different wall patterns.	24
2-11	Left: The mean visual odometer responses of 20 trials. Right: The standard deviations as percentage of the mean visual odometer responses.	25

3-1	Left: The Reichardt model of elementary motion detection. Photoreceptors, high-pass filters, low-pass filters, multipliers, and the subtraction module are wired in series. The output of the last step (subtraction) is an estimate of direction sensitive image speed. Right: The controller circuit for the flying robot and visual odometer. The gray rectangle denotes the panoramic image extracted from the omnidirectional camera on the robot. The image is given to both horizontally and vertically arranged photoreceptor arrays of EMDs. After the integrators and comparator, the outputs are given to motor controller and visual odometer modules.	28
3-2	Top: The autonomous flying robot, Melissa and its gondola, on the bottom of which a miniature panoramic camera is attached. Bottom: An image obtained by the panoramic vision system (left) and its log-polar transformed image (right), which is used in the experiments. . .	29
3-3	Left: Experimental setup for the navigation experiments. The experiments start with the same initial conditions, i.e. initial robot position and orientation. Two video cameras are installed to record the absolute trajectory of the robot for later analysis. Right: Pictures of three different uncontrolled environments, which are tested in the experiments. (EXP 0, 1, 2, from left to right)	31
3-4	3-D trajectories of the flying robot during the experiments. Each plot is extracted from the images recorded with the stereo video camera. The plots denotes the position of the robot at one second time-step, and each graph contains the trajectories of 10 trials. (EXP 0, 1, 2, from top to bottom)	32
3-5	Top: Visual odometer responses of the 10 trials in the 3 experimental setups. The curve profiles show that the visual odometer accurately estimates the distances in the same experimental setup, particularly in EXP0 and 1. Bottom: Visual odometer measurement vs. actual distance. The actual distances that the robot traveled in each trial are extracted from Figure 3-4. The results show that the visual odometer depends on the locations, since the plots from the same EXP are distributed in similar areas of this graph.	33
3-6	The effect of the number of EMDs by standard deviations (SDs) as percent of the mean values in visual odometer measurement. The graphs show that the number of EMDs changes the accuracy of visual odometer measurements.	34
4-1	Stumpy II Robot (Left) and Schematic diagram (Right) of the Stumpy Robot, with variables which are used in modelling and analysis. . . .	40
4-2	Forward walking, produced when $\nu_s^+ = \nu_s^-, \phi = 0^\circ$	41
4-3	Backward walking, produced when $\nu_s^+ = \nu_s^-, \phi = 180^\circ$	41
4-4	Turning left, with a small turning rate, produced when $\nu_s^+ < \nu_s^-$	43
4-5	Turning right, with a small turning rate, produced when $\nu_s^+ > \nu_s^-$	43

4-6	Going backwards and turning right, with a small turning rate, produced when $\nu_s^+ > \nu_s^-$. Simply by changing ϕ to 180° , the robot walks backward, as it slowly turns right.	44
4-7	Going backwards and turning left, with a small turning rate, produced when $\nu_s^+ < \nu_s^-$	44
4-8	Turning right, with a large turning rate, produced when $\nu_s^+ \gg \nu_s^-$. With this controller the robot can effectively turn in place.	45
4-9	Turning left, with a large turning rate, produced when $\nu_s^+ \ll \nu_s^-$. Again the robot can effectively turn in place	45
5-1	Concept of increasing stability	48
5-2	Concept of the locomotion by exploiting friction	48
5-3	Photograph of the Stumpy robot (Left) and schematic illustration of the Stumpy robot (Right), with variables which are used in modelling and analysis.	50
5-4	Intrinsic stability of Stumpy. This graph shows the time series pressure data installed on the right and left feet (top and bottom graphs, respectively). The gait is disturbed by an external force around time step 150. A time step corresponds roughly to 1/20 seconds.	52
5-5	Three typical gaits, Shuffling (Top), Walking (Middle), and Hopping (Bottom). Each diagram includes time series values of pressure sensors on the right foot(Top), the left foot(Middle) and the angle between the upper and lower bodies(Bottom).	53
5-6	Gait distribution diagrams in Terrain 0 (Top) and Terrain 1 (Bottom). Numbers of the texture patches correspond to “4”: Hopping, “3”: Walking, “2”: Shuffling, “1”: Unstable, and “0”:Fall.	54
5-7	Two typical locomotion behaviors of lateral bounding; Ipsilateral bounding (Right) and contralateral bounding (Left).	55
5-8	Gait distribution diagrams of the lateral bounding experiments on Terrain 0 (Top) and Terrain 1 (Bottom).	56
5-9	Locomotion behaviors of Stumpy observed from top (The unit of these graphs is meters). Stumpy can control its movement direction, turning rate (Top and Middle panels), and lateral bounding (Bottom panels) by changing only a few control parameters. Black dots denote the trajectory of the body center, and the line illustrates the orientation of bottom base.	61
5-10	Typical gait patterns of Stumpy (Walking, Hopping, Lateral Bounding from left to right).	62
6-1	Left: A photograph of the quadruped robot. Right: A schematic of the robot. The circles denote passive joints and the circles with a cross inside denote the joints controlled by the servomotors. The triangles with a number show the locations of LEDs which are used for visual tracking of the body geometry during the locomotion experiments. . .	65

6-2	Behavior analysis of a running experiment. The upper graph shows the behavior of whole body extracted from the visual tracking of LEDs attached to the leg joints. The lower graph shows the trajectory of a virtual linear hind leg.	66
6-3	The definitions of touchdown, lift-off angles and body pitch used in the analysis.	67
6-4	The relation between touchdown and lift-off angles. The touchdown angles and lift-off angles are normalized by the corresponding mean touchdown and lift-off angles.	67
6-5	The conceptual illustration of foot placement. If the touchdown angle is appropriate, the trajectory of body mass can be symmetry as shown in (b). Otherwise the lift-off angle can be higher (a) or lower (c). . .	68
6-6	Typical transitions of lift-off angles with different phase parameters. (The phase 0.2 (Top), 0.8 (Middle), and 1.0 (Bottom) radian.) . . .	69
6-7	Relation between the normalized lift-off angles of two successive leg steps. The variable s represents the index of leg step.	70
6-8	Typical time series movement of body pitch with respect to the ground plane. The phase parameter of 0.2 (Top graph) and -0.8 (Bottom) radian.	71
6-9	Average body rotational angular velocity versus the phase parameter.	72
6-10	Average speed versus the phase parameter.	73
7-1	(a) A photograph of the quadruped robot. (b) A schematic of the robot. The circles denote passive joints and the circles with a cross inside denote the joints controlled by the servomotors. The specifications of the robot are shown in Table 1.	75
7-2	A time series photographs during “the gait 0” (a) and “the gait 1” (b). The behavior of the robot is visually registered while running on a treadmill. The interval between two pictures is approximately 30ms. (c) Behavior of simulation model.	77
7-3	Time-series changes of the state variables during one leg step, (a) horizontal, (b) vertical, (c) angular movement and their velocity (d, e, f).	78
7-4	A typical recovery response from the change of the gait. (a) The time-series vertical movement of the body is shown before and after the trigger at $time = 0$, and (b) its phase plot.	79
7-5	Stick figures of behaviors in simulation. The body postures are illustrated every 100 and 1000 simulation steps (gray and black stick figures, respectively). Black dots represent the trajectories of the shoulder joint. (a) $\omega = 4.7Hz$, $\phi = 0.3$ in the ground friction 0.9 (static) and 0.8 (dynamic). (b) the same control parameters in the ground friction 0.7 (static) and 0.6 (dynamic). (c) in the same ground friction as (b) with the control parameters $\omega = 4.9Hz$, $\phi = 0.4$	81

7-6	Sensory information acquired during the behaviors shown in Figure 7-5. From top figure to bottom: Pressure sensor in the hind leg, angle of the hind passive joint, acceleration of the body, and motor output torque of the hind leg.(a)Coefficients of ground friction (CGF) are 0.9(static), 0.8(dynamic), motor frequency 4.8 Hz, (b) CGF 0.7 (static) and 0.6 (dynamic), motor frequency 4.8 Hz, (c)CGF 0.7 (static) and 0.6 (dynamic), motor frequency 4.4 Hz.	82
7-7	Body dynamics during the locomotion experiment measured by a contact detector.(a) distribution of the flight phase durations against the phase parameter, and (b) its standard deviation.	83
7-8	Behavior landscape obtained by a ground contact detector (a-0), and the visual velocity detector (b-0). This landscape is then segmented by threshold in (a-1-3) and (b-1-3).	84
7-9	The different dynamics observed by the contact detector with respect to the different body mass of (a) 0.5, (b) 1.0 and (c)1.5 kg. The landscape is then segmented by threshold in (a,b,c-1).	85
7-10	The different dynamics observed by the speed detector with respect to the different body mass of (a) 0.5, (b) 1.0 and (c)1.5 kg. The landscape is then segmented by threshold in (a,b,c-1).	85
7-11	The different dynamics observed by the contact detector with respect to the different ground friction of (a) 0.5, (b) 0.65 and (c)0.8. The landscape is then segmented by threshold in (a,b,c-1).	86
7-12	The different dynamics observed by the speed detector with respect to the different ground friction of (a) 0.5, (b) 0.65 and (c)0.8. The landscape is then segmented by threshold in (a,b,c-1).	86
8-1	(a) Schematics of the robot design, (b) Photograph of the robot with the supporting rotational bar, (c) Knee and ankle angular trajectories and ground reaction force of human locomotion, and (d) Those from the robot experiment.	93
8-2	From simulation to the real world. Although the overall behavior looks similar in simulation and the real world, the control architectures of these two systems are very much different due to the simplified model of physics in simulation (e.g. the bar does not bend, and there is no friction at the passive joint)[32].	95
8-3	Flying robots: Melissa I, Melissa II, and 10 flying robots built for the Science Fair at the Zurich Main Station (From left to right).	99
8-4	Stumpy robots: Stumpy I, Stumpy II, Stumpy III, Stumpy IV, and Mini-Stumpy.	99
8-5	Dog robots: Geoff, AILab-scout, Puppy, Mini-Dog I, Mini-Dog II, Mini-Dog6M, Mini-Dog1M, and Mini-DogExpo.	100
8-6	Other robots: StumpDog, Monop0, Monop1, Biped, Dumbo, Monkey, and The Fish Robot called Wanda.	100

List of Tables

4.1	Mass and length parameters of the robot mechanical structure	39
5.1	Mass and length parameters of the robot mechanical structure	51
5.2	The observed gaits and identification numbers which are used in Figure 5-6.	55
5.3	Observed gaits and behaviors during the lateral bounding experiments and identification numbers which are used in Figure 5-8.	57
6.1	The specification of the robot mechanical structure	66
7.1	Specification of the robot platform	76

Chapter 1

Introduction

Biological systems explore complex dynamic environments actively and flexibly with a rich variety of behaviors, while artificial systems still suffer from the limited adaptability in the real world. One of the fundamental problems in the study of adaptive behavior seems to lie in the fact that we do not fully understand how the systems (both animals and artifacts) physically interact with the real world. From this perspective, the studies in the field of embodied cognitive science have demonstrated the importance of body and physical system-environment interaction for understanding mechanisms underlying adaptive behavior.

This thesis further explores adaptive behavior in the context of embodied system-environment interaction. By considering the concept of embodiment as a central issue, a set of principles for the design of adaptive systems are investigated. The goal of these principles is not only to actually build robots, but also to obtain additional insights into the adaptive mechanisms of biological systems. In particular, we explore how behavioral diversity and cognitive processes are related to the notion of “cheap design”. With a number of case studies using real-world systems, we introduce ways to achieve behavioral diversity and its relation to cognitive processes.

1.1 Background

In the traditional view of artificial intelligence, one of the underlying implicit assumptions is that symbol processing in the brain is the sole generator of intelligent behavior. The main body of research, therefore, has focused on computation, i.e. constructing a world model and making stepwise decisions based on it. However, this approach faced, among others, the so-called *frame problem* [23, 92]. It is argued that it is impossible to maintain a model of the complex and dynamic environment and at the same time act in real time. The world model must be updated constantly, but the update time grows exponentially as the complexity of the model increases. As a result, the agent will spend most of its time on updating the world model, which leads to a significant degradation of its performance. The traditional approach also suffered from the *frame-of-reference problem*. Adaptive behaviors cannot be explained based on the internal representation in the brain only, because they are highly dependent

on a system-environment interaction [18, 19, 104]. The symbol processing for the internal representation, in particular, was pointed out to be an additional fundamental problem of *symbol grounding* [37, 102]. In the traditional approach, symbols are typically defined in a purely syntactic way by how they relate to other symbols and how they are processed by some interpreter. The relation of the symbols to the real world is rarely discussed explicitly.

In this context, behavior-based robotics was introduced. With only little information about the world, artificial systems are capable of relatively complex adaptive behaviors by having a set of basic parallel processes [10, 11]. This approach provided a significant advance over the traditional paradigm of centralized control. However, the focus was still on the control architecture, and embodiment was not treated as a central issue. More comprehensive observation of biological systems has led to the paradigm of Embodied Artificial Intelligence [89, 54]. This approach deals with adaptive behavior in the context of system-environment interaction, and thus the body as a physical entity became a central issue of interest. One of the implications was that adaptive behavior cannot be reduced to control and symbol processing only. It is essential to consider many different physical aspects of the systems such as morphological properties, control and motor action, and sensory-motor coordination. The principle of cheap design captures the fundamental idea of embodiment, which makes this approach different from traditional artificial intelligence and conventional robotics.

1.2 Motivation

Originally proposed as one of the design principles of autonomous adaptive agents, the principle of cheap design states that designs of adaptive systems must be parsimonious and exploit the physical constraints of the ecological niche [87, 88, 89]. There have been a number of case studies in biological science that support some aspects of cheap design (e.g. [7, 22, 24, 34, 116, 119]). An important aspect of this principle is that behaviors and functions are always dependent on the environment, and they often cease to work when the environment is changed. A good example is the case study of the Passive Dynamic Walker (PDW, [20, 73]). Despite its natural way of walking, a PDW can function only in a very limited ecological niche, i.e. a slope with a specific angle. If the angle of the slope is varied slightly, the PDW is no longer functional and falls over. For an adaptive system, therefore, cheap design cannot be viewed in isolation, but has to be considered in the context of other design principles [87, 89]: it is not only important to exploit physical constraints, but it must be shown how rich behavioral diversity can be achieved, which is the main objective of this thesis.

Firstly, we investigate cheap design in the context of multi-purpose adaptive systems. A system for a simple task (e.g. moving from point A to point B in a pre-determined static office environment) does not always require behavioral diversity, because the system deals with known situations and can always react in the same manner. In contrast, an autonomous adaptive system in a dynamic environment continuously encounters new situations and has to deal with them by using its limited

resources (e.g. limited number of sensors and actuators). This is one of the reasons why cheap design and behavioral diversity are essential for understanding adaptive behavior. In this sense, although the PDWs nicely demonstrate the power of cheap design for the complex task of walking, they have no behavioral diversity. Secondly, we consider how cheap design and behavioral diversity are related to cognitive processes. It will be shown that morphology and physical behavior of an autonomous adaptive system are directly related to cognitive processes. And finally, we pursue the question of how behavioral diversity and cognitive processes lead to the emergence of goal-directed behaviors. Metaphorically this issue was initially pointed out in “the law of requisite variety” [4]: It is necessary for an adaptive system to possess behavioral diversity to regulate and maintain the processes against foreseeable and unforeseeable disturbances. In short, “only variety can destroy variety”. In this respect, the underlying mechanisms for the emergence of goal-directed behaviors are closely related to the notion of cheap design and behavioral diversity.

1.3 Methodology

So far, we have not explicitly discussed what we mean by behavioral diversity. In nature, animals exhibit many different kinds of behaviors such as the different gait patterns of legged locomotion, and handling an object in different manners.

In medical and biological sciences, behaviors are often explained in terms of reflex and voluntary movements, because these movements can be mapped onto different parts in nervous systems such as spinal cord, cerebellum, and cortex. According to the notion of cheap design, however, animals’ behaviors are the result not only of nervous systems, but also of highly complex body structures (e.g. musculoskeletal structure) and interaction with the environment. Functions in nervous systems are only a part of the entire mechanism to generate behavior.

Therefore, for a comprehensive understanding of adaptive behavior, the “ecological balance” between mechanical structures, actuation, control, and information processing has to be investigated. It is not sufficient to decompose a complex system into a number of neural and mechanical substructures. In this sense, the synthetic methodology, i.e. the approach of “understanding by building”, is particularly useful, because different levels of ecological balance can be tested in the real world.

For a systematic investigation, we firstly discuss a way to classify behaviors. There are the following four categories, i.e. Behavior Type I, II, III and IV. As shown in Figure 1-1, behaviors are categorized with respect to actuation and control. Behavior Type I includes those which do not require any active control. In nature, for example, a twisted body automatically turns back to its natural posture without control or actuation. Behavior Type II is controlled and actuated but no sensory information is used. As shown later in this thesis, a simple actuation can be used to attain many behaviors including walking, hopping, running, and swimming. It is difficult to find this type of behavior in nature, because sensory and motor systems are generally tightly coupled in animals. In Behavior Type III, sensory information is used for feedforward motor control. Feedforward control uses the sensory information to

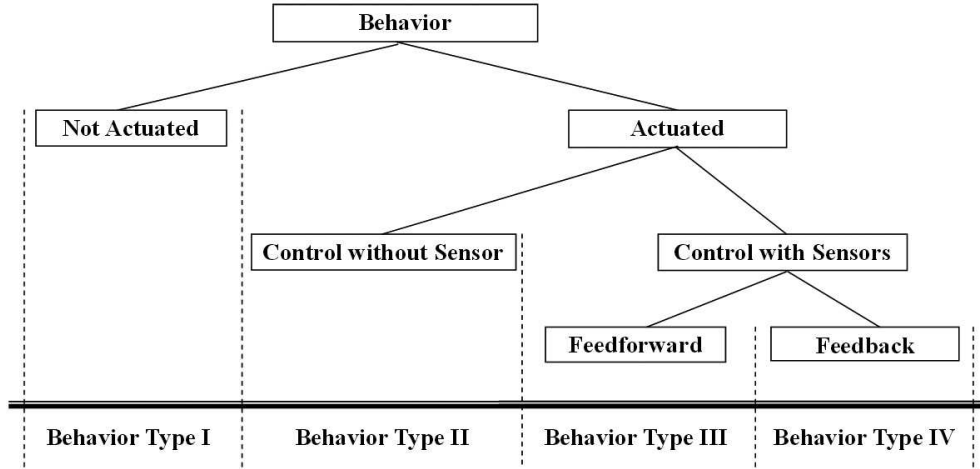


Figure 1-1: Classification of behavior.

exploit the body dynamics. Previously, it has been shown that the models of PDWs can be extended by little actuation such that they are able to walk on a level ground [123, 21, 115]. In this model, the robot swings a leg forward when a sensor detects its lift-off. Sensors are used to control the biped walking of this robot, but control still exploits the body dynamics. Finally, in Behavior Type IV, sensory information is used for feedback control. For this type of behavior, a system has a goal of movement (e.g. a pre-programmed trajectory of the body). The sensory information is used to compensate for the undesired deviation between the current and the desired trajectories. Most of the traditional robots, including industrial robots and the ZMP (Zero Moment Point) based legged robots, are controlled in this manner (e.g. [121]).

In biological systems, it is often difficult to see a clear distinction between these behavior types. During walking, for example, animals make use of all of the behavior types such as passive dynamics of musculoskeletal structure, actuation by muscles, and sensory feedback. This could be one of the reasons why systematic investigation is often difficult in biological sciences. By using the synthetic methodology, we are able to build and test real-world systems. The main contribution of this thesis is, therefore, to explore the potential importance of the different Behavior Types in the context of behavioral diversity and cognitive processes.

In the next section, we will discuss the conceptual principles for cheap design, behavioral diversity and cognitive processes on the basis of this classification. The main focus is centered around Behavior Type II and III, because there we are able to see direct contributions of the morphological properties to adaptive behavior.

1.4 Design Principles

In this section, we summarize the conceptual design principles that have been developed through the case studies described in the rest of the thesis. For the systematic explanation of the concepts, the design principles are formulated into the three aspects, “body dynamics for behavioral diversity”, “body dynamics for sensing”, and

“control for behavioral diversity”. It is important to mention that, because body and control are generally tightly coupled in biological systems, the principles below are also closely related to each other, and some of the principles could be rather obvious in isolation. Given the premature state, however, it is important to focus on how each principle relates to the others in order to see the complete picture.

1.4.1 Design Principles of Body Dynamics for Behavioral Diversity

Embodied systems consist of many different physical components with a variety of properties such as motors with high and low torque, actuated and passive joints, rigid and elastic segments. When such a complex system interacts with the environment, stable periodic behavior patterns, the so-called “attractor states”, can be generated because of the intrinsic body dynamics determined by the morphological properties. In Chapters 4 and 5 of this thesis, a robot called Stumpy will be introduced. It consists of two actuated joints, elastic feet, an upper body acting as an inverted pendulum, and large masses attached in the arms. When one of the joints is actuated at a certain frequency, it hops by exploiting the elastic feet and the properties of the inverted pendulum.

As shown in this example, by exploiting the interactions between the mechanical components, stable periodic behavior can be achieved: The robot will settle into an “attractor state” through a process of self-stabilization without sensory information. Generally, a behavior in an attractor state will self-stabilize if it is disturbed. In this subsection, we focus on two design principles of body dynamics concerning behavioral diversity.

Multiple attractor states by exploiting body dynamics

This design principle states in essence that, because behavior is emergent from the interactions of many mechanical components, a small variation in one control parameter can change the whole dynamics of the system, i.e. the way all components interact with each other. Stated differently, changes in one control parameter can lead to different attractor states.

For example, as shown in Chapter 5, Stumpy exhibits a few different behavior patterns in the locomotion behavior called “lateral bounding” (i.e. a movement pattern between hopping and running in which the robot moves sideways). When the inverted pendulum oscillates in an upright position, it hops in place, whereas it bounds sideways as the center of the oscillation is shifted to one side. Moreover, as another example shown in Chapter 4, Stumpy is able to switch its behavior between forward and backward walking by changing one control parameter of the phase delay between two motor oscillations. Because the behavior of Stumpy is the result of many interacting components (e.g. springs, actuators, and masses), changes in one control parameter (e.g. the center of the oscillation) can lead to different variations of locomotion behavior.

The idea of exploiting body dynamics to achieve multiple attractor states is partic-

ularly important for perception and learning of behaviors. As shown in Chapter 7, by exploiting the interactions between components, the perception and learning mechanisms can be much simpler, because there are fewer control parameters to be explored.

Behavioral diversity by exploiting self-stabilization

This principle states that behavioral diversity can be also increased within one attractor state by exploiting the self-stabilization. Through a change in one of the control parameters, which does not move the robot out of its basin of attraction, considerable behavioral variation can be achieved.

For example, in Chapter 6, a four-legged robot exhibits a form of running behavior simply by swinging the legs at a certain frequency without sensory information. The oscillation frequency is determined by the morphological properties of the robot. Even in this simple method for running behavior, behavioral diversity can be achieved by exploiting the following mechanism: During a stable running behavior, the legs interact with the ground in the same manner in every leg step. Because the legs are exerted by the same ground friction and reaction forces in every leg step, deviation of the leg trajectory results in instability. For example, there is a specific touch-down angle of the legs which enables the same touch-down angle in the next leg step. The touch-down angle of the legs is determined by morphological properties such as elasticity and the length of the leg segments, but the compliant legs have a self-stabilizing function in a sense that a deviation of the touch-down angle can be corrected in the next leg step. Therefore, this running behavior is in an attractor state.

When the frequency of the leg swing is changed, the desired touch-down angle of the legs can rarely be achieved. In other words, the stable locomotion process is “actively” disturbed. What is happening in this case is that, even though the self-stabilization mechanism tries to adjust the angle of touch-down, the preferred oscillation frequency of the legs disturbs the self-stabilization, and as a result the robot runs at a lower forward locomotion speed. Note that Stumpy is also able to control the locomotion velocity of lateral bounding in a similar way (Chapter 4).

1.4.2 Design Principles of Body Dynamics for Sensing

In Behavior Types I and II, changes of the environment directly influence the behavior patterns. For example, a process of running behavior of the four-legged robot (Chapter 7) becomes unstable when the ground friction is changed. When behavior relies on the environmental conditions as in the case of running behavior, the physical properties of the environment can be reflected in the behavior patterns. These behavior patterns are then used for acquiring information about the environment. For this strategy of sensing, there are two design principles which explain the relation between body dynamics and sensory information.

Multi-modal sensing through body dynamics

This principle states that many sensory channels can be used to recognize the physical properties of the environment when a system exploits its body dynamics. As explained in the previous design principle, behavioral patterns are generated as a result of the interplay between many components in the body and the environment.

An example is shown in the running behavior of the four-legged robot which results from many components interacting with each other: The ground reaction force exerted at the feet, the force generated in the elastic passive joints, the output force of the actuators, and the momentum of the large masses in the body, such as the batteries. Even if the robot exhibits running behavior, it often shows a different behavioral pattern when an environmental property (e.g. the ground friction) is changed as shown in Chapter 7. Because the environmental properties are reflected in the behavior patterns of the body, the properties can be estimated through the behavior of each component contributing to the whole body dynamics, such as touch sensors on the ground, joint angle sensors, torque sensors in the motors, and inertial sensors in the body. In this manner, sensing of non-trivial physical properties can be possible: Ground friction and body mass can be measured by a visual sensor and an on-off mechanical switch (Chapter 7).

Multi-modal sensing is particularly important for situated systems, i.e. systems that acquire information about the environment through their own sensory systems. For a situated system, the sensory information acquired through one sensory channel is not very meaningful. Generally in conventional robotic systems, sensory information is interpreted by a human designer and implemented in a control program. For a system which grows through the interaction with the environment, however, grounding is a fundamental issue, as pointed out by the “symbol grounding problem” [37, 102, 127]. For the symbol grounding problem, sensory information becomes more “meaningful” by correlating multi-modal sensory information. Because information from each sensory channel is generated by a certain physical interaction, the robot is able to learn the relation between different physical interactions by correlating the respective information. As another example of legged locomotion, the angle of a slope can be measured with a single sensory channel, an inclinometer. The information extracted from this sensory channel, however, becomes more meaningful if it is combined with information from other sensory channels, e.g. locomotion speed, the force exerted on the legs, energy consumption, and motor signals. The robot might be able to “understand” the meaning of the slope angle or of high friction by correlating sensory patterns from different channels.

It is important to note that this mechanism for multi-modal sensory information does not always work when sensory-motor coordination is implemented. When the behavior is actively stabilized by using sensory information, the behavior of the body might not be changed by different environmental conditions; As a result, multi-modal sensory information cannot be generated. Therefore, it might be important to make the system dependent on the physical changes to some extent in order to acquire multi-modal sensory information.

Information structure acquired through body dynamics

This principle is related to the previous one. It states that the recognition process of the environmental properties can be significantly simplified when sensory information is acquired through behavioral patterns induced by body dynamics. Because a change of an environmental property can result in a considerably different behavioral pattern, the sensory information acquired through body dynamics can be clearly distinctive.

For example, as shown in Chapter 7, the running behavior of the four-legged robot is possible only in a certain environment with a set of control parameters. Although a small change in the environment does not influence the behavioral pattern due to the self-stabilization nature of body dynamics, the stable locomotion pattern disappears and a chaotic pattern is induced when the environment is substantially changed. Because of the self-stabilization mechanism, the transition between stable and chaotic behavioral patterns is salient, thus sensory information acquired through the behavior patterns can be easily distinguished. A threshold can be sufficient for the recognition of ground friction as shown in Chapter 7, for example.

An important implication is the fact that discrete states are generated in continuous space of sensory information, which is originated in the self-stabilization characteristics derived from body dynamics. In other words, the sensory information is “structured” by the body dynamics such that the environmental properties can be discretely recognized. These discrete states are then used for a form of symbolic internal representations, which are the indicators of physical interaction between the body and the environment.

1.4.3 Design Principles of Control for Behavioral Diversity

So far, we have discussed only Behavior Type II, i.e. behaviors generated by a simple controller without any sensory information. Although many behavioral patterns can be generated only with a simple controller by exploiting body dynamics, the integration of sensory information substantially enhances behavioral diversity, which then leads to Behavior Types III and IV as introduced in the previous section. There are many different ways to integrate the sensory information for adaptive control, but here we focus only on the control architecture for Behavior Type III. Namely, the main question is how the control architecture integrates the sensory information by exploiting morphological properties and body dynamics. By integrating sensory information, the control architecture can guide the system for goal-directed behaviors.

Sensory-motor coordination for stable behavior processes

This principle states that, when sensory morphology and temporal sensory information are properly taken into account, sensory-motor coordination can be significantly simplified. The simplification of the sensory-motor coordination is particularly important for the stability and the precision of maintaining complex behavior processes.

For example, although course stabilization in the air is a considerably demanding task, the flying robot introduced in Chapters 2 and 3 is able to recover from most of the potential course deviations with a simple substrate of sensory-motor coordination. This is possible because it exploits temporal sensory information and sensory mor-




Behavior Types	Behavior Type II		Behavior Type III
Robots and Chapters	 Stumpy (Chapt. 4 and 5)	 Dog Robot (Chapt. 6 and 7)	 Flying Robot (Chapt. 2 and 3)
Design Principles	Body Dynamics for Behavioral Diversity		Body Dynamics for Sensing Control for Behavioral Diversity

Figure 1-2: Design principles and their relation to the topics described in this thesis.

phology, i.e. the optic flow information obtained from the omni-directional camera images. More concretely, when the robot rotates clock-wise around its vertical body axis, the optic flow indicates the flow from right to left; When the robot goes down, the flow goes from the bottom to the top; And when it goes straight, the optic flow on both lateral sides indicates opposite directions. Because this optic flow provides sufficient information about the behavior of the system, the robot is able to react to the disturbances.

It is important to mention that sensory morphology is highly related to the body dynamics and the behavioral diversity of the system. In the case of a legged robot, for example, an on-off mechanical switch does not provide any information about a locomotion process if it is not on the foot. In a similar way, the flying robot requires most of the sensors in lateral sides because the robot has particular body dynamics and behavioral diversity, i.e. it mostly travels toward the forward direction.

Control for goal-directed behaviors

This principle states that control for goal-directed behaviors can be significantly simplified when self-stabilization mechanisms are exploited.

In the goal-directed navigation of the flying robot, for example, the optic flow information, which is used for the course stabilization, can also be used for measuring the traveling distance by accumulating the flow over time. By combining both the course stabilization mechanism and the odometry mechanism, this robot is able to perform goal-directed navigation. Theoretically, only a few pixels of visual information are sufficient to be processed for the goal-directed navigation in the air.

As another example, which is highly related to the design principle of body dynamics for behavioral diversity, the four-legged robot can adjust its locomotion velocity by using a simple time delay which is the computationally simplest way to regulate a desired velocity (Chapter 6). This is possible because it exploits the self-stabilization mechanism derived from the compliant legs.

1.5 Overview of the thesis

So far, the conceptual background and design principles have been explored. In the rest of the thesis, we explore three individual research topics that all contribute to our understanding of adaptive behavior. In particular, we focus on the issues of locomotion and navigation, because they are fundamental functions for autonomous systems, and cheap design and behavioral diversity are essential for these functions. The following sections are organized on the basis of about 14 published papers. Here we summarize the case studies in the context of the conceptual contributions described in this section (Figure 1-2).

The first topic investigates visually guided navigation of flying insects (Chapters 2 and 3). The major focus lies on how flying insects can achieve many different functions with a relatively simple brain. In order to understand the behavioral diversity of visual navigation, we have investigated a biological model of flying insects and tested it in a real-world robotic platform (Chapter 2; This chapter is based on the reviewed publications [47, 49]). It is shown that the temporal patterns acquired through the biologically inspired motion detectors can be used for visual odometry given a proper sensor morphology (i.e. the location of motion detectors and their resolution). The visual navigation model is then tested with a freely flying robot (Chapter 3; This chapter is based on the publication [50]). Goal-directed navigation is achieved by implementing mechanisms of course stabilization and visual odometry for sensory-motor coordination. Moreover, it is shown that the proper morphology in the sensory system significantly improves the navigation performance in an unstructured environment.

Chapter 4 presents a dynamic locomotion robot, Stumpy, which takes advantage of its intrinsic body dynamics. Owing to the unique design of its morphology, Stumpy exhibits a variety of locomotion behaviors even though it has only two actuated degrees of freedom (this chapter is based on the publication [48]). The behavioral diversity of Stumpy is explored further in Chapter 5, where it is explained how Stumpy exploits its intrinsic body dynamics and the physical interaction with the environment for behavioral variations (this chapter is based on the publications [51, 53]).

Another kind of locomotion system is introduced in Chapter 6 (this chapter is based on publication [52]). The four-legged robot, Puppy, shows that rapid locomotion can be achieved even without sensory feedback by exploiting a self-stabilization mechanism derived from the elastic material property implemented in its legs. By exploiting this stabilization mechanism, we introduce a unique method to enhance the behavioral diversity. As an example, it is shown that a simple mechanism is sufficient to control a complex running behavior. On the basis of stable dynamic locomotion of Puppy, we explore how body dynamics and the interaction with the environment can be related to the perception in Chapter 7. It is shown how body dynamics is related to the structure of sensory information, which could potentially simplify the perception of situated systems (this chapter is based on the publications [55, 57]).

Finally in Chapter 8, the contributions and perspectives of this thesis are discussed. In particular we consider how this thesis contributes to the challenging issues of evolutionary and developmental artificial systems and artificial cognition.

Chapter 2

A biologically inspired visual odometer for flying robot navigation

Abstract

While mobile robots and walking insects can use proprioceptive information (specialized receptors in the insect’s leg, or wheel encoders in robots) to estimate distance traveled, flying agents have to rely mainly on visual cues. Experiments with bees provide evidence that flying insects might be using optical flow induced by egomotion to estimate distance traveled. Recently some details of this “odometer” have been unraveled. In this study, we propose a biologically inspired model of the bee’s visual “odometer” based on Elementary Motion Detectors (EMDs), and present results from goal-directed navigation experiments with an autonomous flying robot platform that we developed specifically for this purpose. The robot is equipped with a panoramic vision system, which is used to provide input to the EMDs of the left and right visual fields. The outputs of the EMDs are in later stage spatially integrated by wide field motion detectors, and their accumulated response is directly used for the odometer. In a set of initial experiments, the robot moves through a corridor on a fixed route, and the outputs of EMDs, the odometer, are recorded. The results show that the proposed model can be used to provide an estimate of the distance traveled, but the performance depends on the route the robot follows, something which is biologically plausible since natural insects tend to adopt a fixed route during foraging. Further investigation in the simulation shows that goal-directed navigation can be potentially achieved by simple visual processing, and that the design flexibility of this approach leads to high adaptivity to the given task-environment.

⁰This chapter is based on the reviewed publications [47, 49].

2.1 Introduction

Navigation in complex 3-D environments is a challenging issue for both animals and robots. Flying insects solve this task in a robust and adaptive way despite their tiny brains. Being able to navigate in 3 dimensional space offers several advantages. Flying insects, for example, can reach target locations (e.g. food sources, or their nest) faster and easier, they have the birds eye perspective of their environment, and they have increased access to places, that are not reachable by land. However, this also introduces a number of additional issues that need to be addressed. For example, parsimony of control strategies is essential, since flying agents can not simply pause - they must make control decisions in a timely manner. Robustness of control strategies is another issue - while in wheel-based robots it is possible to make a sequence of bad decisions without endangering the integrity of the robot, this will be disastrous for a flying robot. There is also a much higher pressure to develop mechanisms that are able to cope with unanticipated situations. Abilities like flight stabilization, obstacle avoidance, safe landing, or target tracking, will often have to rely on vision. In some cases, required navigational accuracy and small size operating areas preclude the use of most commercially available equipment like GPS or radar. Especially dead reckoning in a small range can only be done supported by visual information, since proprioceptive errors are much larger compared to land-based vehicles [26, 35].

Bees make use of both landmark and dead reckoning information for navigating, and can communicate the distance and direction to a newly found food source to their nest mates. Use of dead reckoning requires that both directional and distance information be available. Whereas in direction estimation there is a lot of evidence (starting with the pioneering work of von Frisch [120]) that celestial cues and especially the polarization pattern of the sky play crucial role [99, 36], the way that bees gain information about the distance traveled has been a point of dispute for many years.

Early studies suggested that the distance is gauged in terms of total energy consumption during a foraging journey, but recent studies of the bees' behavior questioned this hypothesis, and suggested that visual cues, more specifically the amount of image motion, play an important role on estimating the distance traveled [107, 108, 112]. In these studies, bees were initially trained to search for the food source in the vertically striped tunnel. Then the searching behavior of the trained bees was observed when the pattern of stripes on the walls was changed, by using different stripe periods, different width between right and left walls, and walls with horizontal stripes. With horizontal stripes, bees tend to fail searching for the food source at the right location, therefore it was concluded that vertical stripes are used for the visual odometer. With different period of stripes, bees succeed in finding the food source position, which implied that bees measure the distance independent of the spatial frequency of the stimulus in the environment. However, when the distance to both walls was increased or decreased compared to the training situation, bees tend to fail in searching at the right location. The main conclusion from these studies was that the bee's visual odometer provides an estimate of distance that is independent of the spatial frequency of the visual stimulus, i.e., it only depends on the angular

velocity of the image projected on the insect’s retina.

Although there is a lot of behavioral evidence that bees might be using optical flow for estimating distance, there is very little known of how this could be implemented neurally. A visual odometer for mobile robots was proposed, but this odometer is based on an image interpolation algorithm rather than optical flow [109]. On the other hand, there is a lot of work done on insect motion perception and its use on stabilizing flight. The optomotor response of flying insects has been investigated for a long time. Reichardt reported on the optomotor response of the fly almost thirty years ago [97], he demonstrated that a tethered fly inside a striped drum tends to turn in the direction in which the drum is rotated. This response helps the insect maintain a straight course by compensating for undesired deviations. The landing response of the fly was investigated with case studies on the extending leg response for the preparation to land and deceleration of speed before landing [110]. Those studies imply that flies might be using image motion of the texture on the ground for producing a landing response. Such a scheme would take advantage of the fact that texture in the image moves faster as the insect comes close to the ground. In addition, bees appear to use a similar strategy to regulate their flight speed [107], according to which bees decrease their flight speed as the vertically striped tunnel becomes narrower so as to keep the angular velocity of the image constant.

On the basis of above mentioned behavioral experiments as well as electrophysiological studies, a model of motion detection in the insect’s nervous system, the so-called Elementary Motion Detector (EMD), has been proposed [9]. This biological motion detection mechanism is also very interesting from the engineering perspective, because traditional optical flow approaches require large computational resources [3]. Some attempts to incorporate motion detector mechanisms to control artificial agents in both real-world robots and computer simulations have been reported in the last few years. An autonomous agent capable of avoiding obstacles, while moving very fast, by exclusively using optical flow was implemented by Franceschini et al. [30]. The visuomotor system of the robot was based on the study of the neural mechanisms of motion detection in the compound eye of the housefly. It consists of an array of EMDs capable of analog, continuous-time processing, which were used to steer the robot directly. In a similar way, EMDs were used in a simulated flying agent for altitude control, to avoid crushing on the ground [77, 79]. Due to their simplicity, analog VLSI implementation of EMDs has been also proposed [38].

Another advantage of EMDs as can be seen from the above mentioned applications, is that they can be used in different parts of the visual field for different purposes. EMDs at the periphery can be used to evaluate lateral flow as well as the motion of the ground for evaluating flight speed or distance covered, whereas EMDs tuned in the center of the visual field can be used for detecting objects and avoiding them. Being able to reuse the same basic circuit is very important for flying agents since there are normally very strict constraints on the amount of payload the agent can carry.

In this chapter we introduce a biologically inspired visual odometer based on EMDs and present and analyze data of its performance on a robot. Given the results from the real-world experiments, we conduct further investigation of navigation

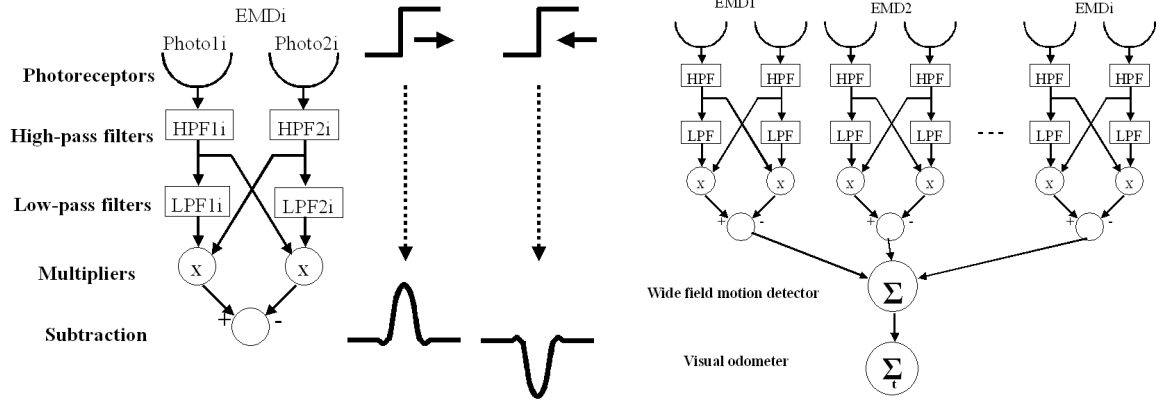


Figure 2-1: Left: the Reichardt model of elementary motion detection. Photoreceptors, high-pass filters, low-pass filters, multipliers, and the subtraction module are wired in series. The output of the last step (subtraction) is an estimate of image speed (see text for details). Right: the visual odometer based on a wide field motion detector. The integrated response of an array of EMDs, each tuned to a different part of the visual field, is used to implement a wide field motion detector. Its outputs are then integrated over time to provide an estimate of the distance traveled (for explanations, see text).

in simulation, in which the minimum requirements of this navigation strategy are explored.

2.2 Elementary Motion Detectors and the Visual Odometer

2.2.1 Basic EMD Circuit

As mentioned earlier a large part of the flying insect’s behavior seems to rely on image motion. Their motion detection mechanism has been investigated in electrophysiological level for a long time [31], and a computational model of motion detection, the Elementary Motion Detector (EMD), has been proposed based on the results from these studies [9]. There are several version of the EMD model, one of the most commonly used is the so-called Reichardt or correlation model, which consists of two photoreceptors, high-pass, low-pass filters, multipliers, and summation functions, as shown in Figure 2-1. An important feature of this model is that it sensitive not only to the magnitude of image motion but also to the direction of the motion, i.e. EMD responses are positive when image moves preferred direction, and negative response with non-preferred.

Here we propose a method to measure distance traveled using the Reichardt model. Since the EMD response provides an angular velocity signal (more exactly, a spatio-temporal signal that depends on the speed of the stimulus as well as its spatial frequency, see next subsection), the distance traveled could be estimated by inte-

grating the EMD outputs over time. The information processing steps we employed in the experiments are as follows. At first, intensity values from two adjacent pixels on a CCD camera image are used to calculate activity of a photoreceptor pair ($Photo1_i(t)$, $Photo2_i(t)$ of the i th EMD). Subsequently the output of the High-Pass Filters $HPF1_i(t)$ and $HPF2_i(t)$ at time t is calculated as follows:

$$HPF1(t) = Photo1(t) - Photo1(t - 1) \quad (2.1)$$

$$HPF2(t) = Photo2(t) - Photo2(t - 1) \quad (2.2)$$

Given output of $HPFs$, the output of the Low-Pass Filters $LPF1_i(t)$, $LPF2_i(t)$ is calculated as follows:

$$LPF1(t) = a \cdot HPF1(t) + (1 - a) \cdot HPF1(t - 1) \quad (2.3)$$

$$LPF2(t) = a \cdot HPF2(t) + (1 - a) \cdot HPF2(t - 1) \quad (2.4)$$

where a is a parameter for the time delay. Then each LPF output is multiplied with the output of its neighboring HPF :

$$MLP1(t) = LPF1(t) \times HPF2(t) \quad (2.5)$$

$$MLP2(t) = LPF2(t) \times HPF1(t) \quad (2.6)$$

The output of an EMD module is finally computed as:

$$EMD(t) = (1 - b) \cdot EMD(t - 1) + b \cdot (MLP1(t) - MLP2(t)) \quad (2.7)$$

where b is another delay parameter implementing a low-pass filter on the EMD's output to reduce noise. By putting many EMD modules in parallel we can increase the visual field size, thus simulating the wide field motion sensitive H1 interneurons in the insect's brain:

$$H1(t) = \sum_i EMD_i(t) \quad (2.8)$$

At the end the visual odometer response, VO , is calculated by integrating the $H1$ output over time:

$$VO = \sum_t H1(t) \quad (2.9)$$

2.2.2 Initial Experiments Using a Panoramic Camera

To evaluate the performance of our model, we developed a miniature panoramic vision system, which consists of panoramic mirror, a CCD camera module, and the housing

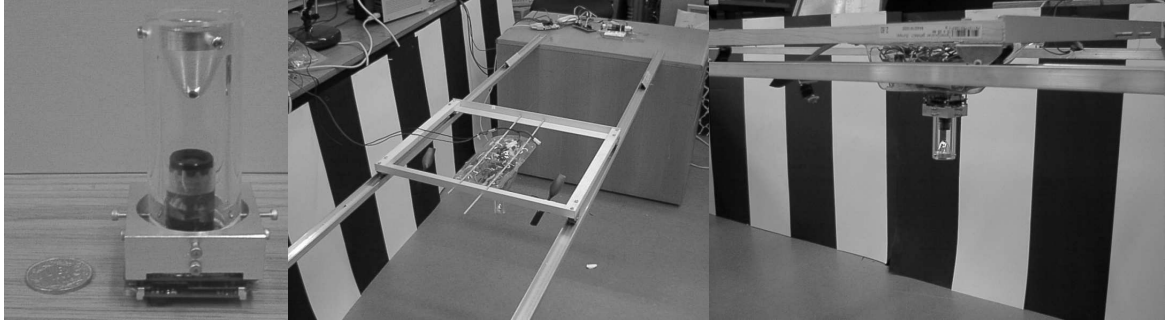


Figure 2-2: Vision system and initial experiment setup. Left: The panoramic vision system we developed for this experiment consists of CCD camera, panoramic mirror, and housing components, which weighs 90 g in total so that it can be embedded in the flying robot. The visual field covers 360 degrees on the horizontal plane, and 260 degrees vertically. Middle and right: This vision system is equipped with the caster-frame on a pair of rails, and an external motor drives the vision system along a straight route at a constant speed. Initially walls with black and white stripes were installed along the rails (20cm width period of black and white, 60cm distance from vision system).

components. The system was designed to weight no more than 90 g in total so that we could later integrate it to the flying robot (Figure 2-2). The panoramic mirror was developed based on a panoramic optics study [16] and it has a hyperbolic surface that provides a visual field of 360 degrees on horizontal plane and 260 degrees vertically. In the first experiment, this vision system was equipped with the caster wheel frame on a pair of rails, and a motor system which drives the vision system at constant speeds along a horizontal straight route (Figure 2-2).

Initially walls with black and white stripes were installed along the railway (20cm width period of black and white, 60cm distance from vision system). Figure 2-3 shows that the typical responses of one EMD module, when the vision system moves 2 m at constant speed of 15 cm/sec. Black and white stripe patterns can be seen as big fluctuation of image intensities, i.e., image edges that activate the *HPFs* and *LPFs*. The EMD responses indicate image motion (as a result of egomotion), and eventually *VO* indicates the distance the vision system moves. Since only one EMD is used in this graph, the response of *VO* seems layered, because *VO* is incremented only when EMD goes through an edge in the image. This layered response in *VO* outputs could be improved by applying wide field of EMDs that cover wide range image angle such that changes in intensity (edges) continuously activate EMDs.

A characteristic feature of the EMD model is that its response depends not only on the speed of the image, but also on its spatial frequency [110]. Thus, it acts more like a spatio-temporal filter rather than a pure speed detector. Its response attains a maximum at a certain speed that induces a specific temporal frequency. In order to test this characteristic, we have carried out another set of experiments, in which the vision system is driven 5 times at 3 different speeds (15cm/sec, 28cm/sec, and 40cm/sec) in the same setup as previous experiment. As shown in Figure 2-4,

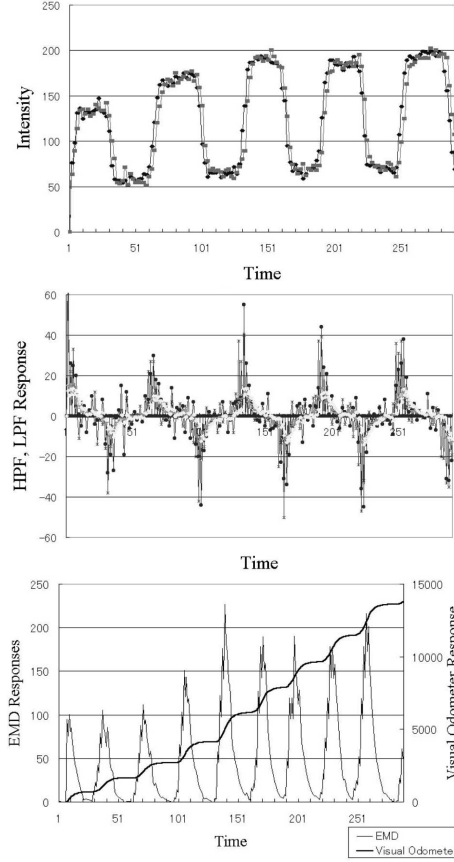


Figure 2-3: Typical responses of the EMD and the visual odometer. Upper: Photoreceptor activity is calculated directly from the image captured by CCD camera. This graph shows the time-series of photoreceptor activity. Fluctuations on the signal correspond to the stripe pattern of the walls when the vision system moves horizontally along the corridor. Middle: The outputs of High-pass and low-pass filters. Fluctuations on these signals correspond to the edges in the image. Bottom: Responses of the wide field motion detectors and the accumulated visual odometer response.

the visual odometer responses at different speeds indicate different distances even though it moves along the same absolute distances, i.e. the responses at middle speed indicate the longest distance. This result is not compatible with the results obtained from the bee experiments that show that distance estimation is independent of the spatial structure of the stimulus [106].

However, as shown in Figure 2-4, the odometer responses at each speed tend to indicate the same distance, which imply this odometer could be used for measuring distance to the target position as long as the agent follows the same route. Considering the fact that this assumption has to be made even in the case of a visual odometer which is independent of the spatial frequency (the bee still needs to encounter the same objects at the same distance), we can conclude that there is no obvious advantage of spatial-frequency independent visual odometer in this context.

With this assumption in mind, we tested this system in the natural office environ-

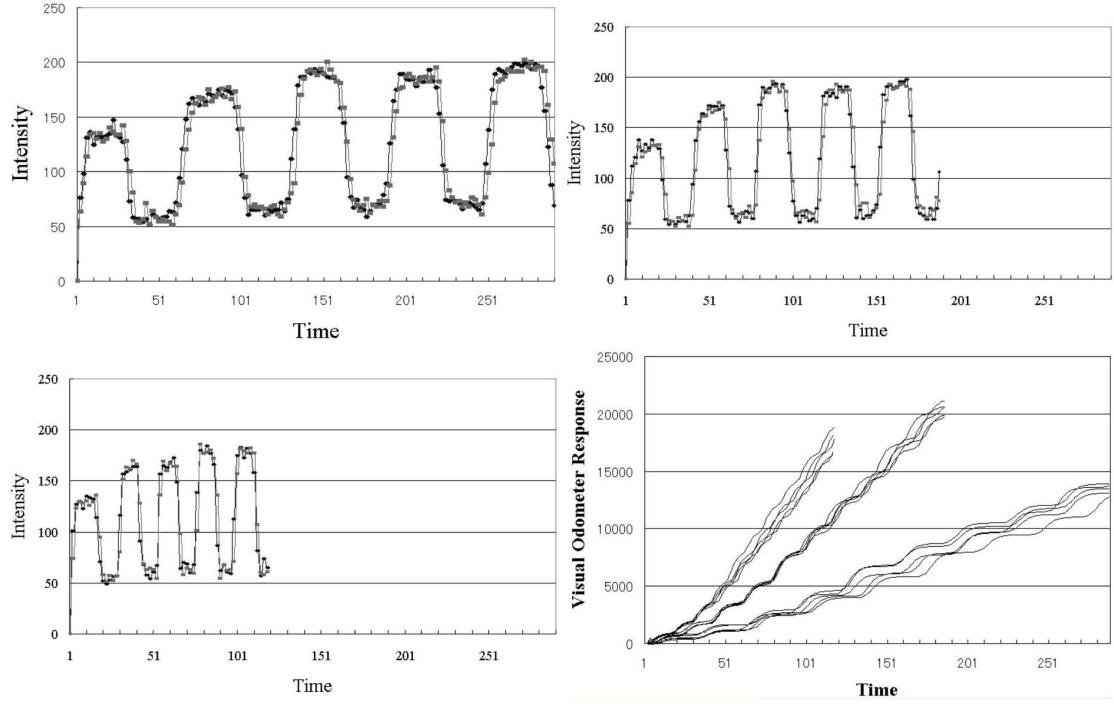


Figure 2-4: Visual odometer responses at 3 different speeds. Time series of photoreceptor activity for 3 different speeds: 15cm/sec (Upper Left), 28cm/sec (Upper Right), and 40cm/sec (Bottom Left). Bottom Right: Visual odometer response. Because the outputs of the EMDs depend on temporal frequency, the odometer produces different distance estimates at different speeds.

ment, in which the vision system moved 5 times at the same speed along the same routes without any artificial walls but by using the surroundings of the office. Photoreceptor inputs and odometer responses are shown in Figure 2-5, which demonstrates that the odometer has the ability to operate even in unstructured office environments when it follows the same route at the same speed.

2.2.3 3-D Navigation with EMDs and the Visual Odometer

In the following, we focus on integration of the EMD-based visual odometer in an autonomous flying robot. Flying agents also need to obtain the flight height information in order to maintain a certain flight altitude, to avoid crushing on the ground, and for reaching a certain target position in 3-D space. One possibility to realize such a mechanism is to use information from the ventral part of the visual field. EMDs receiving input from this part could measure the distance to the ground by using the optical flow induced by ground texture. A strategy of speed and altitude control of flying agents by using a similar mechanism has been evaluated in simulation [77, 79]. An alternative would be to use EMDs tuned to the vertical direction, in such a case the mechanism is the same as the one used in the visual odometer described in the previous section, but this time the EMDs are tuned to motion along the vertical

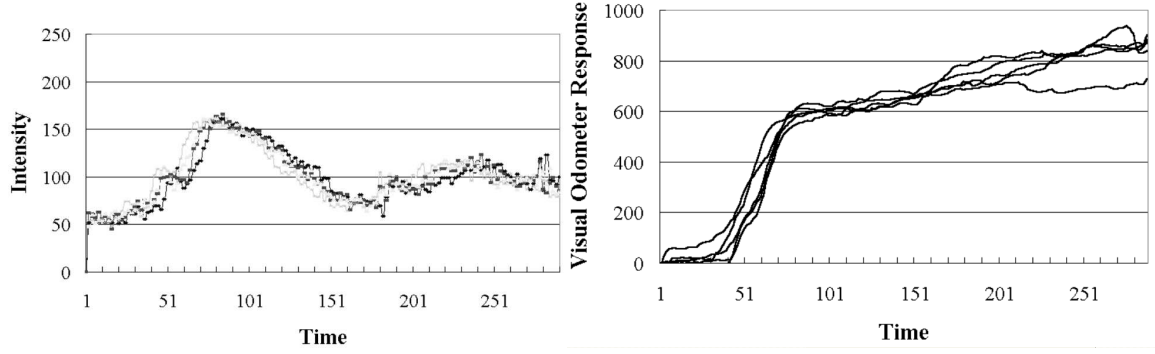


Figure 2-5: The response of the visual odometer in an experiment performed in a natural office environment. Left: Typical output values of four photoreceptors. Their output profile depends on the structure of environment and the light conditions. Right: Visual odometer response. The vision system moved along the same route 5 times at the same constant speed. This graph shows that the proposed odometer mechanism provides a robust distance estimate as long as it moves along the same route.

plane (see Figure 2-7). According to this scheme, the vertical EMDs respond to the vertical motion of the agent (changes in altitude), thus this information could be used for altitude control. Note that, however, this approach does not measure the distance to the ground simultaneously but it depends on the accumulated response of the EMDs, and thus it is prone to cumulative errors. For the purpose for our experiments thought, it proved to be sufficient to keep the robot over a certain height and to avoiding crushing on the ground. This is not general purpose altitude control mechanism neither a model of how insects achieve this.

One prominent feature is that EMDs cannot accurately measure 2-D image motion, i.e. they cannot always distinguish horizontal from vertical motion depending on the image structure [9]. We tested the performance of both vertically and horizontally tuned EMDs in the same experimental setup described in the previous subsection. During the experiment the robot had to move forward at constant height and speed in the office environment. Two arrays, consisting of 80 EMDs each, arranged along the horizontal, vertical directions, were used to provide both horizontal (forward motion) and vertical (changes in altitude) motion cues estimates, respectively. Figure 2-6 shows the panoramic image in an office environment and distribution of the two dimensional EMD array. Figure 2-7 shows the output characteristics of the horizontally and vertically tuned EMDs in terms of the average and the standard deviation of the EMD responses. This result implies that the vertical EMDs could measure vertical motion with a 4% error.

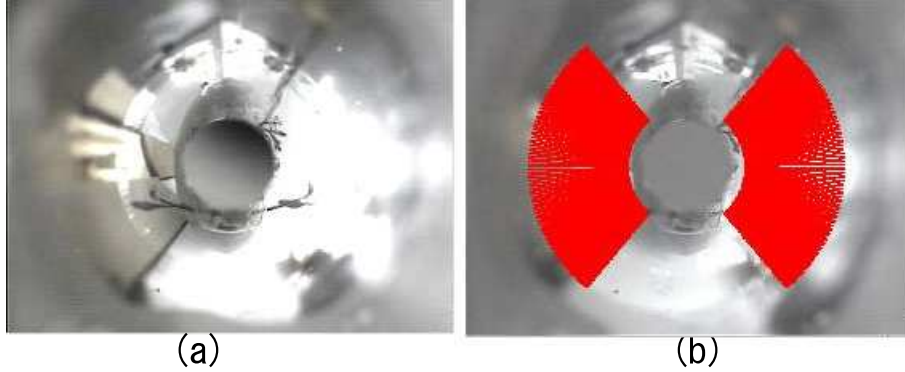


Figure 2-6: (a) Panoramic view of an office environment acquired through the omni-directional camera, and (b) distribution of two dimensional EMD array in the panoramic image.

2.3 Simulation Experiments

2.3.1 Method

This section presents a simple simulation experiment to investigate the influence of parameters on the proposed approach. For the sake of convenience, we conducted the simulations in a 2-D environment. As shown in Figure 2-11, an agent navigates through a corridor, both sides of which have walls with one-dimensional sinusoidal intensity patterns. The controller used in this simulation is shown in Figure 2-9. The left and right visual fields consist of two dimensional arrays of EMDs, in which EMDs are oriented both horizontally and vertically to measure both movements [9]. The number of EMDs in each array can be highly flexible; in the extreme case, one EMD on each side and another for vertical one is sufficient (therefore, only 5 pixels are required for 3-D control). In addition, parameters of the EMDs, such as low-pass filter constants, can be set independently, but only homogeneous distributions are employed. The responses from both horizontal and vertical wide field EMDs are extracted, and provide inputs to the visual odometer as well as to a sensory-motor circuit. In the visual odometer neuron, the given inputs from the horizontal EMDs (EMD_H_R and L in Figure 2-9) are accumulated over time. In the sensory-motor circuit, the right and left horizontal EMDs are connected to the rotation motor neuron. The right and left vertical EMD neurons (EMD_V_R and L) are connected to the elevation motor neuron, whereas the connection weights are chosen in such a way to suppress vertical motion, i.e. to retain height. The thrust motor neuron is connected to a bias neuron that drives the robot forward at a constant speed. The connection weights are set by hand, and are not changed during the experiments. The simulated agent has no inertia or friction, thus the position and the orientation of the agent are simply calculated from visual inputs in the previous step. The agent starts to navigate from the same initial condition and continues until it hits the walls or reaches the end of the experimented area.

We tested 2, 40, and 90 pixels on each lateral view of the agent (therefore the

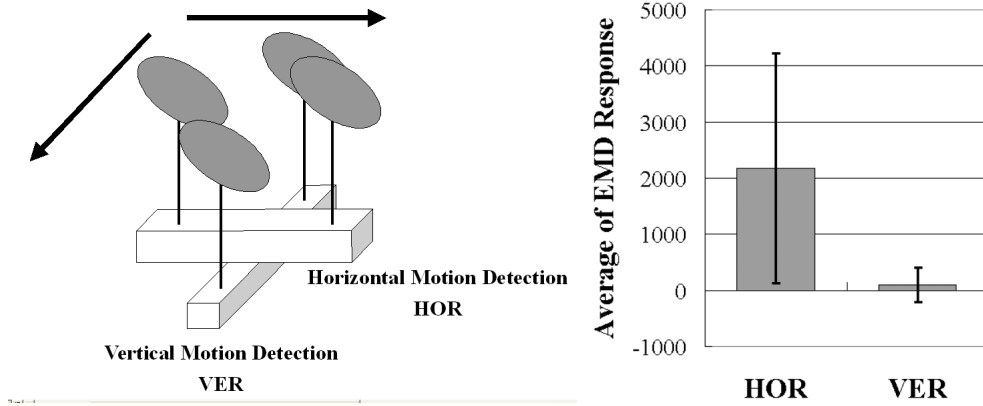


Figure 2-7: Left: Two-dimensional EMDs. Filled ellipses denote photoreceptors, filters and operators are represented by the boxes, and their outputs provide independent estimates of vertical and horizontal image motion. Right: Typical responses of vertical and horizontal EMDs when the vision system moves horizontally straight in the natural environment. This graph indicates that the EMDs could also be used to detect vertical motion with very small errors.

agent has 2, 40, and 90 EMDs in total respectively), each of them are positioned at a constant angular distance of 2 degrees. We began with a simple environment in which walls in the corridor contains sinusoidal intensity patterns. Noise was then added by means of the following equation.

$$I(x) = 128 + 128 \times \sin(x) + 256 \times \text{Noise}_{Level} \times \text{Random} \quad (2.10)$$

where $I(x)$ is the intensity at location x , and Random is a random value between 0 and 1. We tried Noise_{Level} values of 0, 20, 50, and 100 %. This noise corresponds to a variation of spatial structure in the real environment. Figure 2-11 shows the typical sinusoidal patterns at each noise level. With each combination of the number of EMDs and the noise level, 20 trials were tested using the different wall patterns generated by different random seeds.

2.3.2 Result and Discussion

Figure 2-10 illustrates the trajectories from each trial, and Figure 2-11 shows the mean visual odometer responses of 20 trials and the standard deviations (SD) as percentage of the mean visual odometer responses. In case of Noise_{Level} 0%, the proposed method can achieve goal-directed navigation with only 2 EMDs (4 pixels); the agent follows the same route and measures the distance correctly, i.e. zero SD. In the noisy conditions, however, the trajectories spread out in earlier stages of the navigation, which lead to larger odometer errors. In the cases of 40 and 90 EMDs, on the other hand, deviations of routes are relatively small. These results suggest that the larger numbers of EMDs improve the performance in the noisy environments, namely goal-directed navigation can be achieved robustly even when spatial structures of the environment are modified. This also implies the design flexibility of the proposed

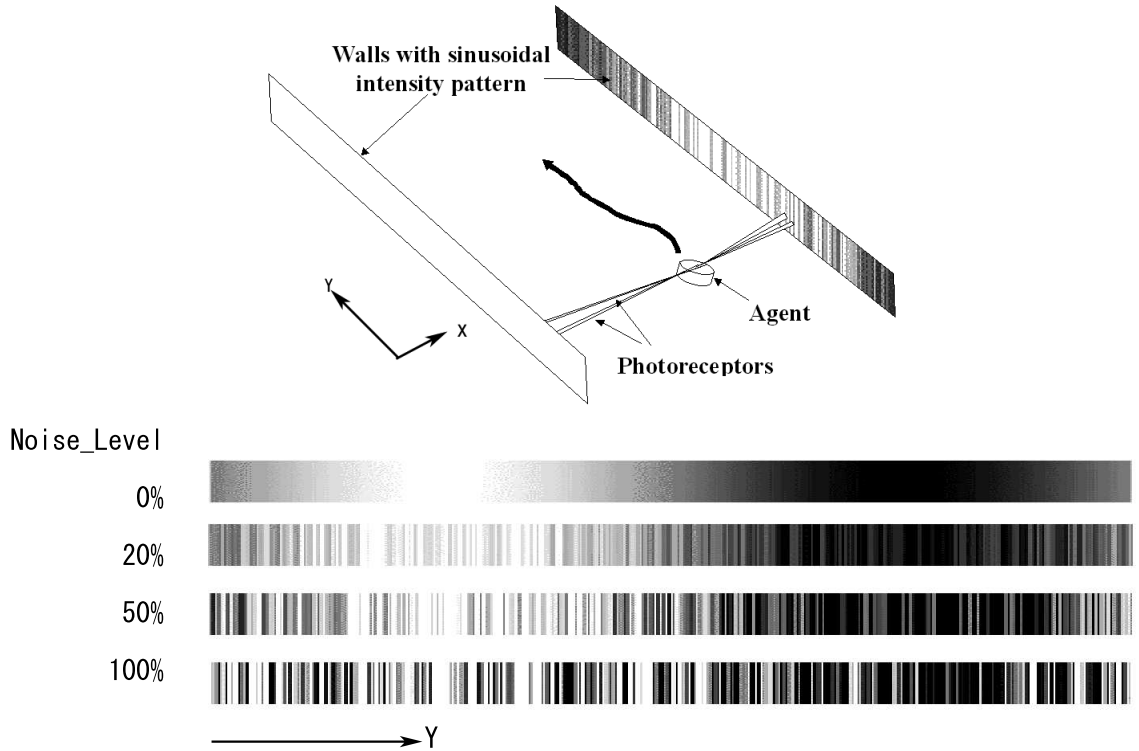


Figure 2-8: Top: The simulation setup. Bottom: The typical patterns used on the wall. (Noise 0, 20, 50 and 100 % from top to bottom.)

approach in a sense that designers (or an evolutionary process) can flexibly change the architecture of the agent to adapt to the complexity of the given task-environments.

2.4 Discussion and Further Work

The experimental results imply that the optomotor response of flying agents would play an important role in a visual odometry scheme using EMDs, because their response tends to be dependent on the structure of environment. In this respect, the visual odometer that we describe here is not compatible with what we currently know about its biological counterpart, because the bee's response seems to be independent of the spatial structure of the environment. However, as we discussed earlier, this does not seem to have an advantage since the bee still has to follow the same route in order to experience the same distances to the objects, which is a prerequisite even for a pure image velocity visual odometer to work.

An interesting property of the navigation scheme described in this chapter, is that the system not only achieves visual odometry but also avoids obstacles, controls its speed, and presumably this mechanism could also be used for safe landing, and these by using the same elementary mechanism, the EMD. For all of these behaviors, the sensory-motor response is, again, a very important issue to consider, because none of these behaviors could have been realized without it. The safe landing mechanism

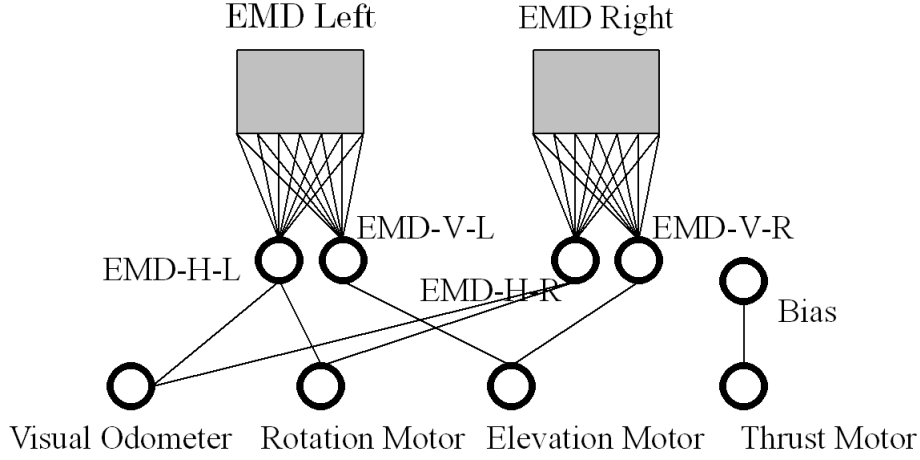


Figure 2-9: Sensory-motor control circuit. Outputs of left and right EMD networks provide the vertical (EMD-V-L, EMD-V-R) and horizontal (EMD-H-L, EMD-H-R) image motion values of each side. The horizontally, vertically tuned EMDs are connected to a motor neuron that controls the robot’s rotation, elevation, respectively. The outputs of the horizontally tuned EMDs are also used by visual odometer. The thrust motor neuron has a connection to bias neuron that implements the default move-forward behavior.

could be implemented by changing the connections between the EMDs and motor neurons. One interesting issue to be studied could be whether an action selection mechanism for switching between conflicting behaviors such as obstacle avoidance and landing would be necessary.

Another issue has to do with EMD design considerations about morphology and heterogeneousness. Considering fly’s tendency of landing control to texture on the ground, it is not only intuitive but also biologically plausible that EMDs focusing on the ground could be used. This is a morphology issue of visual system design. Moreover it is natural to consider a heterogeneous design that would make use of different parameters among EMDs, such as the delay parameters or the connections to the motor neurons, because there would be different optimal parameters for lateral visual fields from ventral ones. Instead of manually tuning these parameters, one possibility would be to use artificial evolution to automatically generate them.

From the information theoretic perspective, this navigation algorithm has many advantages over traditional methods, because of its cheap and flexible design. In the extreme case, only 8 pixel values are required for navigation, because it can navigate as far as ego-motion can be detected, which can be implemented, in principle, with only two EMD modules, for horizontal and vertical motion detection, on each side. The number of EMDs would be determined depending on the task-environment, because, for example, the agent does not need many EMDs when it navigates in a simple environment, with a limited number of visual patterns, like artificial gratings. And it could be also intuitive to imagine that design flexibility would be another advantage, since we, as designers (or by using evolutionary techniques), can easily increment or

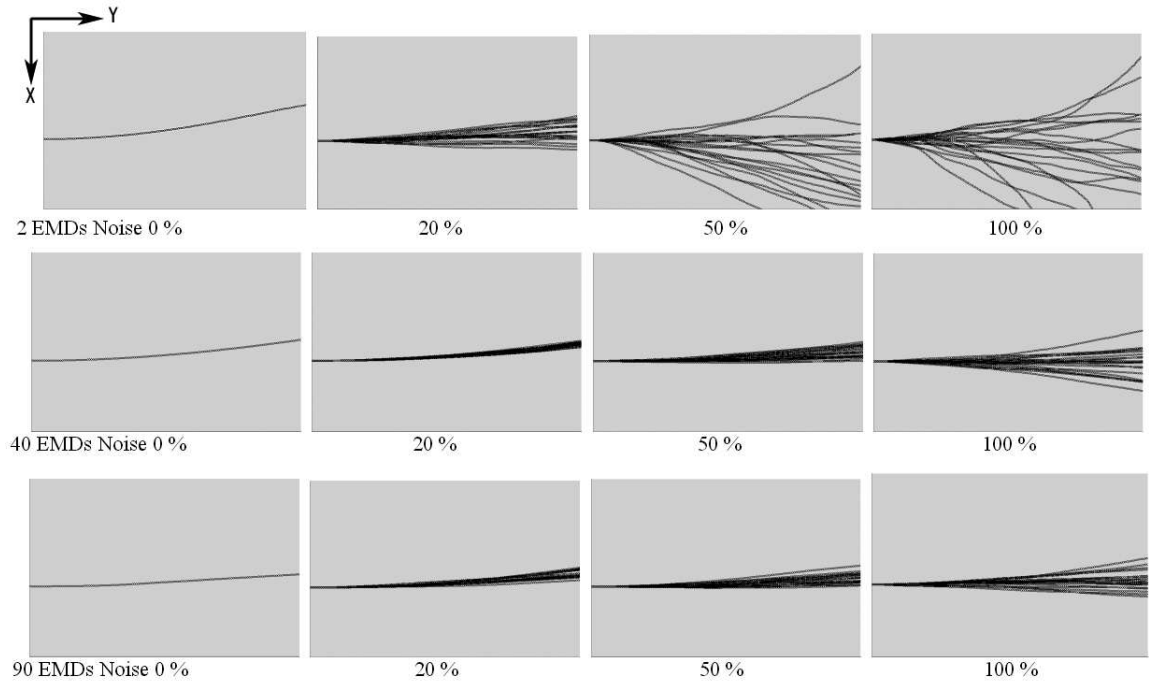


Figure 2-10: Trajectories of the simulated agent. Each graph contains the results from 20 trials with different wall patterns.

decrement the number of EMDs from one to thousands, with the same basic circuit. The relation between EMD design and task-environment could be another interesting issues to be investigated in future work.

To summarize, this chapter presented a navigation algorithm using a biologically inspired visual odometer that is based on Elementary Motion Detectors, and evaluates its performance by using a robot equipped with a panoramic visual system. Since flying agents have to achieve a number of complex tasks in parallel with severe weight and real-time constraints, cheap design could be one of the most important design strategies. The result of the experiments with the autonomous flying robot show that the proposed algorithm can successfully be employed of navigation tasks in a complex indoor environment.

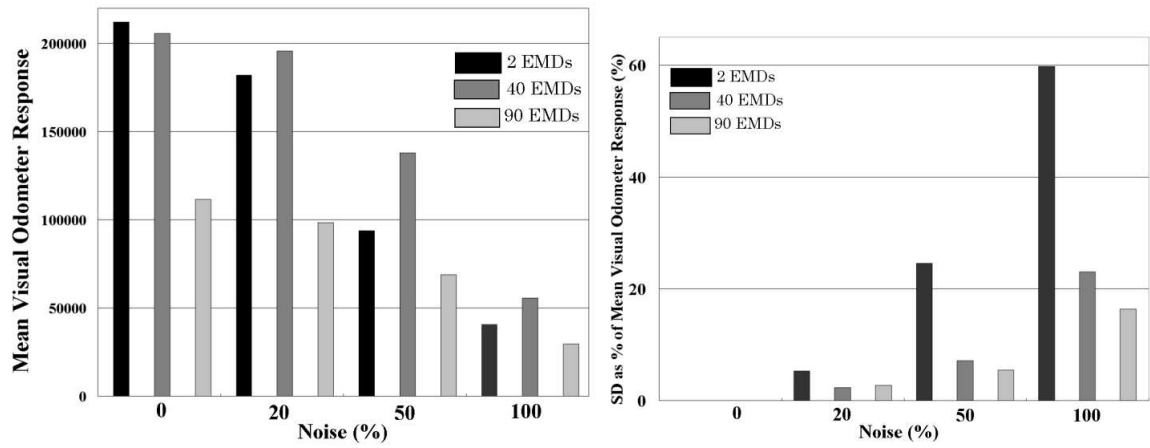


Figure 2-11: Left: The mean visual odometer responses of 20 trials. Right: The standard deviations as percentage of the mean visual odometer responses.

Chapter 3

Biologically Inspired Goal-Directed Navigation of a Flying Robot

Abstract

Experimental research in biology has uncovered a number of different ways in which flying insects use cues derived from optical flow for navigational purposes, such as safe landing, obstacle avoidance and dead reckoning. In this study, we use a synthetic methodology to gain additional insights into the navigation behavior of bees. Specifically we focus on the mechanisms of course stabilization behavior and visually mediated odometer by using a biological model of motion detector for the purpose of long-range goal-directed navigation in 3D environment. The performance tests of the proposed navigation method are conducted by using a blimp-type flying robot platform in uncontrolled indoor environments. The result shows that the proposed mechanism can be used for goal-directed navigation. Further analysis is also conducted in order to enhance the navigation performance of autonomous aerial vehicles.

3.1 Introduction

The ability to navigate in a complex environment is crucial for both animals and robots. Particularly flying insects are capable of surprisingly good navigation despite the small size and relative simplicity of their brains. Biological studies of flying insects have revealed that the animals are largely relying on visual sensory inputs for their navigation. The vision systems of flying insects are exquisitely sensitive to motion, because visual motion induced by ego-motion can tell the animal much about its own motion and also about the structure of its environment. Behavior experiments with flies and bees show a number of different ways in which insects use cues derived from optical flow for navigational purposes (for review, see [110]). Early studies showed that a tethered fly inside a striped drum tends to turn in the direction in which the

⁰This chapter is based on the reviewed publication [50].

drum is rotated [97]. This reaction, so-called optomotor response, serves to help the insect maintain a straight course by compensating for undesired deviations. In addition to such a simple reactive behavior, mechanisms for long distance navigation are also crucial for such insects as honeybees, which navigate accurately and repeatedly from their hive to a food source. This type of navigation has been known to require that both directional and distance information be available. For the direction estimation, there is a lot of evidence that celestial cues, especially the polarization pattern of the sky play a crucial role [36], and recent studies of bees' behavior suggested that the amount of image motion plays an important role to estimate the distance traveled [112].

Inspired by these insect studies, the basic reactive behaviors observed in the animals, e.g. obstacle avoidance and fixation behaviors, have been modeled and implemented into many land-based robotic platforms (e.g. [30, 100, 44, 45, 111]); simulated flying agents were used for altitude control and obstacle avoidance [81]; a robotic gantry demonstrated the landing behavior of flies [113]; a "tethered" autonomous helicopter demonstrated its altitude control using optical flow [80]. A number of aerial robotic applications which employ optical flow based controls have also been extensively explored (e.g. [3, 118, 47]). One of the interesting contrasts between the navigation of these robotics research and those of insects is that, whereas artificial aerial vehicles generally strongly rely on a number of different sensory modalities such as gyros, accelerometer, and GPSs, insects largely depend on vision with a variety of different processing pathways, from the low-level flight stabilization to the high-level long-distance navigation as mentioned above. Toward the comprehensive understanding of flying insects' navigation, which can be applicable for long-distance navigation of aerial autonomous vehicles, in this chapter, we propose a method of goal-directed aerial navigation by exclusively using an embedded omni-directional visual sensor with optical flow. In order to evaluate the performance of the method, the flight experiments with an autonomous flying robot is presented. By comparing the experimental results with the biological experiments and the other robotic navigation studies, we discuss a number of different solutions in order to enhance the performance of the proposed navigation method.

In the following sections, the course stabilization and visual odometer models are proposed, and then we evaluate the performance in the navigation of a freely flying robot. Further issues to enhance the proposed navigation capability are discussed at last.

3.2 Experimental Platform

We developed an autonomous flying robot, shown in Figure 3-2. The flying robot Melissa is a blimp-like flying robot, which consists of a helium balloon, a gondola hosting the onboard electronics, and a host computer. The balloon is 2.3m long and

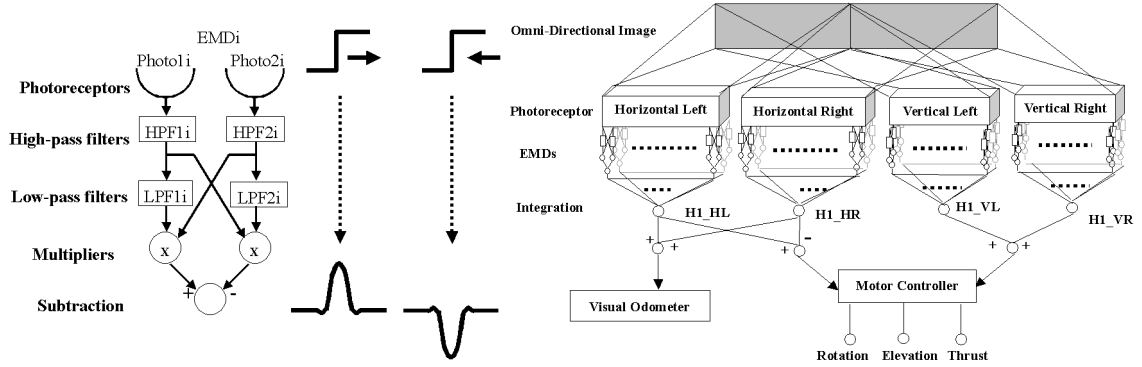


Figure 3-1: Left: The Reichardt model of elementary motion detection. Photoreceptors, high-pass filters, low-pass filters, multipliers, and the subtraction module are wired in series. The output of the last step (subtraction) is an estimate of direction sensitive image speed. Right: The controller circuit for the flying robot and visual odometer. The gray rectangle denotes the panoramic image extracted from the omni-directional camera on the robot. The image is given to both horizontally and vertically arranged photoreceptor arrays of EMDs. After the integrators and comparator, the outputs are given to motor controller and visual odometer modules.

has a lift capacity of approximately 500g. Inside the gondola, there are 3 motors for elevation and thrust control (an additional motor for rotation control is attached directly to the balloon), a four-channel radio link, a miniature panoramic vision system, and batteries. The panoramic mirror has a hyperbolic surface that provides a visual field of 360 degrees on the horizontal plane and 130 degrees vertically. The control process of Melissa can be decomposed to three basic steps. First, the video signal from the CCD camera attached to the gondola is transmitted to the host computer via a wireless video link. Second, the images are then digitized on the host computer, which also performs the image processing in order to determine the target motor command. And third, the motor command is sent to the gondola also via radio transmission. The frame rate of the visual processing is set to a constant speed of 10.0 fps. The robot uses 180 (horizontal) x 60 (vertical) pixels (90 x 30 EMDs), which covers 360 degrees along horizontal plane and 120 degrees along vertical plane in the panoramic image homogeneously, i.e. angular distances between photoreceptors of the EMDs, the sampling bases, are 1.0 degree.

3.3 Course Stabilization and Visual Odometer

3.3.1 Model

On the basis of the biological studies, this section explains models of course stabilization and visual odometer for the flying robot we have developed. These two models will be used for the experiments of goal-directed navigation in the later section.



Figure 3-2: Top: The autonomous flying robot, Melissa and its gondola, on the bottom of which a miniature panoramic camera is attached. Bottom: An image obtained by the panoramic vision system (left) and its log-polar transformed image (right), which is used in the experiments.

3.3.2 Course Stabilization Model

Inspired by the flying insects' optomotor response, here we describe a course stabilization model for our flying robot. For the optical flow measurement, we employ a biologically plausible model of motion detection, the so-called Elementary Motion Detector (EMD) or the Reichardt detector, shown in Figure 3-1 (for review [9]). Two adjacent photoreceptors send their outputs to temporal high-pass filters that remove constant illumination containing no motion information. These signals are then “delayed” by exploiting the phase lag inherent in a first order temporal low-pass filter. Delayed channels are then correlated with adjacent, non-delayed channels by means of a multiplication operation. Finally the outputs of two opponent EMDs are subtracted to yield a direction-sensitive response. Although the nature of the neural mechanisms and the location in the visual pathway remains to be elucidated, some behaviors of the motion sensitive neurons in insects can be well characterized by this motion detector model [110]. The salient properties of the movement-sensitive mechanism underlying these responses are that it is directional, and that it does not encode the pure speed of the moving image, rather it is sensitive to the temporal frequency of intensity fluctuations generated by the moving image, and therefore confounds the speed of the image with its spatial structure.

Figure 3-1 illustrates the control procedure: At first, image from the panoramic vision system (see next section for the details) is log-polar transformed (the gray rectangle in Figure 3-1), the intensity information of which is given to four 2-dimensional EMD arrays, i.e. Horizontal Left (HL), Horizontal Right (HR), Vertical Left (VL), and

Vertical Right (*VR*). These arrays extract horizontal motion and vertical motion from the left and the right lateral images. The outputs of each EMD array are then integrated in order to simulate the wide field motion sensitive interneurons H1 as follows.

$$H1_HL(t) = \sum_i \sum_j EMD_HL_{ij}(t) \quad (3.1)$$

$$H1_HR(t) = \sum_i \sum_j EMD_HR_{ij}(t) \quad (3.2)$$

To estimate the rotational ego-motion of the robot, the right and left horizontal motions are compared by a simple subtraction.

$$S_{rot}(t) = H1_HL(t) - H1_HR(t) \quad (3.3)$$

The vertical motion, i.e. changes in height, is also estimated in a similar manner. The vertically arranged EMDs in the 2-dimensional EMD arrays give the estimate of vertical motion. The outputs of these EMDs are integrated as S_{alt} :

$$\begin{aligned} S_{alt}(t) = & \sum_i \sum_j EMD_VL_{ij}(t) \\ & + \sum_i \sum_j EMD_VR_{ij}(t) \end{aligned} \quad (3.4)$$

These rotation and height sensory information induced by ego-motion is then given to a motor controller module. The three parameters are required for the control of the flying robot (see the next section for the details), i.e. rotation, elevation and thrust motor outputs, M_R , M_E and M_T , respectively, which are determined by the following equation.

$$\begin{bmatrix} M_R \\ M_E \\ M_T \end{bmatrix} = \begin{bmatrix} W_{RS} & 0 & 0 \\ 0 & W_{ES} & 0 \\ 0 & 0 & W_{bias} \end{bmatrix} \cdot \begin{bmatrix} S_{rot} \\ S_{alt} \\ 1 \end{bmatrix} \quad (3.5)$$

In this motor controller, W_{RS} and W_{ES} are heuristically determined so that S_{rot} and S_{alt} should be minimized, and W_{bias} is set such that thrust motors are driven at constant speed.

3.3.3 Visual Odometer Model

The same horizontal EMD arrays that are used for course stabilization control are again used for the visual odometer (Figure 3-1). Since the EMD response provides an angular velocity signal, the distance traveled could be estimated by integrating the EMD outputs over time. The responses from both right and left horizontal EMD arrays are integrated every time step, which is given to the visual odometer module, then accumulated over time. Namely the visual odometer response, VO , is calculated

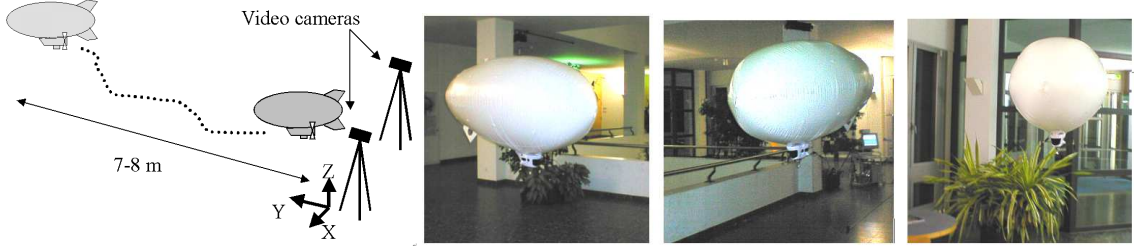


Figure 3-3: Left: Experimental setup for the navigation experiments. The experiments start with the same initial conditions, i.e. initial robot position and orientation. Two video cameras are installed to record the absolute trajectory of the robot for later analysis. Right: Pictures of three different uncontrolled environments, which are tested in the experiments. (EXP 0, 1, 2, from left to right)

by integrating the $H1_HL$, $H1_HR$ output over time:

$$VO = \sum_t (H1_HR(t) + H1_HL(t)) \quad (3.6)$$

3.3.4 Experiments

This section presents a series of navigation experiments by using an autonomous flying robot. The models explained in the previous section are implemented in the robot, and then tested in uncontrolled indoor environments.

3.3.5 Method

The W matrix of the equation (5) is heuristically determined before experiments, since it is strongly dependent on the hardware conditions (floating balance of the robot etc.) and environmental factors (air currents etc.). Three sets of experiments are conducted in three different uncontrolled indoor locations (EXP0, EXP1 and EXP2 shown in Figure 3-3), where we installed two video cameras to track and record the absolute trajectories of the robot for later analysis (Figure 3-3 Left). The experiments in each location consist of 10 flight trials: in one trial, the robot starts controlling at the same initial conditions, i.e. initial positions and initial orientations, and stops the operation after the same time duration. Due to the limitation of the experimental environments, the time duration is set to 25 seconds.

3.3.6 Results

In Figure 3-4, the plots show 3-D trajectories of the robot. From the stereo video camera images recorded externally, absolute positions of the robot are extracted by tracking a fixed point of the robot in one second step. In these graphs, each trial starts from left toward right. Most of the trajectories in these graphs show that the robot maintains straight routes by balancing the right and left lateral image speeds.

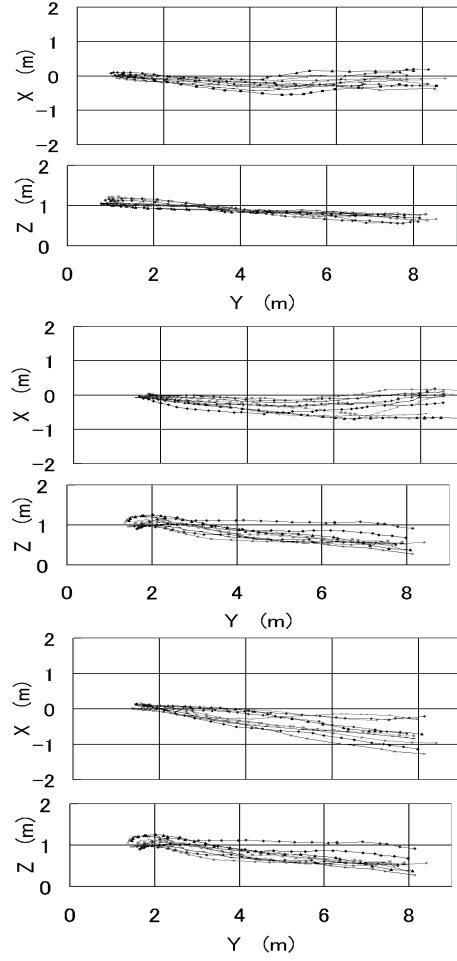


Figure 3-4: 3-D trajectories of the flying robot during the experiments. Each plot is extracted from the images recorded with the stereo video camera. The plots denotes the position of the robot at one second time-step, and each graph contains the trajectories of 10 trials. (EXP 0, 1, 2, from top to bottom)

However a small difference in the initial orientations of the robot results in a relatively large deviations at the goal position, as shown in the X-Y plane figure of EXP 2 in particular. For the height control, the robot tends to lose the height at the beginning of experiments, but eventually maintains the height in a certain range in all of the trials.

Figure 3-5 shows the visual odometer responses that the robot experienced during each trial. The proposed visual odometer model measures almost the same distances in each experimental setup, EXP 0, 1, and 2. Especially in EXP 0 and 1, the curve profiles of the visual odometer values over 10 trials show the similarity in their accumulation patterns, which indicates that the proposed visual odometer could potentially be capable of measuring the traveling distance. The relatively large deviations in EXP 2 could be due to the course deviation of the robot route trajectories as shown in Figure 3-4. Further issues will be discussed in the next section.

In addition, in Figure 3-5, the visual odometer responses are plotted against the cor-

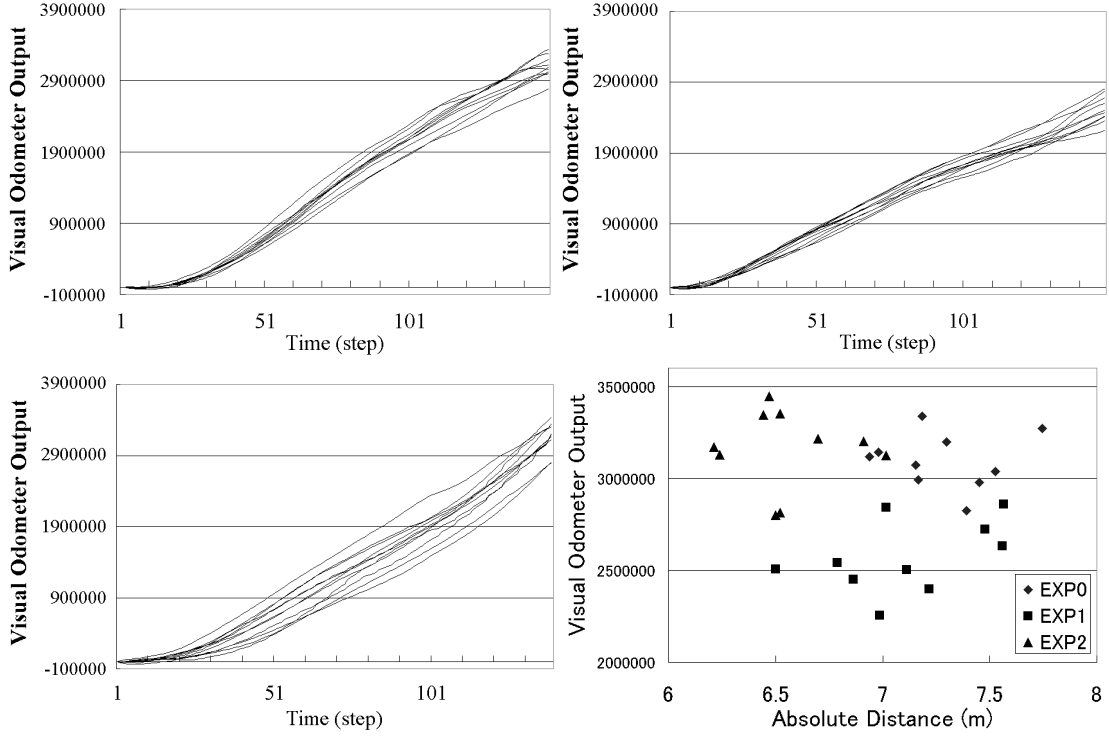


Figure 3-5: Top: Visual odometer responses of the 10 trials in the 3 experimental setups. The curve profiles show that the visual odometer accurately estimates the distances in the same experimental setup, particularly in EXP0 and 1. Bottom: Visual odometer measurement vs. actual distance. The actual distances that the robot traveled in each trial are extracted from Figure 3-4. The results show that the visual odometer depends on the locations, since the plots from the same EXP are distributed in similar areas of this graph.

responding actual distances the robot travels. The actual distances in this figure are estimated from the externally observed 3D trajectories shown in Figure 3-4. Despite the same flight duration of 25 sec, the variance of the visual odometer measurement is relatively large. However, the distributions from EXP 0 and 1 tend to monotonously increase as the actual distances increase. The result from EXP 2 seems to be, again, caused by the route deviation. From these experimental results, the proposed model is potentially capable of measuring the travelling distances visually, however the measurement prones to depend on the route the robot experiences.

Further analyses are conducted with respect to the effects of the number of EMDs. In these analyses, from the stored data of EMD outputs, we re-calculated the visual odometer outputs by using the different numbers of EMDs; 1, 10, 20, 30, and 45 EMDs are selected over each left and right laterally distributed EMDs; then integrated their outputs over time. These results are normalized by the corresponding actual distances, and their standard deviations (SDs) are calculated as percent of mean values (Figure 3-6). Therefore, when a SD results in a smaller value, it indicates that the visual odometer with the corresponding number of EMDs contains smaller error.

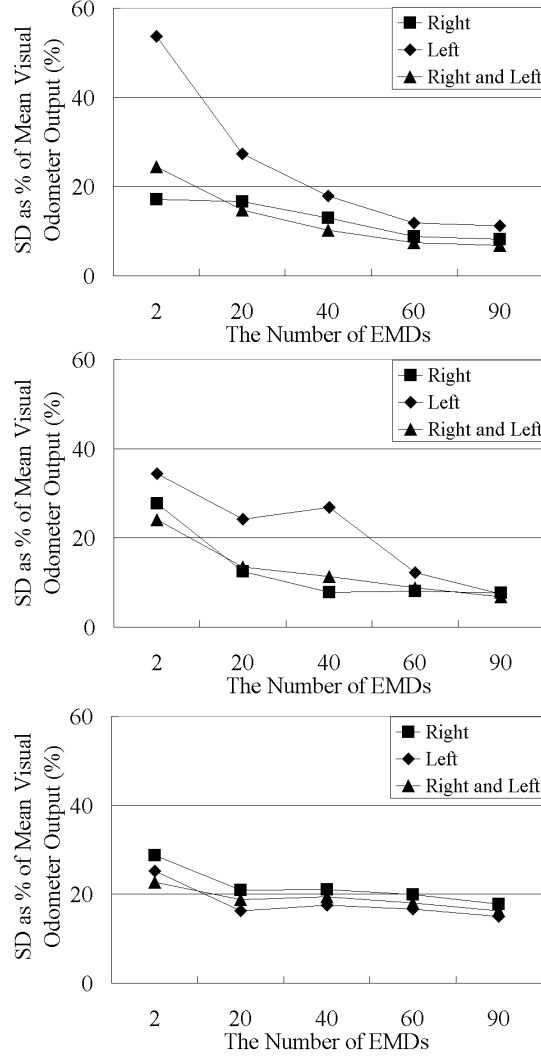


Figure 3-6: The effect of the number of EMDs by standard deviations (SDs) as percent of the mean values in visual odometer measurement. The graphs show that the number of EMDs changes the accuracy of visual odometer measurements.

There are two implications that should be mentioned from this analysis. Firstly, in principle, one EMD is essentially the minimum requirement of the proposed visual odometer model, although redundancy improves the measurement errors for all EXP 0, 1, and 2. Secondly, these results indicate that the performance of the proposed visual odometer could be improved by adaptively choosing a preferable visual field. For example, in EXP 0 and 1, the SDs of the left visual field are significantly larger than those of right, especially in the smaller numbers of EMDs. Therefore in order to improve the performance, the robot should use the left visual field for the odometer. More generally, if the robot would have a task in which it should visit the same goal location, the robot could adaptively choose/learn the appropriate number and positions of EMDs in order to improve the odometer performance.

Given the experimental results, in this section, we discuss further issues of the

proposed navigation model and possible solutions to improve the performance of the goal-directed navigation.

For flight stabilization using optical flow, the robot has to visually extract the translation and rotation motions of its own body and compensate for them. While a flat visual projection area with a narrow view angle, such as a standard camera view, has a great disadvantage for this problem, the panoramic vision system makes the problem easier as employed in our experiments, where we compared the mean motion direction at the contralateral part of the panoramic image for the yaw rotational control. Furthermore, if necessary, the same principle can be applicable for the roll and pitch controls in the case of flying insects or the other robotic platforms with an omni-directional vision. For the altitude controls, in this chapter, we employed the vertical EMDs to measure the vertical image movement. Most probably pure image speed detectors, rather than spatio-temporal filter such as EMDs which have non-linear responses with respect to image speed, would improve the performance of altitude control. Alternatively, measuring the apparent ground speed could be another solution to control altitude as demonstrated in [80]. The advantage of this solution is that the similar mechanism could be also used for safe landing [113].

Although the experimental results showed that the combination of course stabilization behavior and visual odometer could be used for goal-directed navigation, there are some potential solutions to improve the accuracy of the proposed visual odometer model. Since the performance of the visual odometer relies on the spatial structure experienced during the navigation as shown in Figure 3-5, minimizing route deviations could improve the accuracy. Sensory feedback from compass information, for instance, is desirable to maintain a straight route, considering that celestial cues play an important role as a global compass in natural systems. Landmark navigation could also be a biologically plausible alternative solution to enhance the performance of course stabilization. In another solution, as suggested in Figure 3-6, the EMD locations and the number of EMDs in the visual field need to be carefully considered for the better performance of the visual odometer, especially in unstructured environments. Considering that bees increase the accuracy of goal-directed navigation after learning phase, an adaptive learning mechanism in visual odometer model is expected. Alternatively, visual odometer could be based on a pure speed detector, rather than spatio-temporal filters. However, as long as the robot follows the same route repeatedly, a spatio-temporal filter can be also usable.

3.4 Discussion

Given the experimental results, in this section, we discuss further issues of the proposed navigation model and possible solutions to improve the performance of the goal-directed navigation.

For flight stabilization using optical flow, the robot has to visually extract the translation and rotation motions of its own body and compensate for them. While a flat visual projection area with a narrow view angle, such as a standard camera view, has a great disadvantage for this problem, the panoramic vision system makes the

problem easier as employed in our experiments, where we compared the mean motion direction at the contralateral part of the panoramic image for the yaw rotational control. Furthermore, if necessary, the same principle can be applicable for the roll and pitch controls in the case of flying insects or the other robotic platforms with an omni-directional vision. For the altitude controls, in this chapter, we employed the vertical EMDs to measure the vertical image movement. Most probably pure image speed detectors, rather than spatio-temporal filter such as EMDs which have non-linear responses with respect to image speed, would improve the performance of altitude control. Alternatively, measuring the apparent ground speed could be another solution to control altitude as demonstrated in [80]. The advantage of this solution is that the similar mechanism could be also used for safe landing [113].

Although the experimental results showed that the combination of course stabilization behavior and visual odometer could be used for goal-directed navigation, there are some potential solutions to improve the accuracy of the proposed visual odometer model. Since the performance of the visual odometer relies on the spatial structure experienced during the navigation as shown in Figure 3-5, minimizing route deviations could improve the accuracy. Sensory feedback from compass information, for instance, is desirable to maintain a straight route, considering that celestial cues play an important role as a global compass in natural systems. Landmark navigation could also be a biologically plausible alternative solution to enhance the performance of course stabilization. In another solution, as suggested in Figure 3-6, the EMD locations and the number of EMDs in the visual field need to be carefully considered for the better performance of the visual odometer, especially in unstructured environments. Considering that bees increase the accuracy of goal-directed navigation after learning phase, an adaptive learning mechanism in visual odometer model is expected. Alternatively, visual odometer could be based on a pure speed detector, rather than spatio-temporal filters. However, as long as the robot follows the same route repeatedly, a spatio-temporal filter can be also usable.

3.5 Summary

In this chapter, inspired by the navigation mechanisms of bees, we propose a method for goal-directed aerial navigation exclusively using a panoramic vision system. We performed experiments using a blimp-type robotic platform in unstructured indoor environments, and the combination of course stabilization and visual odometer models successfully demonstrates goal-directed navigation in the 3D indoor environments. In addition, the further analysis leads to potential solutions to enhance the navigation capability of the proposed models. Although the control of our blimp-type robotic platform is by far simpler than those of other platforms such as helicopters, it is expected to realize more sophisticated controls in more demanding situations with a vision-based architecture, as the natural evolution has found a solution for flying insects.

Chapter 4

Design and Control of a Pendulum Driven Hopping Robot

Abstract

In this chapter a new kind of hopping robot has been designed which uses inverse pendulum dynamics to induce bipedal hopping gaits. Its mechanical structure consists of a rigid inverted T-shape mounted on four compliant feet. An upright “T” structure is connected to this by a rotary joint. The horizontal beam of the upright “T” is connected to the vertical beam by a second rotary joint. Using this two degree of freedom mechanical structure, with simple reactive control, the robot is able to perform hopping, walking and running gaits. During walking, it is experimentally shown that the robot can move in a straight line, reverse direction and control its turning radius. The results show that such a simple but versatile robot displays stable locomotion and can be viable for practical applications on uneven terrain.

4.1 Introduction

The design and implementation of the Stumpy II¹ hopping robot is an exploration of a novel morphology for locomotion, with an inverted pendulum inducing rhythmic hopping and a transverse rotational degree of freedom for direction control. Its unique structure and dynamics are capable of producing both biped-like and quadruped-like gaits. In addition it can also display some effective non-biomimetic gaits.

Such use of pendulum dynamics in movement has been only partially explored. Hayashi *et al* [39] have designed a pendulum-type jumping machine which uses inverted pendulums as swinging arms to propel the robot to jump. This machine was capable of jumping up stairs, but not of regulating its movement direction or velocity. In another interesting example, Ioi *et al* [60] applied pendulum dynamics to the problem of wheeled locomotion and designed a robot comprised of two big parallel

⁰This chapter is based on the reviewed publication [48].

¹Videos available at <http://www.ifl.unizh.ch/ailab/people/iida/stumpy/>

wheels, with a pendulum hanging between them. This robot was able to roll up slopes and control forward velocity and turning. However, the use of pendulum dynamics to drive legged locomotion has not been previously considered².

The control of gait and balance in hopping robots has been widely studied by Raibert and his colleagues, for one-legged, two-legged and four-legged hopping robots, in two and three dimensions [93, 94, 96, 95]. Such robots have been shown to successfully produce bounding gaits, through control of hopping height and forward velocity. They have also been able to perform somersaults [90]. These robots have long narrow legs each with a single spring-loaded prismatic joint. The legs are attached to the body mass, by a roll and (for 3D motion) a pitch degree of freedom, by which they can influence foot placement. Due to this mechanical structure, these robots are statically unstable, and therefore must continue to hop in order to stabilize their body. For practical applications this presents a considerable limitation. In the Stumpy robot, the four legs also consist of a spring loaded prismatic joints, but are much shorter. Also, they do not have any other degrees of freedom with respect to the robot’s upper body, and control of foot placement is accomplished by the upper body. This has the advantage that the structure is statically stable, while allowing for dynamically stable locomotion. This enables the robot to smoothly transition between standing still, walking, running, and coming to a stop again, which is more practical for real world applications.

The dynamic stability of the Stumpy robot is comparable to that of the monopod hopping robot developed by Ringrose [98]. The monopod was able to achieve self-stabilizing running, without any sensors or active control, by simply moving the single actuator of the robot, through a fixed repetitive cycle. Due to the interaction of this simple control with a carefully designed self-stabilizing mechanical structure, the robot was able to correct its posture despite the effects of destabilizing forces. According to Murphy [78], self-stabilizing posture of the body can be achieved in a two legged robot during bounding gait, if the normalized moment of inertia of the mechanical structure is less than 1. Since the interaction between controller and the mechanical structure of the Stumpy robot fulfills this condition, it displays a similar self-stabilizing property. Thus, it is able to perform locomotion with high tolerance to environmental disturbances.

The mechanical structure of the robot has been designed according to the principles of *cheap design* and *ecological balance* described by Pfeifer *et al* [89]. Thus, only the minimum number of sensor and actuators that are necessary to perform the task have been used. This is similar to the design of the Scout robot, built by Buehler *et al* [14], which uses a small number of actuators for quadruped locomotion. The design of Stumpy has also incorporated the use of mass distribution in control, an optimization method described by Paul *et al* [84]. The controller for the robot is designed according to the principles of behavior based control [13].

The following section, Section 2, describes the design of the Stumpy robot. The behavior of the robot is then mathematically modeled in Section 3. Then the control

²This is conceptually different from using inverse pendulum dynamics in ZMP-based balance control, which is common in legged robots

Table 4.1: Mass and length parameters of the robot mechanical structure

Parameter	Description	Value
r_1	rest length of feet	10 cm
l_b	length of base	15 cm
l_1	length of lower vertical beam	21 cm
l_2	length of the upper vertical beam	26 cm
l_3	length of shoulder horizontal beam	41.5 cm
m_1	mass of lower body	1.2 kg
m_2	mass of upper body	0.43 kg
m_3	mass on shoulder	0.12 kg

of straight line movement, direction, and turning radius are developed in Section 4. These controllers are tested on the robot, and data is presented from real world experiments. In Section 5, a short discussion of the robots performance on these tasks follows, with implications for future work. Section 6 ends with conclusions.

4.2 Robot Mechanical Structure

The robot (Fig. 5-3) was designed through the development of three prototypes. The Stumpy II robot's lower body is made of an inverted "T" mounted on wide springy feet. The upper body is an upright "T" connected to the lower body by a rotary joint providing one degree of freedom in the frontal plane (see Figure 1). This enables the upper body to act as an inverted pendulum. For simplicity in nomenclature, we call this the "waist" joint. The horizontal beam of the upright "T", is weighted on the ends to increase its moment of inertia. It is connected to the vertical beam by a second rotary joint, providing one rotational degree of freedom, in the plane normal to the vertical beam of the upper "T". This joint is labeled the "shoulder" joint. Stumpy's vertical axis is made of aluminum, while both its horizontal axes and feet are made of oak wood.

The total mass of the robot is approximately 1.9 kg. The mass and length parameters of the robot are detailed in the Table 7.1.

The joints are actuated using Minimotor DC-Micromotors. The waist motor is a 3042 012C with a 43:1 gear reduction, and shoulder motor is a 2342 012C, also with 43:1 gear reduction. The joint angles are measured using rotary potentiometers. The control is performed via off-board motor control boards with a PIC16F877 microcontroller and a standard motor driver with PWM output.

4.3 Modelling and Analysis

The following variables are used in the analysis of the robot:

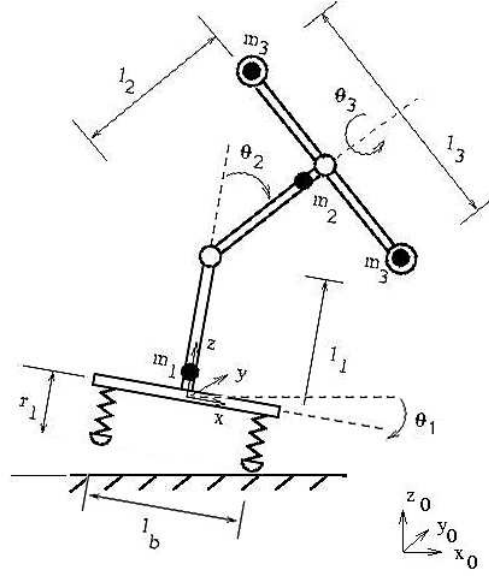
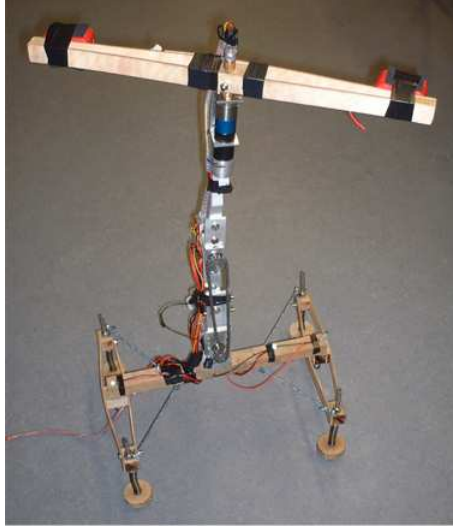


Figure 4-1: Stumpy II Robot (Left) and Schematic diagram (Right) of the Stumpy Robot, with variables which are used in modelling and analysis.

x_0, y_0, z_0 : origin of the world coordinate system

$[x, y, z], \theta_1$: origin of the robot, inclination in frontal plane

τ_1, τ_2 : waist motor torque, shoulder motor torque

θ_2, θ_3 : joint angles of the robot

J_l : moment of inertia of the lower body

To analyze the behavior of the robot, the model is orthogonalized into models for the frontal and sagittal planes. In the frontal plane, the waist motor serves to accelerate the waist joint and induce hopping motion.

$$\tau_1 = m_2 l_2 \ddot{\theta}_2 - m_2 g l \sin(\theta_1 + \theta_2) \quad (4.1)$$

We assume that in this motion, the effects of external forces are negligible, and that conservation of angular momentum holds. According to this the following relation can be stated:

$$J_l \dot{\theta}_1 = m_2 l_2 \dot{\theta}_2 \quad (4.2)$$

where J_l is the moment of inertia of the lower body.

During walking, where at least one foot is always on the ground, the following relations arise:

$$x = l_b \cos \theta_1, z = l_b \sin \theta_1 \quad (4.3)$$

By substitution of Equation 4.3 into Equations 1 and 2, the following relations result:

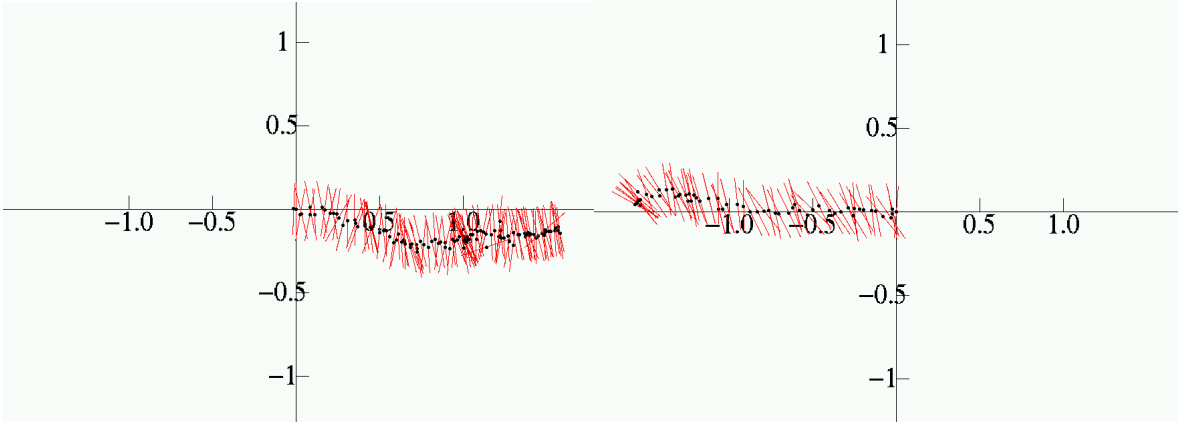


Figure 4-2: Forward walking, produced when $\nu_s^+ = \nu_s^-, \phi = 0^\circ$

Figure 4-3: Backward walking, produced when $\nu_s^+ = \nu_s^-, \phi = 180^\circ$

$$J_l \dot{x} = (\tau_1 + m_2 g l \sin \theta_2)(-r \sin \theta_1) \quad (4.4)$$

$$J_l \dot{z} = (\tau_1 + m_2 g l \sin \theta_2)(-r \cos \theta_1) \quad (4.5)$$

In the sagittal plane, motion is induced by application of torque at the shoulder joint. The shoulder torque first accelerates the shoulder beam.

$$\tau_2 = m_3 l_3 \ddot{\theta}_3 \quad (4.6)$$

This motion causes two effects. One is a reaction torque, $\tau_r = -\tau_2$, which must be produced to conserve the angular momentum due to the rotation of the shoulder beam. The second is an impulse torque produced due to the collision of the shoulder beam with the joint stop τ_c . At any given angular velocity of the shoulder joint $\dot{\theta}_3$, the reaction torque τ_r will have the opposite sign as $\dot{\theta}_3$, and τ_c will have the same sign.

The rotation of the lower body in the plane normal to the reaction torque, θ_{τ_r} , caused by shoulder motion, is thus given as follows:

$$\tau_r + \tau_c = J_l \ddot{\theta}_{\tau_r} - \tau_f \quad (4.7)$$

where τ_f is the friction torque produced by the coefficient of static friction between the ground and the feet.

In this locomotion model, the elastic linear passive joints in the feet are neglected for the sake of simplicity. Although it provides a significant influence to the stability of locomotion behavior and the intrinsic body dynamics for hopping behavior, the overall walking behavior of this robot can be well characterized by this model. The hopping dynamics exploiting the elasticity will be investigated further in the next chapter.

4.4 Control

Stumpy is controlled to move in a unique way by actuating its waist joint, with a back and forth swinging motion. This motion of the upper body imparts angular momentum to the base which creates a rhythmic hopping motion.

During hopping, each lateral pair of foot contacts which can be considered together as a “foot”, experiences two phases: stance phase, in which the foot is on the ground and flight phase, during which the foot is airborne. At low frequencies of the upper pendulum, one foot completes its flight phase and returns to stance phase, before the second foot initiates flight phase. As a result, there are two phases in the gait cycle: single support and double support. Therefore, we term this gait “walking”. At higher frequencies, one foot is still in flight phase when the next foot enters flight phase, so the two phases in the gait cycle are single support, and airborne. Therefore we term this gait “running”. At the transition frequency, there is only one phase: single support.

If the “shoulder” joint is unused, the robot will hop in place. The shoulder joint can be used to control movement in the sagittal plane. When a lateral forward rotation of the shoulder joint occurs, the foot will acquire a slight angular momentum during flight phase, which serves to project the foot forward. Thus the shoulder joint can be used to control movement direction, forward velocity and turning rate.

The control parameters are the frequency ω_1 , amplitude α_1 and setpoint θ_1^* of the waist joint oscillation, the frequency ω_2 , amplitude α_2 and setpoint θ_2^* of the shoulder joint oscillation, and the phase difference, ϕ , between ω_1 and ω_2 , when they are oscillating at the same frequency.

The basic control for the waist motor is a simple reactive algorithm, which outputs a constant motor voltage until the joint angle sensor detects the maximum amplitude α_1 , and then reverses the direction. Thus, the waist motor oscillates approximately between α_1 and $-\alpha_1$. The control of the shoulder joint is reactively coupled to the waist and functions in a similar way. The shoulder motor voltage remains constant, until the waist joint angle sensor detects that it has crossed the maximum amplitude α_1 . At this instant, the shoulder joint instantaneously reverses the motor torque. Due to this coupling, the waist and the shoulder joints are phase locked, such that the phase relationship ϕ between the waist and the shoulder joint is constrained to be either 0° or 180° .

The hopping height of the robot mainly depends on the angular acceleration of the waist joint periodic motion. The maximum amplitude of the swing determines the region of stability of the structure during hopping. As in Raibert’s hopping robots, it has been experimentally found that the control of hopping height in this robot can be separated from the control problems of forward velocity, gait direction, and the radius of curvature of the robots turning trajectory. As the main focus was the control of movement direction, the hopping was tuned to a constant frequency, which produced a suitable hopping height and allowed for a wide range of motions. Controllers were then developed for straight walking, reversing direction and turning.

These controllers were implemented and tested on the robot. Data on position and velocity of the robot during locomotion was collected using a CCD camera suspended

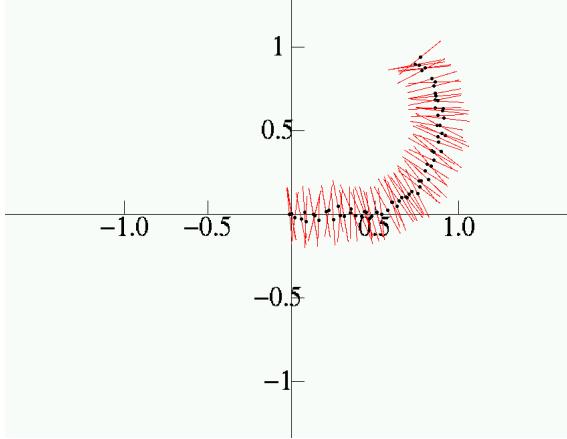


Figure 4-4: Turning left, with a small turning rate, produced when $\nu_s^+ < \nu_s^-$.

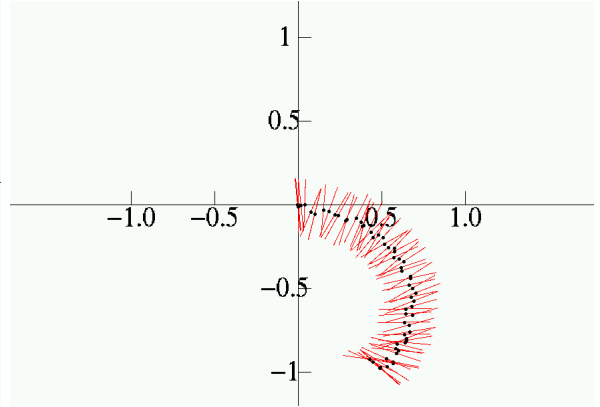


Figure 4-5: Turning right, with a small turning rate, produced when $\nu_s^+ > \nu_s^-$.

from the ceiling above a 3.0 m x 2.0 m experimental arena, and a framegrabber which recorded the movement of the robot at 25 frames/sec. For each experiment, the robot was initially positioned at the center of the image. It was equipped with four high-intensity LEDs, two on each side of the base and recorded in a darkened room. The camera image was then processed to identify the locations of the LEDs, from which the robots position and orientation was extracted and plotted once every second. The following sections describe the design and implementation of the controllers and present experimental data collected using this setup.

4.4.1 Tuning the Hopping Height

The hopping height and frequency were experimentally tuned by adjusting the motor voltage of the waist motor. It was found that if the motor voltage is too low, the angular acceleration is not fast enough to lift the feet off the ground for a significant amount of time. As, the motor voltage gets higher a stepping motion is induced but the frequency is not in tune with that of the mechanical structure. Within a small range of motor voltages, resonance with the mechanical structure produces a stable hopping pattern is produced with high dynamic stability. Informal tests show that even large disturbances caused by accidental human intervention, such as “stepping on the robot’s foot”, are corrected by its self-stabilizing nature. In this range, the robot produces a “walking” gait, where one foot is always on the ground, and therefore lends itself to good direction control.

4.4.2 Straight Walking

As described above, the shoulder joint is coupled to the waist joint angle, and reverses the motor voltage at the maximum amplitude values. Thus, the basic control is such that ν_s^+ , the motor voltage applied to the shoulder during clockwise rotation, and ν_s^- which is the motor voltage applied to the shoulder during counter-clockwise rotation

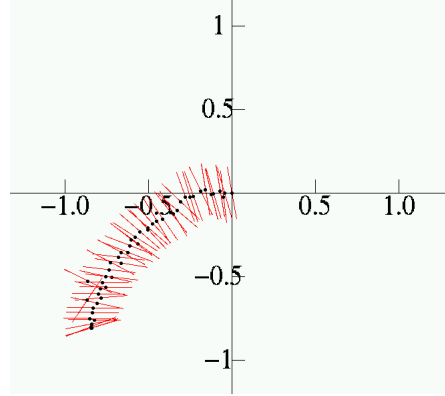
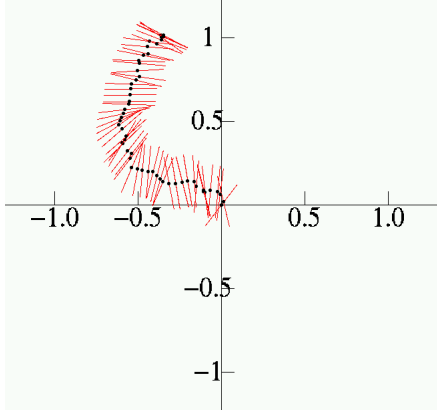


Figure 4-6: Going backwards and turning right, with a small turning rate, produced when $\nu_s^+ > \nu_s^-$. Simply by changing ϕ when $\nu_s^+ < \nu_s^-$ to 180° , the robot walks backward, as it slowly turns right.

are related by relationship, $\nu_s^+ = -\nu_s^-$.

In this situation, the forward momentum acquired by the left foot during flight phase, is equal to the forward momentum acquired by the right foot and, therefore, the alternating step sizes of the left and right foot are equal and the robot walks in a straight line. Results of the robot performing this behavior are shown in Figure 4-2. (The axes in this figure, and all other performance graphs are in metres).

It was found that the direction of the robot, that is whether it would move in the forwards or backwards direction, was only dependent on the phase parameter ϕ . The following graph in Figure 4-3 shows how changing the phase from 0° to 180° , makes the robot move in the opposite direction from that in Figure 4-2.

4.4.3 Control of Turning Rate

The control of turning rate is achieved using an enhanced forward walking controller. In forward walking, the step lengths on the left and right sides are approximately equal. Using a similar controller, but by increasing the step length of one foot and shortening the other, the robot can achieve turning. Thus, we focus on the turning rate induced by the difference between the clockwise and counter-clockwise voltages applied to the shoulder motor. The turning rate, R , can be approximately given as $\dot{R} = K(\nu_s^+ - \nu_s^-)$. Thus, for example, in the case of $\nu_s^+ > \nu_s^-$, while the motor rotates clockwise, the foot in flight phase takes a large step, but while the motor rotates counter-clockwise, the other foot takes a smaller step, causing the robot to turn at a constant rate. The control of movement in the forward or backward direction, discussed in the previous subsection, is also independent of turning rate. Various combinations of ν_s^+ and ν_s^- have been tested, to exhibit different turning rates in both forward and backward walking. Figure 4-4 shows a small turning rate produced by the motor control of $\nu_s^+ < \nu_s^-$. Figure 4-5 also shows the performance with the

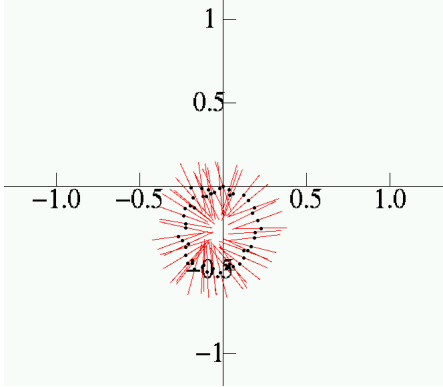


Figure 4-8: Turning right, with a large turning rate, produced when $\nu_s^+ \gg \nu_s^-$. With this controller the robot can effectively turn in place.

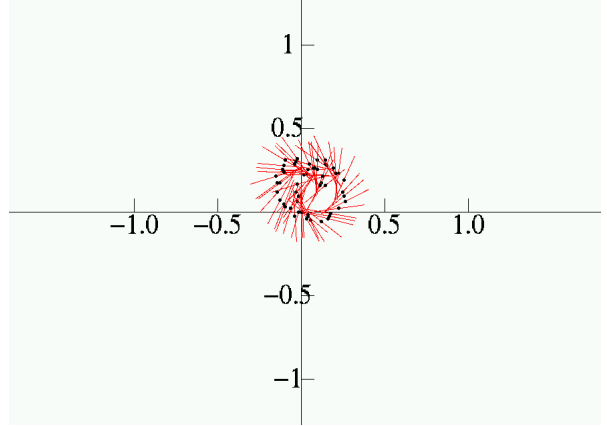


Figure 4-9: Turning left, with a large turning rate, produced when $\nu_s^+ \ll \nu_s^-$. Again the robot can effectively turn in place

same turning rate, but in the other direction, that is where $\nu_s^+ > \nu_s^-$. Figures 4-6 and 4-7 show the same behaviors but in the reverse direction. Then, larger turning rates are produced, when the difference between ν_s^+ and ν_s^- is greatly increased, which effectively produces turning in place, as shown in Figure 4-8 and 4-9.

4.5 Discussion

The controllers tested for control of forward motion, change of direction and turning rate, as described in the previous sections, achieved considerable success in displaying the desired behavior in real world experiments. The results showed that the preliminary controller concepts developed, were sufficient to fulfil the requirements of the tasks. However, the controllers were all open loop with respect to movement direction and velocity, and were thus sensitive to slight changes in mechanical biases in the robot, and environmental irregularities such as frictional differences on the ground and slight ups and downs of the terrain. To account for these uncertainties closed-loop control using sensor feedback must be added to these controllers. The selection of appropriate sensors and their use in a closed-loop control algorithm, are topics of further investigation. For example, if a sensory device is able to detect a fixed point (e.g. salient visual cues for landmarks of navigation) in the environment, angular deviation toward a target location can be adjusted by using the sensory-motor coordination exploiting the mechanism of turning behavior which was described in this chapter.

In addition, many other interesting issues with respect to the performance and control of this robot remain to be investigated. One of the topics includes the self-stabilizing property of the robot. In this chapter, this property was exploited to achieve high dynamic stability during locomotion. However, it would be interesting to focus on this aspect more closely, and explicitly analyze the domain of attrac-

tion and its relationship to mechanical and control parameters. (This issue will be discussed in the next chapter.) Another topic of potential interest would be the accurate control of forward velocity. Finally, it would also be interesting to investigate different gait patterns. The Stumpy mechanical structure is capable of moving in a variety of different ways, one of which (walking) has been investigated in this work. The exploration of some of the other dominant modes of locomotion such as running, quadruped-like lateral bounding, and “diagonal” gaits, will be exciting topics of further investigation, which will be explained in the next chapter.

4.6 Summary

In this chapter a new kind of hopping robot with two feet, and no legs, has been presented. It consists of an inverted T-shaped base, connected to a T-shaped pendulum by a rotary joint. The hopping of the feet is induced indirectly by the motions of the upper body. Control of this novel mechanical structure has been investigated for walking, changing direction and control of turning radius. Experimental evidence shows that although it lacks legs, surprisingly, such a robot is capable of efficiently producing numerous modes of locomotion, while maintaining dynamical stability. Future work will consider the use of more sensors for achieving further precision in control and dealing with increased uncertainty in real world applications.

Chapter 5

Exploiting Friction for the Locomotion of a Hopping Robot

Abstract

For the locomotion of animals and machines, the friction between the body and the ground is one of the most crucial factors for stability and mobility. In this chapter, we investigate how the friction could be exploited for the purpose of adaptive locomotion. At first, we propose two conceptual working hypotheses, especially focusing on two important issues, (1) how to control the friction to increase the stability of a locomotive system, and (2) how the friction could mobilize a system for a form of adaptive locomotion. Secondly, by using a hopping robotic platform we have developed, we evaluate the proposed ideas with three experimental case studies. The experimental results show the statistical plausibility of the proposed idea of increasing the stability of locomotion. Furthermore, it is shown that, by properly taking advantage of the friction, the robot could enlarge the repertoire of locomotion behaviors, which could presumably enhance the adaptability of robot locomotion.

5.1 Introduction

Compared to artificial locomotive systems, animals are capable of remarkable adaptive locomotion in an unpredictable environment. One interesting phenomenon is that, for locomotion purposes, biological systems adaptively take advantage of the friction between the ground and the contact points of their body. Moreover, the use of such a mechanism of locomotion covers a wide variety of species in nature, from worm/snake style locomotion to shuffling locomotion of legged-animals. In this chapter, by using synthetic methodology, we investigate how the friction between a system and the ground could be exploited for the purpose of locomotion.

A number of the snake-like robots developed by Hirose and his colleagues is one of the pioneering studies in which artificial robotic systems actively exploit the friction

⁰This chapter is based on the reviewed publications [51, 53].

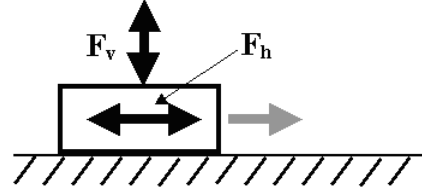
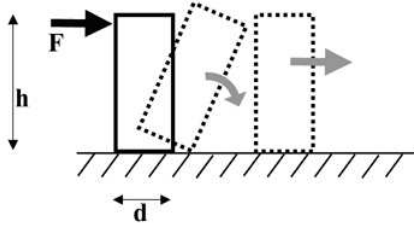


Figure 5-1: Concept of increasing stability Figure 5-2: Concept of the locomotion by exploiting friction

for a form of adaptive locomotion [41]. In these studies, inspired by biological studies of snakes, they have successfully demonstrated snake-like locomotion. For legged-locomotion, although the designs of robotic morphology and controllers largely take account of the friction force, the friction is only partially exploited, i.e. in a hold-or-release fashion. For example, the ZMP-based control generally assumes that the friction force should be sufficient to prevent sliding of the legs [121]. One of the disadvantages of such a design strategy is that the ecological niche of a robot is quite often very limited, and that it results in a restricted locomotion capability.

To complement these points, in this chapter we propose two working hypotheses with which artificial systems could actively exploit the friction for locomotion in the real world. The first hypothesis concerns the stability of the robot locomotion process. And, for the second hypothesis, we propose a conceptual design principle with which a legged-robot could actively take advantage of ground friction to mobilize itself. These hypotheses are then tested by using a hopping robotic platform we have developed.

The structure of this chapter is as follows. We first propose two conceptual design principles of such a form of locomotion based on simple physics. By using a hopping robot described in section 3, these design principles are then tested with 3 case studies explained in sections 4, 5 and 6. We will discuss further issues in section 7.

5.2 Design Principle to Exploit Friction for the Locomotion

In this chapter, we consider how friction could be exploited for a form of locomotion. We propose two working hypotheses; (1)friction could contribute to increase the stability of locomotion processes and (2)it could be possible to mobilize a system for a form of adaptive locomotion by properly exploiting the friction. In this section, we consider simple physics as a basis of argument. Since the physics of friction is highly complicated and depends on many parameters, the purpose of the following consideration is not to prove the hypotheses, rather we attempt to characterize the concepts above.

5.2.1 Increasing the Stability of Locomotion

Figure 5-1 shows a schematic to consider locomotion stability of a robot. When an external force F is exerted to an end of the rectangular object on the ground, the movement of the object could be either translational or rotational with respect to the ground. In other words, it would slip or fall down. The parameters which determine the movement are, at least, the friction (coefficient of the friction and mass of the object), the external force F , and the shape of the object (h and d in Figure 5-1).

Although it is difficult to derive the necessary conditions from this static analysis, a design principle of a stable system could be shape and mass of the object and coefficient of the friction. We will discuss further issues of this working hypothesis in the following sections.

5.2.2 Locomotion by Controlling the Friction

In this subsection, we propose the second hypothesis in which we consider how the friction could be actively exploited for locomotion. The conceptual idea is illustrated in Figure 5-2. In this figure, there are two oscillatory forces generated (for instance, by motors) in an object, F_h and F_v , that are represented as follows.

$$F_h = A_0 \sin(\omega_0 t) \quad (5.1)$$

$$F_v = A_1 \sin(\omega_1 t + \phi) + B_1 \quad (5.2)$$

where A_0 and A_1 are amplitude, ω_0 and ω_1 are frequency, ϕ is a phase between two oscillations, and B_1 is a set point. Here, we assume that the friction F_r between the object and the ground can be approximated by the following equation.

$$F_r = \begin{cases} \mu \cdot F_v & : F_v > 0, F_h > 0 \\ -\mu \cdot F_v & : F_v > 0, F_h < 0 \\ 0 & : F_v < 0 \end{cases} \quad (5.3)$$

where μ is a nominal coefficient of friction. Friction force can be generated only when there is vertical force (i.e. $F_v > 0$). The equation of the object movement, therefore, can be represented as follows.

$$\begin{aligned} \frac{d(mv)}{dt} &= F_h - F_r \\ &= \begin{cases} A_0 \sin(\omega_0 t) - \mu(A_1 \sin(\omega_1 t + \phi) + B_1) & : F_v > 0, F_h > 0 \\ A_0 \sin(\omega_0 t) + \mu(A_1 \sin(\omega_1 t + \phi) + B_1) & : F_v > 0, F_h < 0 \\ A_0 \sin(\omega_0 t) & : F_v < 0 \end{cases} \end{aligned} \quad (5.4)$$

This equation shows the relation between the control parameters and resultant behaviors. In the case of locomotion, B_1 can be regarded as a gravitational force induced by the mass of the object itself, therefore it can be assumed as a constant. From this equation, there are many different forms of locomotion behavior. For example, under the constraints of $\omega_0 = \omega_1$ and $\phi = 0$, forward locomotion is always

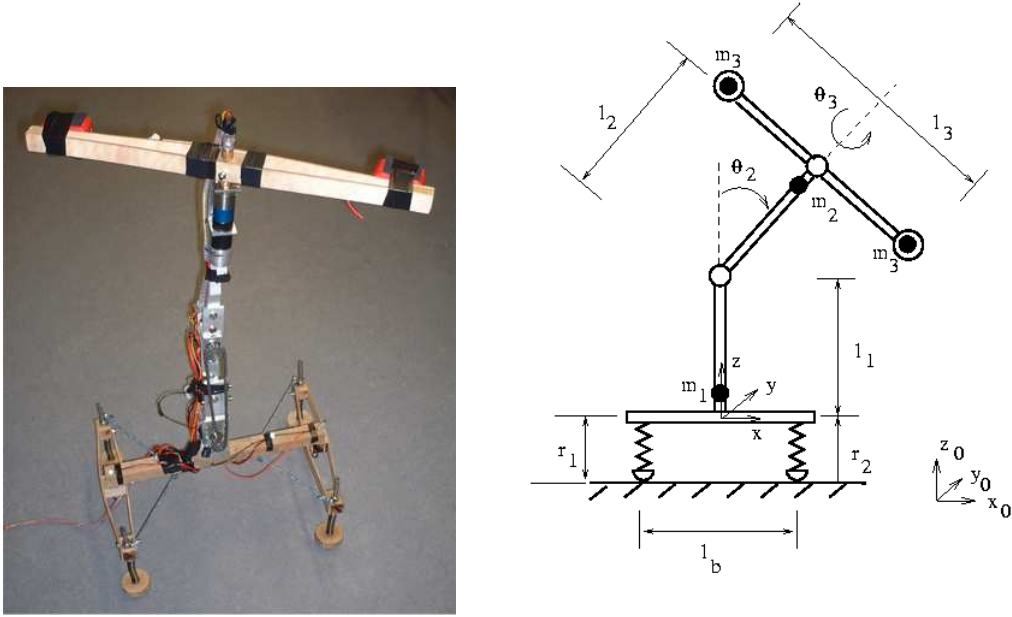


Figure 5-3: Photograph of the Stumpy robot (Left) and schematic illustration of the Stumpy robot (Right), with variables which are used in modelling and analysis.

possible when $A_0 > -\mu \cdot (A_1 + B_1)$ and $A_1 > B_1$.

The intention of introducing this equation is to characterize a conceptual form of locomotion. Therefore, one of the purposes of this chapter is to elucidate to what extent this conceptual form of locomotion can be applicable. In the following sections, we investigate this concept by using a robotic platform we developed.

5.3 Robotic Platform

In this section, we describe the design and control of the Stumpy robot [48, 85, 51] we have developed as an experimental platform. In the later sections, the behaviors of this robot will be analyzed to examine the hypotheses explained in the previous section.

5.3.1 Mechanical Design of the Stumpy Robot

The morphology of the Stumpy robot consists of two “T” shape components, called “upper body” and “lower body” (Figure ??). The Stumpy robot’s lower body is made of an inverted “T” mounted on wide springy feet. The upper body is an upright “T” connected to the lower body by a rotary joint providing one degree of freedom in the frontal plane. This enables the upper body to act as an inverted pendulum. For simplicity in nomenclature, we call this the “waist” joint. The horizontal beam of the upright “T”, is weighted on the ends to increase its moment of inertia. It is connected to the vertical beam by a second rotary joint, providing one rotational

Table 5.1: Mass and length parameters of the robot mechanical structure

Param.	Description	Value
r_1, r_2	rest length of feet	10 cm
l_b	length of base	15 cm
l_1	length of lower vertical beam	21 cm
l_2	length of the upper vertical beam	26 cm
l_3	length of shoulder horizontal beam	41.5 cm
m_1	mass of lower body	1.2 kg
m_2	mass of upper body	0.43 kg
m_3	mass on shoulder	0.12 kg
s	spring constant of feet	1.11 kg/cm

degree of freedom, in the plane normal to the vertical beam of the upper “T”. This joint is labeled the “shoulder” joint. Stumpy’s vertical axis is made of aluminum, while both its horizontal axes and feet are made of oak wood. Table 1 shows more detailed specifications.

5.3.2 Control of the Robot

Stumpy is controlled to move in a unique way by actuating its waist joint, with a right and left swinging motion. This motion of the upper body imparts angular momentum to the base which creates a rhythmic hopping motion. In this study, we employ a proportional control to track simple sinusoidal target trajectories for this upper body oscillation. For the sensory feedback, the angular position of the upper body with respect to the base is acquired by a potentiometer incorporated in the waist joint. The parameters we tested in the following experiments are, therefore, set point, amplitude, and frequency of the sinusoidal oscillation. The second motor which is equipped in the shoulder joint is also controlled in a oscillatory manner, although we did not use the potentiometer feedback, but it is simply synchronized to the control of waist motor.

5.3.3 Friction

The friction during the operation of Stumpy is very difficult to measure, but a good estimate to represent the friction between the robot and the floor would be a nominal coefficient of friction. In the following sections of this chapter, we will conduct comparative studies of robot’s behaviors in two different flat terrains in order to compare the effect of different friction force to the behaviors of robot, which we call “Terrain 0” and “Terrain 1” for the sake of convenience. The nominal friction coefficients are approximately, 0.29 in Terrain 0, and 0.46 in Terrain 1. This data provide us a good approximation of the slipperiness of these two environments, i.e. Terrain 0 is more slippery than Terrain 1 for the robot.

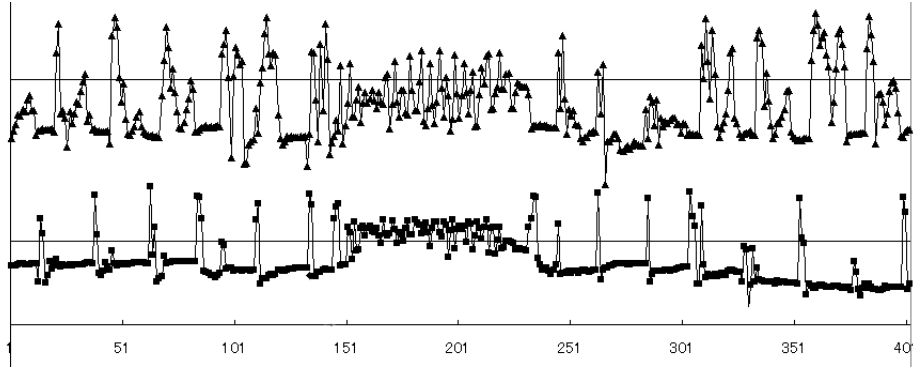


Figure 5-4: Intrinsic stability of Stumpy. This graph shows the time series pressure data installed on the right and left feet (top and bottom graphs, respectively). The gait is disturbed by an external force around time step 150. A time step corresponds roughly to 1/20 seconds.

5.4 Stability and Gait Analysis

In addition to the static stability which is achieved by a wide base and four feet, the dynamical stability is one of the major features in the behavior of Stumpy. Figure 5-4 shows the time-series pressure data measured at the feet of Stumpy. At around time step 150 an external force disturbance is exerted. The rhythmic pattern of the ground contact is generally retrieved after a certain period of chaotic behavior, in the figure after roughly 100 time steps. In this section, we explain the first set of experiments, in which we analyze Stumpy’s typical gaits and its stability by using only the waist motor (Figure 5-10). Note that, in this chapter, we use the term “gait” in a broad sense. Generally a gait represents a spatiotemporal pattern of ground contacts of an interested subject, however, in this chapter, we call the spatiotemporal “pressure” patterns at the ground contacts instead. Namely, we call two different pressure patterns two different gaits, even if all of the feet are on the ground and stay at the same positions.

For the purpose of measuring such pressures at the ground contacts, we installed pressure sensors on the right and left soles of the robot. These sensors output analog signals which are digitized with 10-bit resolution and stored in a host computer.

5.4.1 Method of the Experiment and Observed Gaits

In the first set of experiments, we use only the waist motor and a potentiometer. The target trajectory is a sinusoidal oscillation of the upper body with a fixed set point at the middle, i.e. the center of oscillation is upright with respect to the lower body. Under this condition, we analyzed the relation between the gait of the robot and the target oscillation trajectories, i.e. the amplitude and the frequency parameters. We conducted 100 experiments each in Terrain 0 and 1. In each experiment, we set different parameters of amplitude and frequency in which the amplitude ranges from 2.5 to 25 degrees in steps of 2.5 degrees, and the frequency from 0.3 to 2.3 Hz at

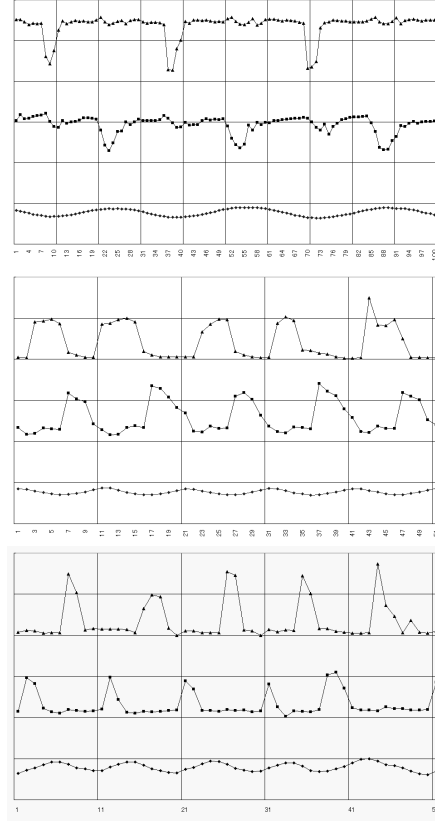


Figure 5-5: Three typical gaits, Shuffling (Top), Walking (Middle), and Hopping (Bottom). Each diagram includes time series values of pressure sensors on the right foot(Top), the left foot(Middle) and the angle between the upper and lower bodies(Bottom).

0.2 Hz stepwise. At the same time the potentiometer and pressure sensor signals were registered for 500 operation cycles of the host computer (one operation cycle is 20ms). By analyzing the pressure sensor data, we categorized the gait observed during each experiments into 5 categories listed in Table 2. The time series data of three typical pressure patterns, thus “gaits”, are plotted in Figure 5-5. The first gait, “Shuffling gait”, is usually observed when the upper body oscillates at a smaller amplitude. In this gait, the robot simply swings the upper body which does not affect lower body very much. From Figure 5-5 (Top), the feet of the robot are mostly on the ground during the shuffle gait, and the pressure sensors indicate the lower state only for a short time in one cycle of the upper body oscillation. The second gait, “Walking gait”, can be observed when the amplitude and frequency of the waist motor oscillation are increased, in which one of the feet is off the ground while the other foot is on the ground. As shown in Figure 5-5, this behavior is clearly distinguishable from the shuffling gait by comparing the period of time during which one of the feet is on the ground. The “Hopping gait” is then emerged at even larger amplitude of the waist motor oscillation, in which both of the feet are off the ground during a certain period in a cycle of the upper body oscillation. This gait

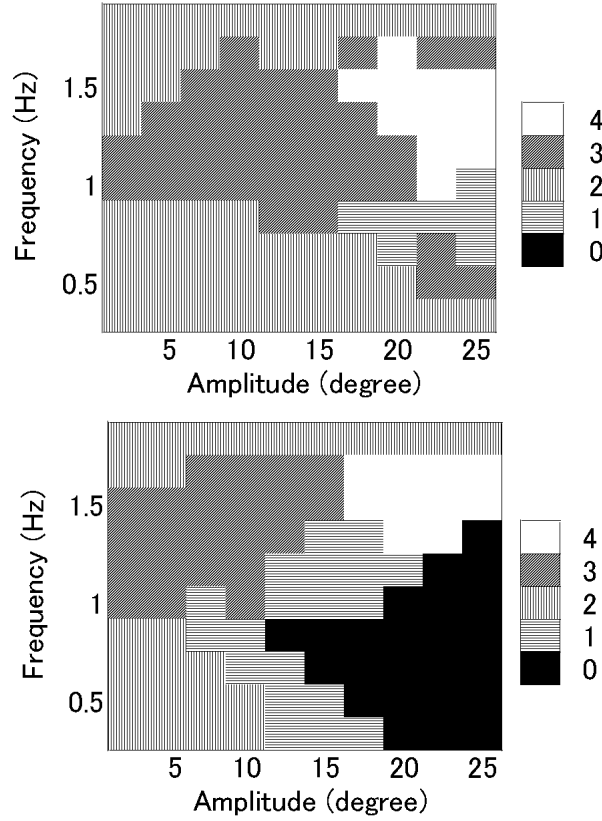


Figure 5-6: Gait distribution diagrams in Terrain 0 (Top) and Terrain 1 (Bottom). Numbers of the texture patches correspond to “4”: Hopping, “3”: Walking, “2”: Shuffling, “1”: Unstable, and “0”:Fall.

can be also clearly distinguished from the shuffling and walking gaits by comparing the two pressure sensor values on the right and left soles. Another category of the gaits is called the “unstable gait”, in which there is no stable gait pattern. The typical behavior in this category shows two foot-steps during one foot-step of the other foot. A similar behavior can sometimes be observed during a mixture of the walking and hopping gaits, which is also included in this category. Finally, the fifth category is called “Fall”, in which the robot falls down to the ground and fails to continue the operation.

5.4.2 Stability Analysis

Based on the category above, we analyze the gait at each amplitude and frequency of the oscillation. Figure 5-6 shows the result of this analysis, in which rectangular texture patches denote the observed gait. Comparing these two gait distribution diagrams, a salient difference is the large regions of “Fall” and “Unstable” in the diagram of Terrain 1. Moreover, there is a relatively larger regions of the walking and hopping gait in the diagram of Terrain 0, whereas these regions are squeezed by the “Fall” and “Unstable” regions in the diagram of Terrain 1.

Table 5.2: The observed gaits and identification numbers which are used in Figure 5-6.

No.	Gait
4	Hopping
3	Walking
2	Shuffling
1	Unstable
0	Fall

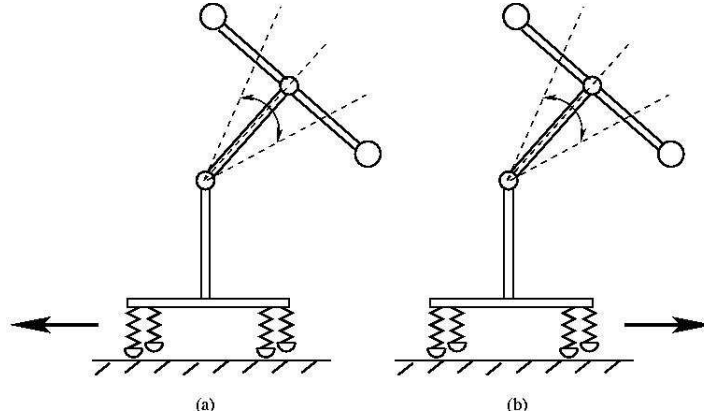


Figure 5-7: Two typical locomotion behaviors of lateral bounding; Ipsilateral bounding (Right) and contralateral bounding (Left).

The main conclusion derived from these experimental results is that, statistically, slippery interactions between the robot and the ground, such as the experiments in Terrain 0, could increase the stability, particularly during the hopping and walking gaits. In addition, a design which exploits such a slippery property could suppress instability of oscillatory processes and avoid fatal crash.

5.5 Lateral Bounding

A novel locomotion method called the “lateral bounding” was previously proposed and tested in [85]. By using the “waist” motor with a biased set point of the oscillation, Stumpy can move in lateral direction. The previous experiments have shown two unique lateral locomotion behaviors, so-called “ipsilateral bounding” and “contralateral bounding”, which are illustrated in Figure 5-7 and Figure 5-10. In this section, we investigate this interesting phenomenon further.

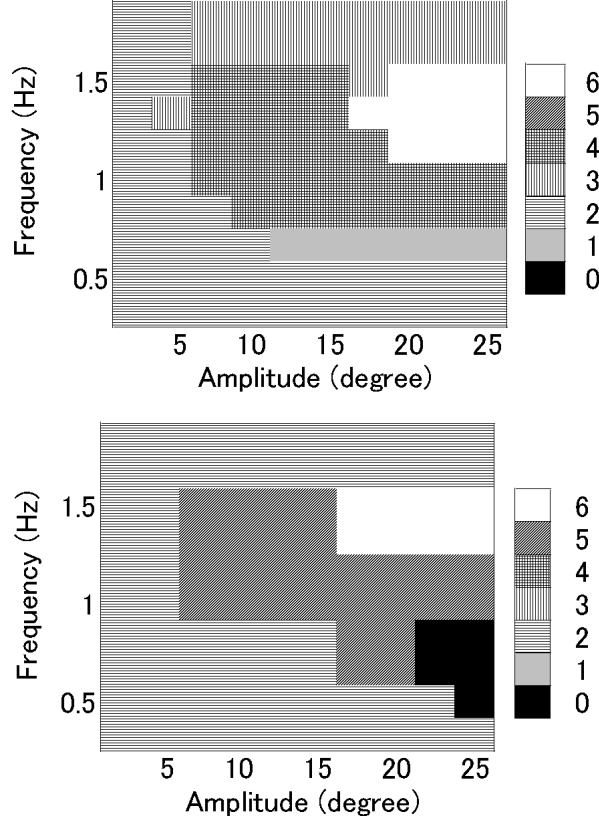


Figure 5-8: Gait distribution diagrams of the lateral bounding experiments on Terrain 0 (Top) and Terrain 1 (Bottom).

5.5.1 Experiments of the Lateral Bounding and the Observed Gait

We have performed another set of experiments in a similar manner to the experiments described in section 4. In this experiment, however, we set the set point at 30 degree to the right side and conducted 100 sets of experiments each on Terrain 0 and Terrain 1. We applied the same range of amplitude and frequency parameters as were used for the experiments in section 4.

There are 4 different locomotion behaviors observed during these experiments, i.e. ipsilateral locomotion, contralateral locomotion, the mixture locomotion of these two behaviors, and “Fall”. Again we define the categories for these behaviors, “Right”, “Left”, “Stay”, and “Fall”, respectively. These behavior categories are determined by measuring the physical displacement (a threshold of 30 cm from the starting location) of the robot, after 500 operation cycles. Concerning the gait in the lateral bounding, we did not observe the walking gait, only shuffling and hopping gaits, by applying the same categorization framework which was used in section 4. In total, therefore, there are 7 different patterns of behaviors in these experiments as shown in Table 3.

Table 5.3: Observed gaits and behaviors during the lateral bounding experiments and identification numbers which are used in Figure 5-8.

No.	Gait	Behavior
6	Hopping	Right
5		Stay
4		Left
3	Shuffling	Right
2		Stay
1		Left
0		Fall

5.5.2 Gait Analysis

Figure 5-8 shows the gait distribution diagrams of the lateral bounding experiments. One of the major contrasts between the gait distributions in Terrain 0 and 1 is a region of the “Fall” category shown in the Terrain 1 diagram, whereas it does not appear in the Terrain 0 diagram, which is similar to the results shown in Figure 5-6 explained in the previous section. This result can also be another evidence that supports the hypothesis of increasing the stability of locomotion by exploiting friction.

Another interesting contrast of the diagrams in Figure 5-8 is the fact that the number of different types of behaviors observed in Terrain 0 is greater than that in Terrain 1. More specifically, in the Terrain 0 diagram, “Right” and “Left” behaviors were observed in both “Hopping” and “Shuffling” gaits. On the contrary, the Terrain 1 diagram shows mostly “Stay” behavior except for a relatively small region of the “Hopping Right” behavior.

Note that the informal experiments have shown that the gait distribution is also dependent on the set point. For example, the gait distributions of the set points 30 degrees and 45 degrees would be different. Further comprehensive analysis of this phenomenon is expected.

An important aspect of these experimental results is that, by using a simple 1-DOF inverted pendulum oscillation, Stumpy shows 6 qualitatively different behaviors in one dimensional lateral locomotion, which are controlled by 4 partially coupled redundant parameters, i.e. friction coefficient, amplitude, frequency and the set point of the oscillation. This variety of behaviors could probably enhance the adaptability of a locomotive system. For instance, the ipsilateral bounding is faster and more unstable than contralateral bounding [85]. Therefore, the ipsilateral behavior could be used for emergency situation. The contralateral one is, on the other hand, stable and robust which can be viable for practical long-term applications.

5.6 Controlling the Turning Rate

In this section, we reconsider another locomotion method of Stumpy originally proposed in [48], in which the robot is capable of moving forward, reversing direction, and changing the turning rate as shown in Figure 5-9.

The control of moving forward/backward direction can be realized as follows. The waist motor oscillation with constant amplitude and frequency generates a periodic gait of either hopping or walking. And at the same time, the robot rotates the shoulder motor also in a oscillatory fashion by synchronizing with the waist motor oscillation. With this control, the oscillatory yaw momentum produced by the swing of the shoulder beam drives one foot in the air moving forward or backward. Thus, the periodic operation of this control results in either moving forward or backward, and the direction of the robot's movement can be controlled by changing the phase between the waist and shoulder motors by 180 degrees.

The control of turning rate uses the same principle, although the speed of shoulder beam oscillation should be biased, i.e. the clockwise speed is faster than that of counter-clockwise, or vice versa. Therefore the turning rate of the locomotion can be approximately proportional to the speed difference between clockwise and counter-clockwise.

The control of turning rate is a very good practical case study in which the second hypothesis described in section 2 is effectively used. In this control of Stumpy, by analogy, the oscillation of the waist motor produces F_v and the oscillation of the shoulder motor gives F_h . It is observed that, for the control of the robot moving direction and turning rate, the gait of the robot does not need to be walking, but it can also be hopping or shuffling. The significance of this fact is, again, that the qualitative diversity of the behaviors.

An interesting argument is that, Stumpy has a rotational oscillation provided by the swing of its shoulder, whereas the second hypothesis in section 2 assumes a linear oscillation. Interestingly, due to its rotational momentum, rather than a linear one, Stumpy can produce 3 degrees-of-freedom movement in two-dimentional space, i.e. moving forward/backward, right/left, and rotating on its own axis. This argument needs to be elaborated in the future.

5.7 Discussion

In this chapter, we propose two working hypotheses described in section 2 with respect to how the friction could contribute to a form of locomotion. In this section, we discuss further issues on these hypotheses.

Concerning the first hypothesis mentioned in subsection 2.1, the experimental results in section 4 and 5 show that the friction can be one of the significant parameters which largely increases the stability of a locomotion process. However, it is still an open question regarding to what extent this hypothesis could be applicable. As mentioned in section 2, the principle of increasing the stability depends not only on the friction force, but also on the shape of the object (e.g. d and h in Figure 5-1),

the external force, at least. Additional comprehensive experiments and analysis on this issue is expected, including Stumpy's morphological design of l_b , r , l_1 , and l_2 in Figure 4.

Another interesting discussion would be whether the variety of locomotion behaviors on Terrain 0 in Figure 5-8 could be explained by the second working hypothesis described in subsection 2.2. In these experiments, by analogy, one could assume that the swing of the inverted pendulum (i.e. the oscillation of the upper body) produces both the vertical force F_v and horizontal force F_h in equation(4). If this is the case, the friction coefficient μ could be a control parameter for locomotion as well as amplitude A and frequency ω . However, it has to be mentioned that these control parameters are only partially independent in such a sense that the friction force cannot be larger than the horizontal force F_h .

As mentioned in section 2, there are two possible ways to control the friction. According to equation (3), one is to control the coefficient of friction, μ , and the other is to control the vertical force F_v at the ground contact. The former one mainly depends on the material property, and the latter is mostly realized by shifting the center of gravity of a locomotive system. The material property of the sole, therefore, plays a very important role in locomotion of the robot, which can be categorized as the first point. However an active control of the friction coefficient could be potentially an alternative parameter to control the locomotion.

In relation to the vertical force F_v , the springs which are vertically installed in the Stumpy robot would also be a point of dispute, since they significantly affect the force F_v and most probably also the phase ϕ in equation(4). As has been known in biological studies of running animals (e.g. [1]), the passive spring component can increase the energy efficiency, i.e. converting the kinetic energy to the potential elastic energy. However, the vertically equipped springs could also be an additional control and design parameter for the locomotion exploiting the friction force.

Finally, the concept of locomotion presented in Figure 5-2 assumes two oscillatory forces given to the system. In this chapter, therefore, we have applied only simple sinusoidal oscillation controls. Considering that the friction is usually a highly non-linear interaction, an adaptive control method (e.g. one used by [114]) might enhance the locomotion stability of the system as well.

5.8 Summary

In this chapter, we propose two working hypotheses in which we discuss how an artificial system could actively exploit the interaction between a system and the ground for the purpose of adaptive locomotion. In order to test these hypotheses, we have conducted three case studies by using a robotic platform which we have developed. The experimental results show the statistical plausibility of the first hypothesis, where stability of locomotion could be increased by properly exploiting the friction. Furthermore, it is shown that, by properly taking advantage of the friction, the robot could enlarge the repertoire of locomotion behaviors. A criticism to what we discuss in this chapter might be whether it is worth exploring all the possible locomotion behaviors

exploiting the slippery interaction between a system and the ground, since the energy efficiency of locomotion is always lower with respect to traveling distance as long as there is a friction force. However, our interest of this research is not to focus on the efficiency, rather we are interested in a comprehensive understanding of adaptive locomotion, where a repertoire of locomotion behavior would play an important role.

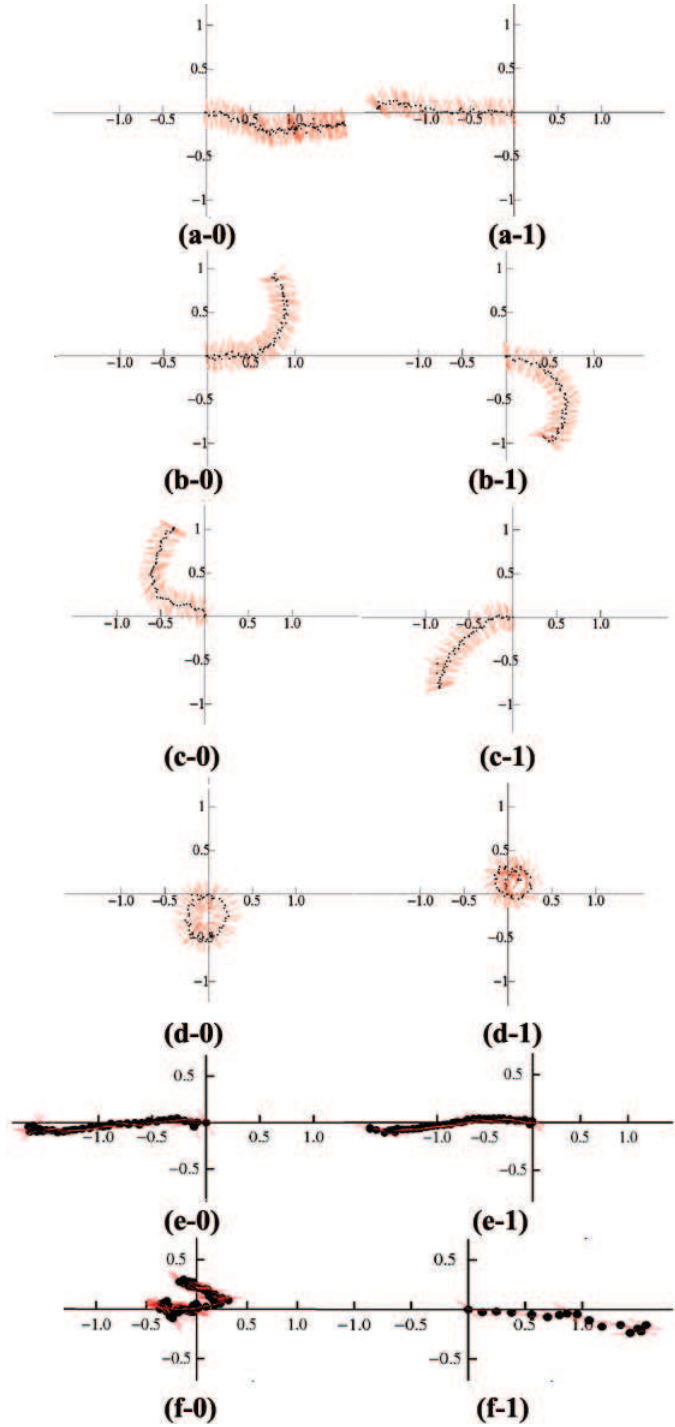


Figure 5-9: Locomotion behaviors of Stumpy observed from top (The unit of these graphs is meters). Stumpy can control its movement direction, turning rate (Top and Middle panels), and lateral bounding (Bottom panels) by changing only a few control parameters. Black dots denote the trajectory of the body center, and the line illustrates the orientation of bottom base.

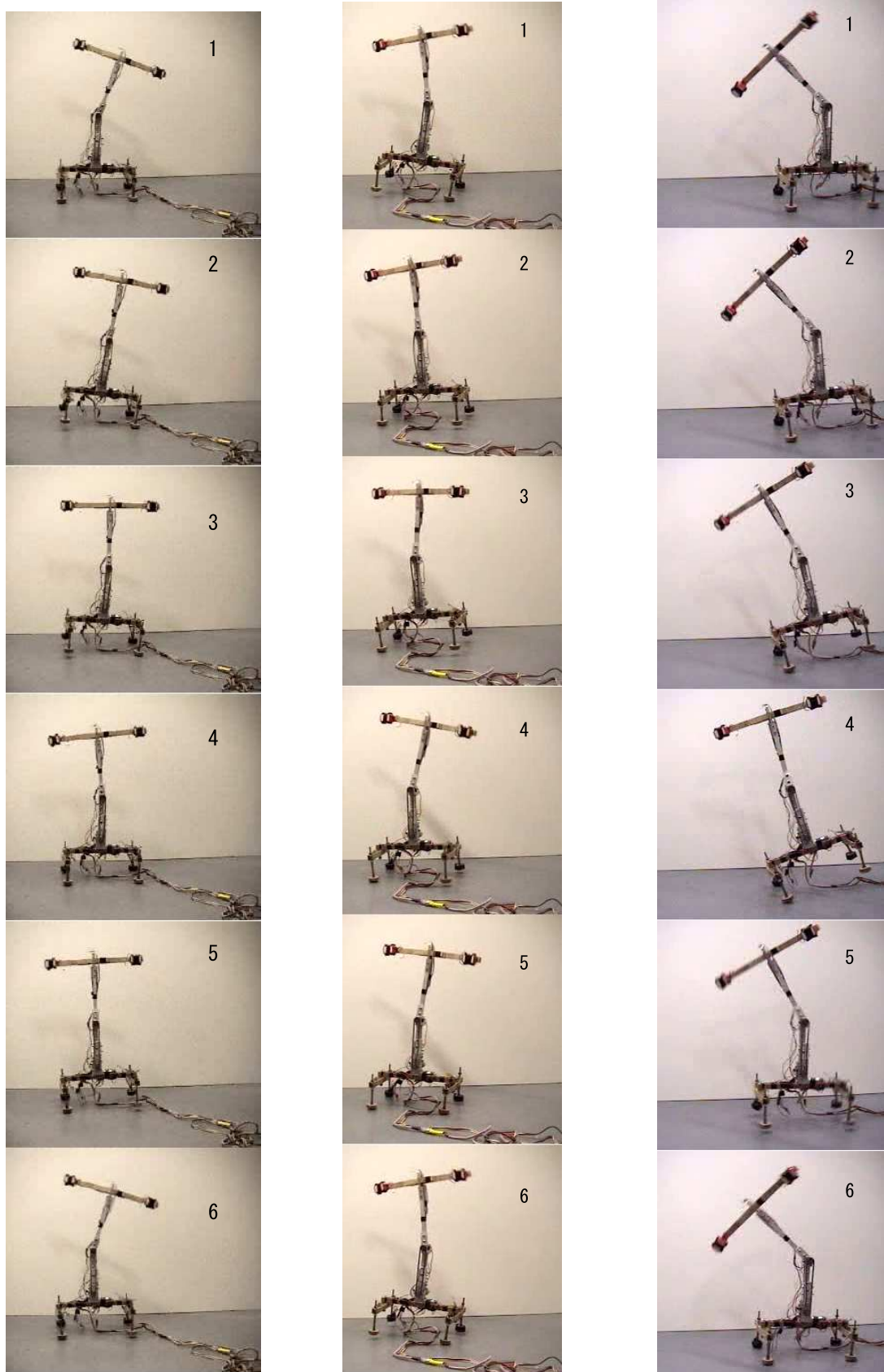


Figure 5-10: Typical gait patterns of Stumpy (Walking, Hopping, Lateral Bounding from left to right).

Chapter 6

Cheap Rapid Locomotion of a Quadruped Robot

Abstract

The legged animals are capable of rapid, energy efficient, and adaptive locomotion in a complex environment. Toward a comprehensive understanding of the nature of such ecologically balanced legged locomotion, in this chapter, we propose a novel method to achieve a form of bounding gait for a quadruped robot by using a minimalistic approach. Although this method uses a simple sinusoidal position control with no global sensory feedback, it is shown that the rapid bounding is possible in a relatively robust manner by properly exploiting the intrinsic dynamics and the interaction with the environment. The behavioral analysis with the robot experiments show that this relatively complicated dynamic locomotion is achieved even with a simple controller mainly because of a self-stabilization mechanism. Moreover, by exploiting this mechanism of self-stabilization, we propose a unique approach to control the forward velocity of the locomotion.

6.1 Introduction

The locomotion capability is one of the most essential functions for an adaptive robot. However, in order to understand the nature of adaptability, locomotion cannot be seen in isolation, rather a multi-functional perspective is crucial. From this viewpoint, a set of design principles have been proposed for the autonomous agents, which include the principle of “cheap design” [89]. This principle suggests that if a robot could properly exploit the given ecological niche, the control effort could be significantly simplified. The studies of the passive dynamic walking have nicely illustrated this principle [73, 20]. Even without any control and actuation, a robot can achieve a relatively complicated behavior of dynamic walking if it is properly designed for its ecological niche. Another good example is the rapid legged locomotion, since the use

⁰This chapter is based on the reviewed publication [52].

of cheap design is particularly important when the temporal constraint of the system is demanding.

The bounding gait is a form of legged locomotion, which is generally observed when a quadruped animal is running at the highest speed. In this gait, the animal lands with both of its front feet and brings the hind legs forward, then lands with both of the hind feet to swing the front legs forward for the next leg step. Biomechanics studies have extensively investigated the mechanisms of this running behavior of the legged animals. The use of the elastic components in the muscle-tendon system has been analyzed and a theoretical model of legged animals, the so-called “spring-mass model” was proposed [1, 75]. In this model, it was hypothesized that an animal’s leg could be approximated by a spring loaded inverted pendulum. Interestingly the studies of the spring-mass locomotion models have shown that, with a proper implementation of the self-stabilization mechanisms, many aspects of rapid legged locomotion can be passive or they require extremely simple controls (e.g. [64, 103]). Based on these biomechanical investigations, the study of running robots has been conducted during last couple of decades, and the mechanism of running behavior has been successfully engineered. The pioneering work by Raibert [96] has shown that the task of a hopping machine can be decomposed into three problems, namely (1) regulating periodic hopping height; (2) maintaining body attitude; and (3) controlling the desired forward speed. Then these control problems can be solved by switching between two control strategies for stance and flight phases. During the stance phase, the robot controls for problems (1) and (2), and during the flight phase, the problem (3) is dealt with. On the basis of this principle, monopod, biped, and quadruped robots have demonstrated dynamical hopping/running behaviors [96]. By following a similar approach, it has been shown that, only by regulating the appropriate angle of attack at touchdown during a flight phase, a quadruped can maintain its balance and control the forward velocity [91, 14]. All these studies are based on a method in which there are two independent control phases. Therefore the robot needs to identify the phase at every computational step by using contact detectors on the feet.

By following the hypothesis of the spring loaded inverted pendulum model, the challenge addressed in this chapter is whether it is possible to achieve the bounding behavior of a quadruped robot without sensory feedback at the level of global body function, i.e. no sensory feedback from, for example, gyros, inclinometers and contact detectors. In order to realize such a locomotion method, we have to carefully consider the intrinsic body dynamics which self-stabilizes into a periodic stable gait. Compared to the phase based control scheme, this approach provides a physiologically cheaper design, i.e. no wire transmitting sensory signals is required, and a coherent controller, which reduces the computational cost. Moreover, as shown later in this chapter, the coherent control scheme provides the significant flexibility in controlling the locomotion behaviors such as the forward locomotion velocity.

The structure of this chapter is as follows. In section 2, we describe the design and control of our quadruped robot which is used for the experiments explained in section 3. Issues leading to further design principles will be discussed in section 4.

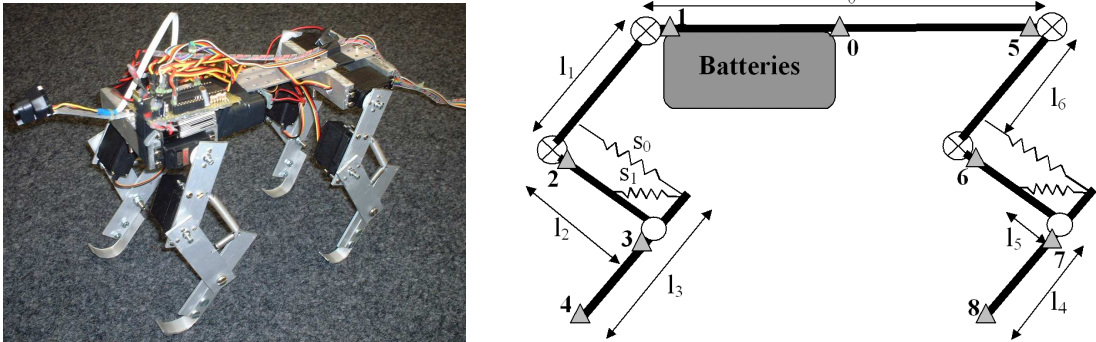


Figure 6-1: Left: A photograph of the quadruped robot. Right: A schematic of the robot. The circles denote passive joints and the circles with a cross inside denote the joints controlled by the servomotors. The triangles with a number show the locations of LEDs which are used for visual tracking of the body geometry during the locomotion experiments.

6.2 Design and Control of a Quadruped Robot

6.2.1 Morphological Design

The robot is designed based on the so-called spring-mass model, which is an abstract model of musculoskeletal structure in legged animals (Figure 7-1). Despite its simplicity, it has been shown that legged locomotion of biological systems are very well characterized by this model [75, 7, 103].

The physical dimensions of the robot body are as follows: It is 170mm long, 135mm wide and approximately 200mm high (refer to Table 1 for more detailed specifications). The robot has 8 standard digital servomotors (Hitec HS-5945MG) in the shoulder, elbows, hip, and knees. Batteries and a micro controller are also implemented in the robot body, which results in a body weight of 1.5 kg. We employ a three-segment model of animal legs, where two motors and one springy passive joint in the ankle are implemented. We have applied exactly the same leg design to all four legs for the sake of simplicity, whereas the hind and fore legs of animals are generally very different.

In the experiments shown in the following section, we deliberately installed slippery materials on the soles of the robot. The intention of this slippery interaction is two fold: On the one hand, the informal experiments showed that the robot locomotion requires more torque and it is unstable if the robot has non-slippery interaction. On the other hand, for the running/hopping behavior, the high friction force would not always be required, because of the relatively high vertical force against the ground induced by hopping dynamics. Although it is difficult to quantitatively measure the slipperiness during dynamic interaction between legs and ground, a good estimate could be the coefficient of friction. The static and dynamic coefficients of friction are approximately 0.20 and 0.13, respectively.

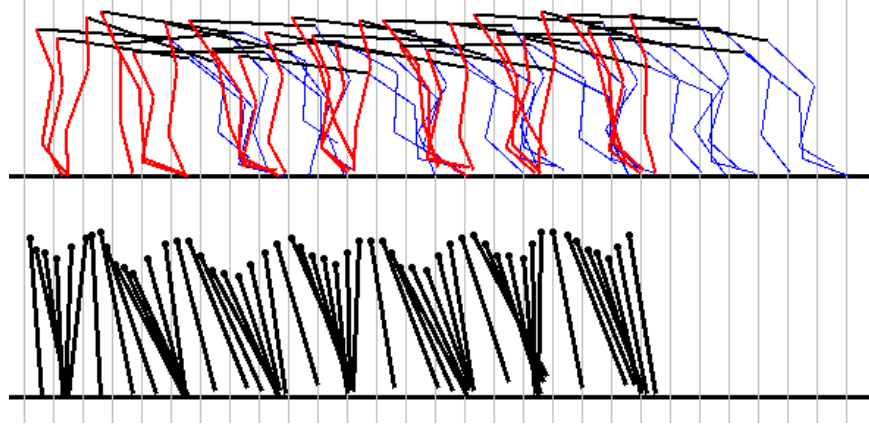


Figure 6-2: Behavior analysis of a running experiment. The upper graph shows the behavior of whole body extracted from the visual tracking of LEDs attached to the leg joints. The lower graph shows the trajectory of a virtual linear hind leg.

Table 6.1: The specification of the robot mechanical structure

Param.	Description	Value
l_0	length of body	170 mm
l_1	length of upper leg limb	70 mm
l_2	length of middle leg limb	80 mm
l_3	length of lower leg limb	120 mm
l_4	point of lower joint attachment	70 mm
l_5	point of s_1 attachment	45 mm
l_6	point of s_0 attachment	30 mm
s_0	spring constant	13.9 g/mm
s_1	spring constant	20.8 g/mm
m	mass of the robot	1.5 kg

6.2.2 Controller

In this chapter, we focus only on the hip and shoulder motor controls, i.e. the motors in the elbows and knees are fixed. For the control of shoulder and hip motors, we employ a simple oscillatory position control, and the motor commands are symmetric in terms of the sagittal plane, i.e. the control of two fore legs is the same. The target motor positions are determined as follows.

$$P_f(t) = A_f \sin(\omega t) + B_f \quad (6.1)$$

$$P_h(t) = A_h \sin(\omega t + \phi) + B_h \quad (6.2)$$

where P_f and P_h indicate the target angular positions of the fore (shoulder) and hind (hip) motors, respectively. A and B determine the amplitudes and the set points of the oscillation, and ϕ determines the phase delay between these two oscillations of the fore and hind legs. The parameters used in the following experiments are heuristically

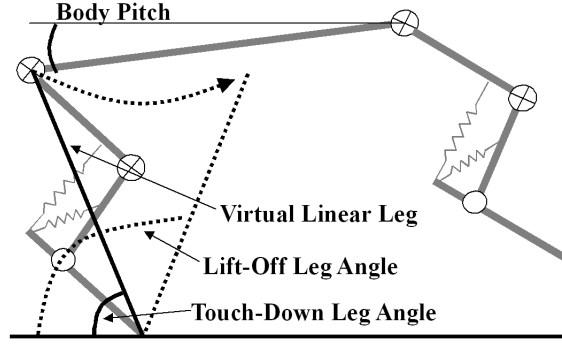


Figure 6-3: The definitions of touchdown, lift-off angles and body pitch used in the analysis.

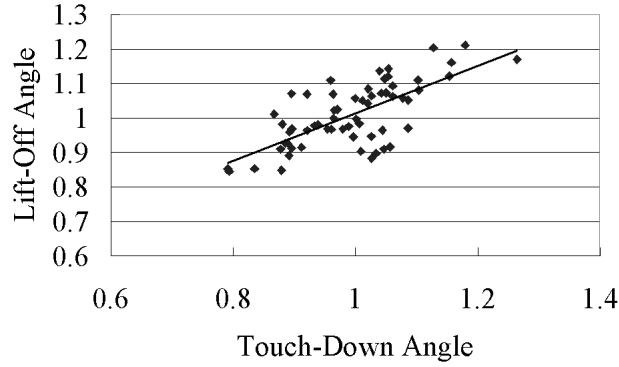


Figure 6-4: The relation between touchdown and lift-off angles. The touchdown angles and lift-off angles are normalized by the corresponding mean touchdown and lift-off angles.

determined as follows. $A_f = A_h = 25(\text{degree})$, $B_f = 20(\text{degree})$, $B_h = 10(\text{degree})$, $\omega = 7.0$ (1/sec, 0.90 Hz). The coordinate of these set points is set to perpendicular with respect to the spine. This control method does not require any global sensory feedback: The controller does not need to distinguish stance and flight phase, the body attitude or leg angles with respect to the absolute ground plane. Therefore, the main interest of the following experiments is how the robot could self-organize into a periodic gait primarily by the intrinsic body dynamics and its interaction with the environment.

6.3 Experiments

In this section, firstly, we explain the methods of experiments and behavior analysis. Then, we analyze how the stabilization of the periodic bounding gait can be achieved in the proposed locomotion control. Finally, by exploiting the stabilization mechanism, a control scheme of forward locomotion velocity is proposed.

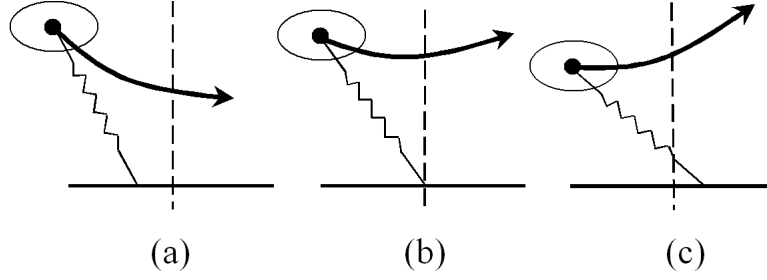


Figure 6-5: The conceptual illustration of foot placement. If the touchdown angle is appropriate, the trajectory of body mass can be symmetry as shown in (b). Otherwise the lift-off angle can be higher (a) or lower (c).

6.3.1 Experimental Method

We conducted behavior analysis of the robot movement during the running behavior. In this analysis, first, we attached 9 LEDs at every joint as visual tracking points labeled LED 0 to 8 as shown in Figure 7-1. Then we recorded the running behavior from a side view by using a standard video camera. These tracking points were extracted by visual tracking processing at 25 frames per second. Figure 6-2 shows a typical running behavior of the robot as acquired from this visual tracking analysis.

For further analyses explained in this section, we use “a virtual linear (hind) leg”, i.e. a virtual line between the hip joint and toe (LED 5 and 8). For reasons which become clear later in this chapter, the running behavior of the robot is well characterized by analyzing the virtual linear leg, instead of using all of the joint trajectories including knees and ankles. A typical behavior trajectory of the virtual linear (hind) leg is shown in Figure 6-2.

A set of experiments have been conducted in terms of the phase parameter ϕ in equation 7.2. The reason to focus on the phase parameter is that the self-stabilization mechanism and its use are very well characterized as explained in detail later. In the following experiments, we analyzed the behavior of 6 leg steps from a side view. We repeated the same experiments by changing the phase parameter ϕ from -1.6 to 0.2 (radian) by 0.2 step. This range of the parameter is chosen based on informal experiments, in which a stable bounding gait is possible.

6.3.2 Stability Analysis

To achieve the stable periodic gait, the legs need to touchdown and lift-off at constant angles with respect to the ground plane. In this subsection, we first analyze the behavior of a hind leg and elaborate the self-stabilization mechanism of the bounding gait. More specifically, by analyzing touchdown and lift-off angles of a virtual linear leg, we explain how the controller is interacting with the environment which leads to the stable gait. Secondly we focus on how the self-stabilization mechanism could result in a whole body coordination by analyzing the dynamics of body pitch. (The touchdown, lift-off angles and the body pitch are explained in Figure 6-3.)

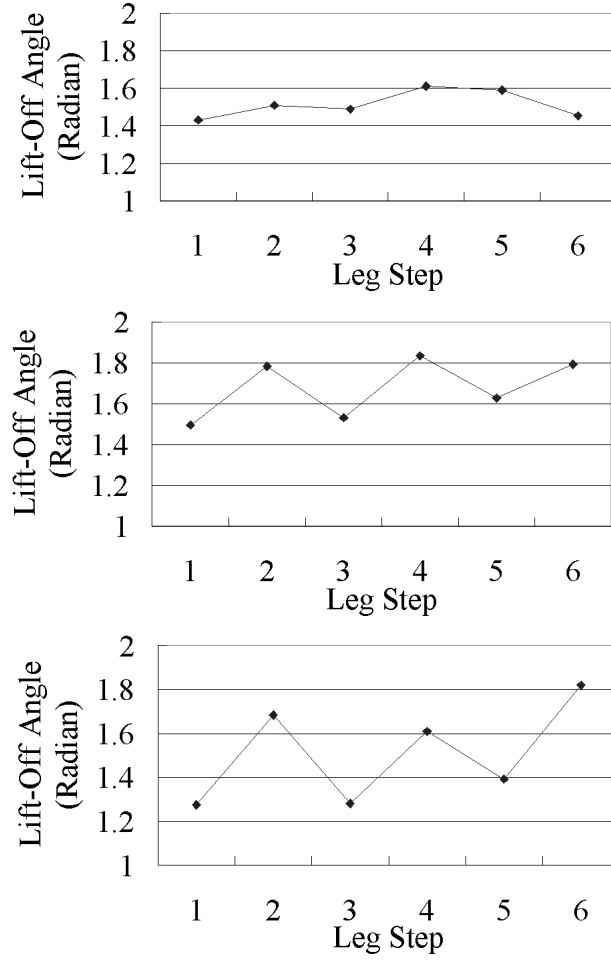


Figure 6-6: Typical transitions of lift-off angles with different phase parameters. (The phase 0.2 (Top), 0.8 (Middle), and 1.0 (Bottom) radian.)

Self-stabilization during the Stance Phase

In the first analysis, we measured the touchdown and lift-off angles of the virtual linear hind leg with respect to the ground plane (the absolute coordinate) by using joint geometries gained from the visual tracking. The touchdown angles and the successive lift-off angles (the lift-off angles following the corresponding touchdown angles) of 60 leg steps are normalized by the mean touchdown and lift-off angles respectively, and are plotted in Figure 6-4. As shown in the figure, the lift-off angle is, on average, proportional to the touchdown angle, i.e. the lower touchdown angles result in lower lift-off angles, and vice versa.

It has been found that the angle of attack at touchdown is one of the most important parameters for a legged running behavior [96, 103]. The basic principle is illustrated in Figure 6-5. In this principle, if the touch down angle of a linear springy leg is appropriate, the trajectory of the body mass can be symmetric with respect to the vertical line at the foot contact, as shown in the middle illustration. Otherwise the lift-off angle can be lower or higher. Figure 6-4 shows that this principle holds

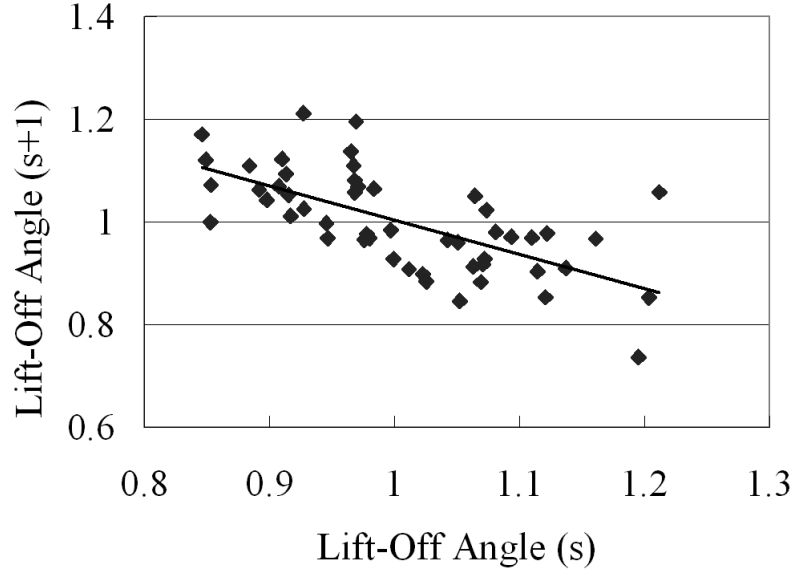


Figure 6-7: Relation between the normalized lift-off angles of two successive leg steps. The variable s represents the index of leg step.

also for the experimental results of the virtual linear leg.

Self-stabilization during the Flight Phase

In the next analysis, we analyze the stabilization of locomotion during the period of several leg steps by using the same joint geometry data above. As shown in Figure 6-6, the fluctuations of successive lift-off angles against the ground are generally maintained within a certain range. To show this more clearly, the relation between two successive lift-off angles is plotted in Figure 6-7. This figure shows that, when a lift-off angle is lower than average, the subsequent lift-off angle tends to be larger, and vice versa. Given the relation between touchdown and lift-off angles during the stance phase, the leg behavior during the flight phase is typically such that a lower lift-off angle leads to a higher touchdown angle and vice versa, which results in the stable gait over multiple leg steps.

It has been shown that the principle of foot placement can be used for the speed control of some legged hopping robots by adjusting the touchdown angle during a flight phase [96, 91]. However, in this experiment, the angle of attack was not controlled but self-stabilized without sensory feedback; the robot cannot recognize flight/stance phase nor the body pitch to estimate the touchdown angle of the legs.

Full Body Coordination

By using the same joint geometry data above, we analyzed the movement of the body pitch. The body pitch is measured as the angle of spine with respect to the ground plane as shown in Figure 6-3. Figure 6-8 shows a few typical angular movements of the body pitch. As shown in these graphs, the spine rotation is changed from a steep zigzag movement to a relatively stable flat movement depending on the phase. The

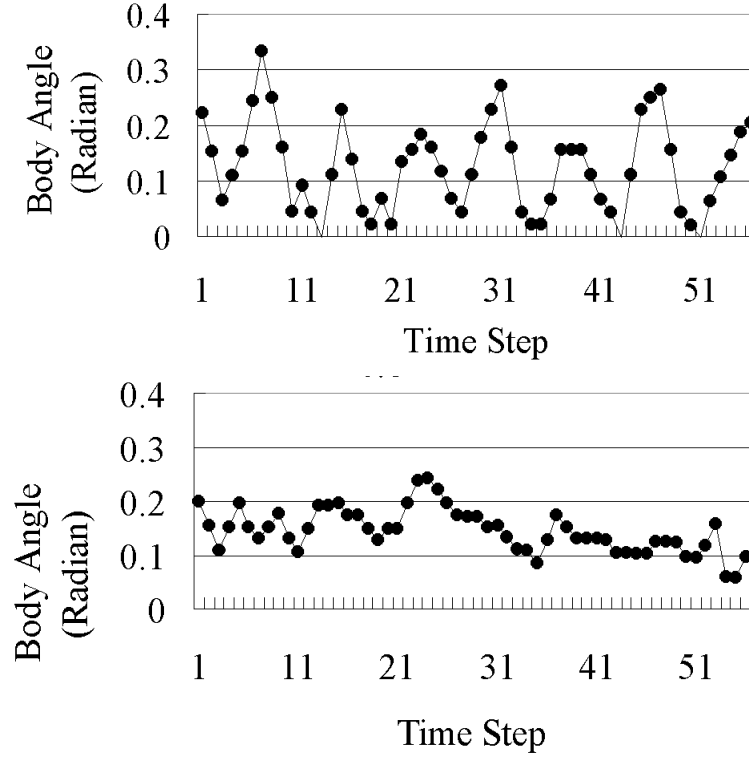


Figure 6-8: Typical time series movement of body pitch with respect to the ground plane. The phase parameter of 0.2 (Top graph) and -0.8 (Bottom) radian.

average angular velocity against the phase parameter is plotted in Figure 6-9, which shows that the movement of body pitch as measured by angular velocity accurately corresponds to the phase between front and hind leg oscillations. This is possible only when the front and hind legs are self-stabilizing their touchdown angles. More precisely, to maintain a constant touchdown angle with respect to the ground plane, the motor angles of hip at touchdown, i.e. $P_h(touchdown)$ in equation 7.2, should be changed according to the phase parameter, which would result in this characteristics of body pitch movement.

6.3.3 Forward Speed Control

In this section, the forward locomotion speed with respect to the phase parameter ϕ is analyzed. The velocity is also visually estimated by using the center of the body (LED 0), where we measured the horizontal distance traveled and the duration during 6 leg steps for the values of the phase parameter ϕ . As shown in Figure 6-10, the speed can be controlled in the range from 20 to 50 cm/sec by changing the phase. A possible explanation of the speed difference shown in this figure could be that, considering the fact that relatively higher velocity is achieved at a larger body movement, i.e. the phase range from -0.4 to 0.2, the fluctuation of body pitch could provide smaller touchdown angle even with the same amplitude of motor oscillation,

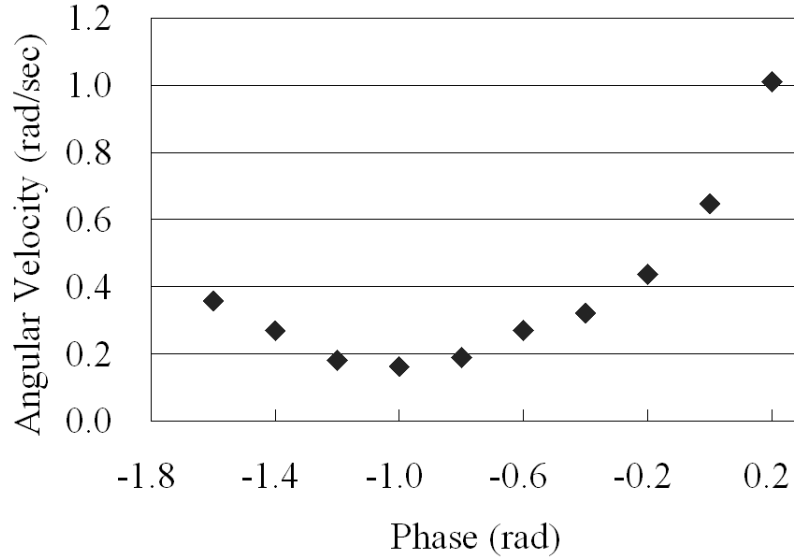


Figure 6-9: Average body rotational angular velocity versus the phase parameter.

which is required for the faster legged locomotion. An explanation of the relation between the phase and the forward locomotion speed need to be corroborated, but, at least, this experimental result shows that the speed of locomotion can in principle be controlled by changing only the phase parameter.

6.4 Discussion

The findings discussed in this chapter are of potential interest to both engineers and biologists. One of the most significant contributions is that the proposed control scheme adds another variation of rapid bounding locomotion method. In most of the existing controllers for the bounding behavior, the controllers need to detect two states, i.e. flight and stance phases, whereas it requires no need of the global state recognition in the proposed method.

From an information theoretic viewpoint, there are a number of interesting aspects. Firstly, the flow of information is unidirectional and there is no signal feedback loop running all through the body, but the loop is only local, i.e. only in the servomotors. This experimental result achieved by a synthetic investigation could help understanding the physiological nature of legged rapid locomotion. Secondly, the control of speed cannot be computationally cheaper than the proposed phase control, since there is no sensory feedback, on the one hand, and the phase is equivalent to a low-pass filter or a simple time delay, on the other. Given the fact that the property is possible mainly due to the self-stabilization mechanism, the design of controller strongly depends on the stabilization mechanism including the morphological design of legs and body. From this perspective, although we only focus on a simple sinusoidal position control, the adaptability of the controller (e.g. the biological controller models investigated by [63, 33]) would be another interesting topic to be investigated

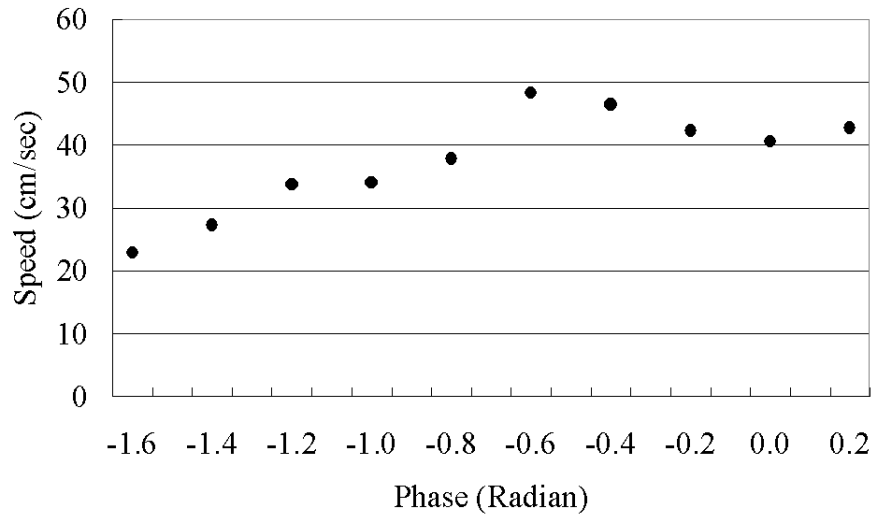


Figure 6-10: Average speed versus the phase parameter.

in the future. Thirdly, it is also worth to mention that, owing to the self-stabilization mechanism, there are many other parameters such as the frequency, the set points, and the spring constants (if possible) which can potentially control the forward velocity in addition to the phase parameter. The diversity and the flexibility of the proposed control scheme is another interesting aspect to be explored further.

Chapter 7

Sensing through Body Dynamics

Abstract

Passive dynamics has generally been investigated for generating energy efficient behaviors of robots. This paper explores another aspect of passive dynamics for the purpose of sensing. Through particular system-environment interaction derived from intrinsic body dynamics, the system is able to acquire sensory information with a set of discrete states in a continuous multi-modal sensory space. A locomotion model of a four-legged robot in both simulation and real world is used for a case study. It is demonstrated that this locomotion model is able to achieve stable behavior by using a simple control architecture which provides a basic setup for sensing. A comprehensive analysis of behavior and sensory information leads to additional insights of the relation between control, body dynamics and sensory information processing, which provides further conceptual implications for the task of object recognition and category learning of autonomous robotic systems.

7.1 Introduction

While design principles of traditional robotic systems assume rigid body materials and high-gain control, there has been an increasing interest in broader ranges of material properties and adaptive control. In particular, the use of passive dynamics for behavior control has provided a significant conceptual impact. One of the most fundamental aspects of passive dynamics, or more generally body dynamics, lies in the fact that behaviors and functions should be viewed as a result of the interplay between morphological properties, control and environment. The studies of passive dynamic walkers and rapid legged locomotion have nicely demonstrated how morphological properties are related to behavior of the system. When a system exploits morphological properties (e.g. shape, stiffness, friction, weight distribution, etc.), it is possible to simplify control and to achieve energy efficient behavior. Even without any actuation, for example, passive dynamic walkers are able to walk down a slope in a very natural way [73, 20], and they require extremely small amount of energy for

⁰This chapter is based on the reviewed publications [55, 57, 56].

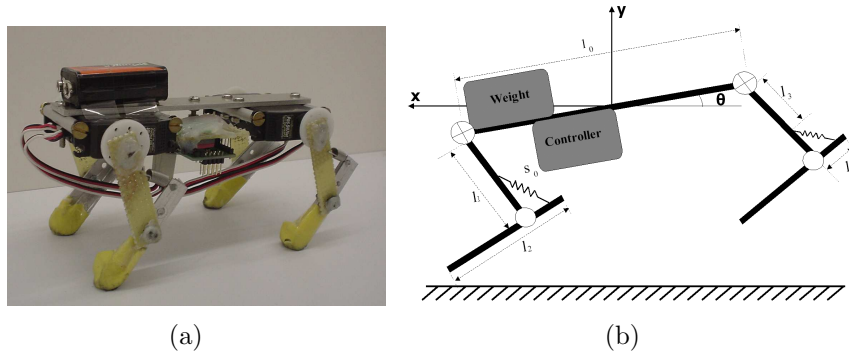


Figure 7-1: (a) A photograph of the quadruped robot. (b) A schematic of the robot. The circles denote passive joints and the circles with a cross inside denote the joints controlled by the servomotors. The specifications of the robot are shown in Table 1.

walking even on the level ground [123, 21]. By exploiting compliant material properties, as another example, a number of robots demonstrated energy efficient rapid legged locomotion [96, 17, 14].

A common characteristics of the systems exploiting body dynamics is that their behavior is generally dependent on the physical conditions of the environment. For example, the passive dynamic walkers can function only in a very limited environmental conditions, i.e. a slope with a specific angle and a limited range of the ground friction. If the angle of the slope is varied slightly, the passive dynamic walker is no longer functional and falls over. Although the dependency of behavior to the environment is not preferable for design and control of certain desired behavioral functions, it is potentially important for the purpose of sensing. When material properties and active control are exploited, a system is able to obtain more sensory information about the physical properties of the environment. There are a few related issues that partially cover this concept. Previously, by implementing various materials in some parts of the body (e.g. elastic fingers, feet, or whiskers), it has been shown that slight differences of physical properties in the environment and the objects can be categorized (e.g. [43, 105, 27]).

This paper explores the sensory information acquired during dynamic behavior exploiting whole body dynamics in order to gain broader perspective of the relation between body dynamics, control, behavior and sensory information. A four-legged robot model will be examined in this paper as a case study of body dynamics for sensing. Because it exploits a self-stabilization mechanism derived from passive dynamics, the locomotion behavior is intrinsically stable, but at the same time, dependent on the physical conditions of environment. A comprehensive analysis of the behavior and the corresponding sensory information will demonstrate that, when the system exploits the intrinsic stability derived from body dynamics, sensory information acquired during the interaction with the environment contains discrete states in multi-modal continuous sensor space. We will then speculate how such sensory information provides further insights in the mechanisms of object recognition and

Table 7.1: Specification of the robot platform

Param.	Description	Value
l_0	length of body	142 mm
l_1	length of upper leg limb	42 mm
l_2	length of lower leg limb	56 mm
l_3	spring attachment	15 mm
l_4	spring attachment	20 mm
s_0	spring constant	40 g/mm
m	mass of the robot	273 g

category learning.

7.2 Body Dynamics of a Quadruped Robot

The use of elastic muscle-tendon systems during rapid locomotion has been investigated in biomechanics, which leads to the theoretical model of legged animals, the so-called “spring-mass model” [15, 1, 2, 75, 7]. In this model, it was hypothesized that animal’s leg could be approximated by a spring loaded inverted pendulum. The studies of the spring-mass locomotion models have shown that, with a proper implementation of the self-stabilization mechanisms, many aspects of rapid legged locomotion can be passive or they require extremely simple control (e.g. [64, 103]). In this section, we introduce how a stable locomotion behavior can be achieved by a minimalistic control architecture in a four-legged robotic platform [52, 56].

7.2.1 Morphological Design

The design of the robot is inspired by the spring-mass model studied in biomechanics. As shown in Figure 7-1, the robot has four identical legs each of which consists of one standard servomotor (KOPROPO PDS947FET) and a series of two segments connected through a passive elastic joint. We used aluminum for the design of body frame and legs. The physical dimensions of the robot body are 142mm long, 85mm wide and approximately 75mm high (refer to Table 1 for more detailed specifications). The robot has 4 servomotors, a micro-controller (Microchip PIC 16F877) and a small weight to adjust the weight distribution of the body, which result in a total weight of 273g. The control signal for the motors and the electricity are supplied externally through the cables. We used the standard serial communication protocol to send the positions of the servomotors from a PC to the micro-controller that produces the modulated signals for the servomotors.

To gain a higher forward velocity, the robot requires higher ground friction. For this reason we implemented a rubber surface at the ground contact in each leg. Although it is difficult to quantitatively measure the slipperiness during dynamic interaction between legs and ground, a good estimate could be the coefficient of friction.

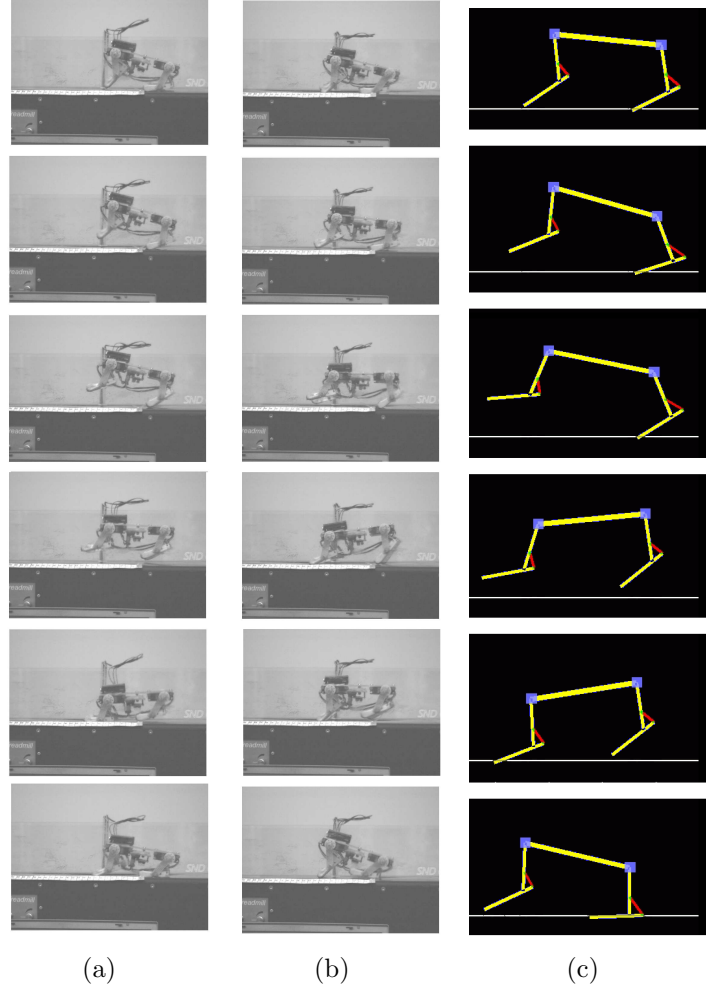


Figure 7-2: A time series photographs during “the gait 0” (a) and “the gait 1” (b). The behavior of the robot is visually registered while running on a treadmill. The interval between two pictures is approximately 30ms. (c) Behavior of simulation model.

The static and dynamic coefficients of friction are approximately 0.73 and 0.55, respectively.

7.2.2 Motor Control

For the detailed observation of the intrinsic body dynamics derived from the morphological properties, we apply a minimalistic control strategy, in which no sensory feedback is used at the level of global function. In the following experiments, the motors are controlled by a simple oscillatory position control as follows:

$$P_f(t) = A_f \sin(\omega t) + B_f \quad (7.1)$$

$$P_h(t) = A_h \sin(\omega t + \phi) + B_h \quad (7.2)$$

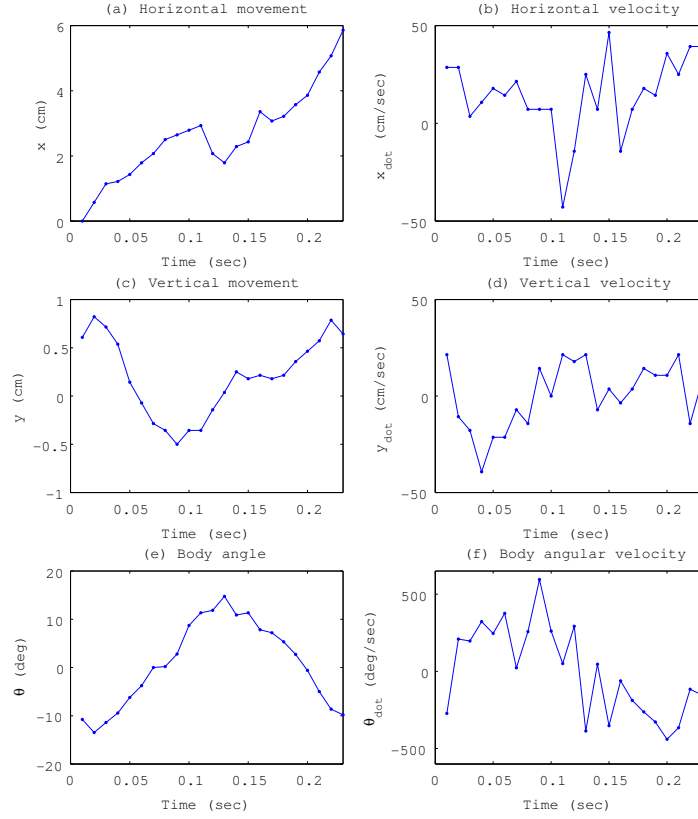


Figure 7-3: Time-series changes of the state variables during one leg step, (a) horizontal, (b) vertical, (c) angular movement and their velocity (d, e, f).

where P_f and P_h indicate the target angular positions of the fore (shoulder) and hind (hip) motors, respectively. A and B determine the amplitudes and the set points of the oscillation, and the frequency ω and the phase ϕ determines the phase delay between these two oscillations of the fore and hind legs. Control of the motors is symmetric in terms of the sagittal plane, i.e. the control of two fore legs is the same. The parameters used in the following experiments are heuristically determined as follows. $A_f = A_h = 25(\text{degree})$, $B_f = 20(\text{degree})$, and $B_h = 10(\text{degree})$. The control parameters of frequency ω and phase ϕ will be used for the parameter search. The coordinate of these set points is set as illustrated in Figure 7-1.

7.2.3 Intrinsic Stability

Although most of the compliant legged robots use sensory information to achieve stable rapid locomotion (e.g. [103, 91, 46]), this locomotion model does not; The controller does not need to distinguish stance and flight phase, the body attitude or leg angles with respect to the absolute ground plane, but stable locomotion behavior

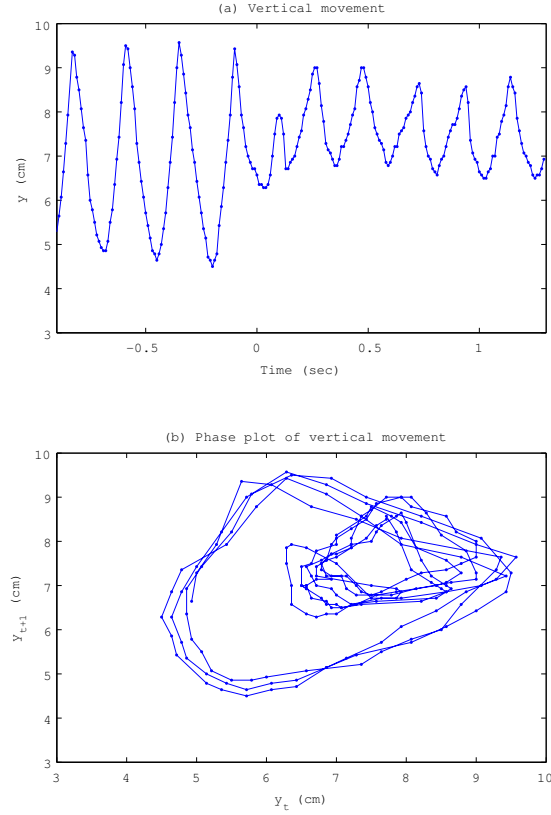


Figure 7-4: A typical recovery response from the change of the gait. (a) The time-series vertical movement of the body is shown before and after the trigger at $time = 0$, and (b) its phase plot.

can be achieved by a self-stabilization mechanism exploiting the compliant legs [52]. In the first set of experiment, we evaluate the stability of the locomotion method without sensory feedback. Figure 7-3 illustrates typical time-series state variables which characterizes the movement of the robot body during one leg cycle. For this analysis, the locomotion behavior was registered by a high-speed camera (Basler Basler A602fc, 100fps), and the movement of the body segment was extracted by a standard visual tracking method. As shown in this figure, all five state variables (i.e. \dot{x} , y , \dot{y} , θ , and $\dot{\theta}$) go back to the states at the beginning of the leg step, that ensures the periodic gait cycle.

By searching through the control parameters, we observed, at least, two qualitatively different locomotion gaits which are labeled “gait 0” and “gait 1”, as shown in Figure 7-2. In the gait 0, the hopping height is relatively larger than the gait 1, which results in the four legs clearly off the ground for some duration in a leg cycle. And the gait 1 generally exhibits larger forward velocity. The intrinsic stability of the locomotion method can be demonstrated by switching between the control para-

meters of these gaits. A typical response induced by the change of the gait is shown in Figure 7-4 (the control parameter of phase ϕ is varied at time $t = 0$). Generally the stable gait patterns can be recovered within one or two leg steps after the switch of the control parameters.

In general, there exist multiple stable gait patterns in this framework of quadrupedal locomotion, and the number of stable patterns are largely dependent on the ground friction. However, even during the unstable locomotion, it is possible to maintain the locomotion process owing to the intrinsic stability of the locomotion model.

7.2.4 Simulation Model

For the sake of comprehensive behavior analysis, we have constructed a simulation model of the running quadruped robot. The simulation was conducted in Mathworks Matlab 7.01 together with SimMechanics toolbox. We developed this simulation model in the same scale as that of real robot in a planar environment; It consists of 5 body segments (a pair of two-segment legs and a body segment), two linear springs, and two motors in shoulder and hip joints with angular position feedback. With a biomechanical ground friction model, the simulated dynamic locomotion is fairly comparable to the real one, as shown in Figure 7-2. The following experimental results are obtained by using this simulation model.

7.3 Behavior and Sensory Information

Sensory information acquired during the locomotion process is explored in this section. We conducted three simulation experiments to characterize the relation between locomotion behavior, control and the sensory information.

By tuning control parameters, the simulated robot is able to achieve a stable running behavior as shown in Figure 7-5(a). During this locomotion process, we registered time-series response of several different sensory channels, i.e. a pressure sensor on the sole of hind leg, a angle sensor of the hind passive joint, an inertia sensor in the body segment, and a motor torque sensor in the hip joint. As shown in Figure 7-6(a), all of the sensory signals show a periodic response due to the stable locomotion behavior.

In the second experiment, the coefficient of ground friction is varied, which results in unstable locomotion behavior with the same control parameters. Figure 7-5(b) illustrates a typical unstable behavior of the system; The behavior is mostly chaotic, and some periodic patterns are generally disappeared after a few leg steps due to accumulation of small slippage and undesired touch-down angles of the legs. Consequently, the sensory response also shows chaotic patterns; The ground reaction force and the motor torque particularly represent substantial differences compared to the previous ones in Figure 7-6(a).

In the third experiments, the control parameters are tuned for a stable locomotion behavior even in the coefficient of friction used in the second experiment. Although this locomotion exhibits slightly slower forward speed and larger hopping height, it is

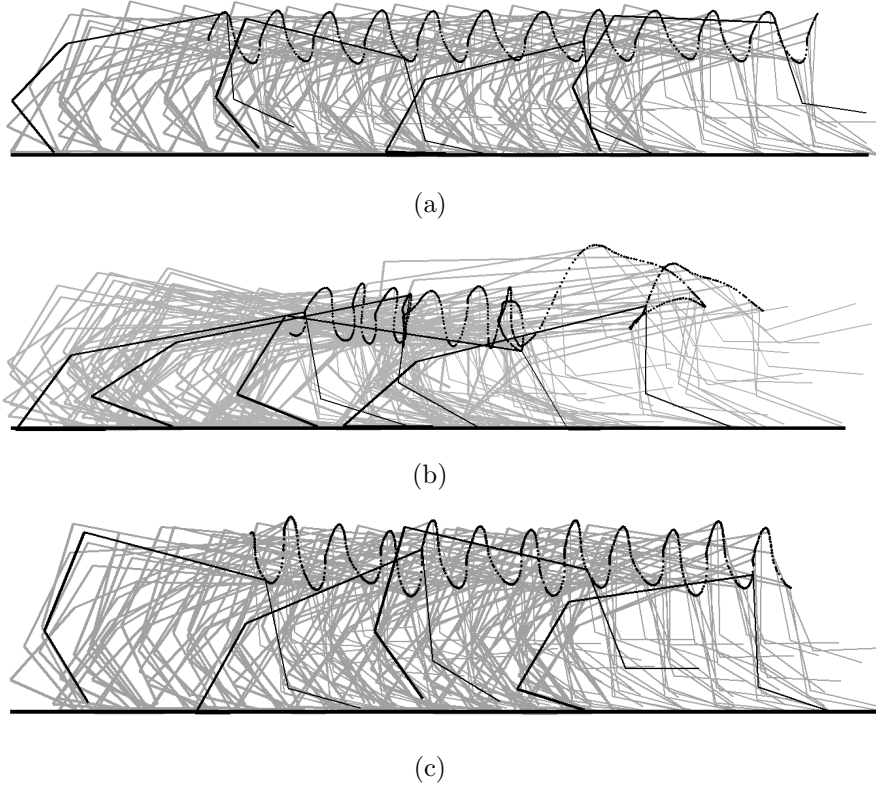


Figure 7-5: Stick figures of behaviors in simulation. The body postures are illustrated every 100 and 1000 simulation steps (gray and black stick figures, respectively). Black dots represent the trajectories of the shoulder joint. (a) $\omega = 4.7Hz$, $\phi = 0.3$ in the ground friction 0.9 (static) and 0.8 (dynamic). (b) the same control parameters in the ground friction 0.7 (static) and 0.6 (dynamic). (c) in the same ground friction as (b) with the control parameters $\omega = 4.9Hz$, $\phi = 0.4$.

possible to achieve comparable stability as the first experiment (Figure 7-5(c)). The sensory information also shows stable periodic patterns very similar to the first ones.

There are two implications from these experimental results. One point is that the different ground friction is reflected on four sensory channels. This is possible because the intrinsic stability of the locomotion process is achieved through the body dynamics; The system is, on the one hand, able to maintain the (unstable) locomotion process without any control in different environment, and on the other, a number of different physical interactions react to it. In this case study, for example, there are, at least, the ground reaction force exerted at the feet, the force generated in the elastic passive joints, the output torque of actuators, and the momentum of the large masses in the body.

Secondly, the relation between stable behavior pattern and sensory information has to be considered further. It was shown that, when the behavior is stabilized by tuning the control parameters, the amount of information about the environmental properties can be reduced considerably. In the third experiment, for example, because

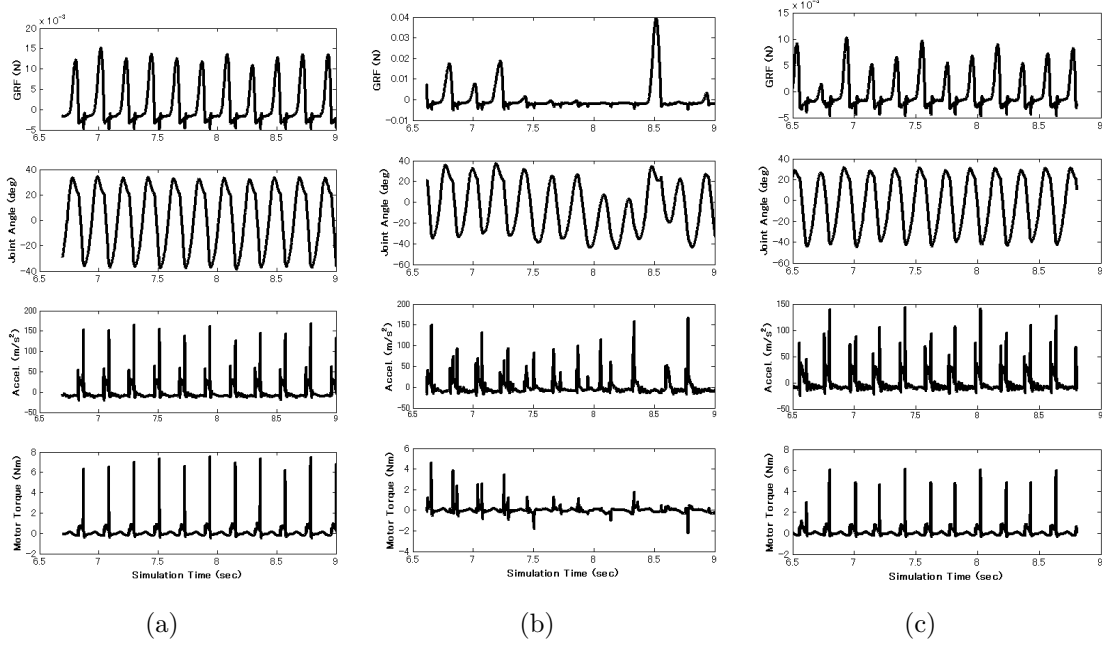


Figure 7-6: Sensory information acquired during the behaviors shown in Figure 7-5. From top figure to bottom: Pressure sensor in the hind leg, angle of the hind passive joint, acceleration of the body, and motor output torque of the hind leg. (a) Coefficients of ground friction (CGF) are 0.9(static), 0.8(dynamic), motor frequency 4.8 Hz, (b) CGF 0.7 (static) and 0.6 (dynamic), motor frequency 4.8 Hz, (c) CGF 0.7 (static) and 0.6 (dynamic), motor frequency 4.4 Hz.

the control parameters are tuned for the different environment, the sensory patterns of the first and the third experiments are difficult to distinguished.

7.4 Situated Sensing of Body Dynamics

In the following experiments, we investigate the influence of frequency ω and phase ϕ to the locomotion behavior. These parameters significantly change the locomotion behavior; it exhibits a stable rapid locomotion; it runs slowly or hops at place; it exhibits chaotic behavior; or it falls over.

This dynamic locomotion behavior can be recognized in a relatively simple manner by analyzing temporal patterns of the sensory signals. We implemented two sensors in the simulation model, i.e. the ground contact detector in the fore foot and the speed detector at the body segment. First, a ground contact detector (an on-off mechanical switch in the fore foot) is tested. By measuring the duration of a swing phase (i.e. the duration of the leg in the air), the stability of locomotion can be estimated. In Figure 7-7, the duration of the swing phase during 10 seconds of experiment are plotted with respect to the phase parameter ϕ . This figure shows that the stability of the locomotion can be identified by measuring the duration. For instance, with

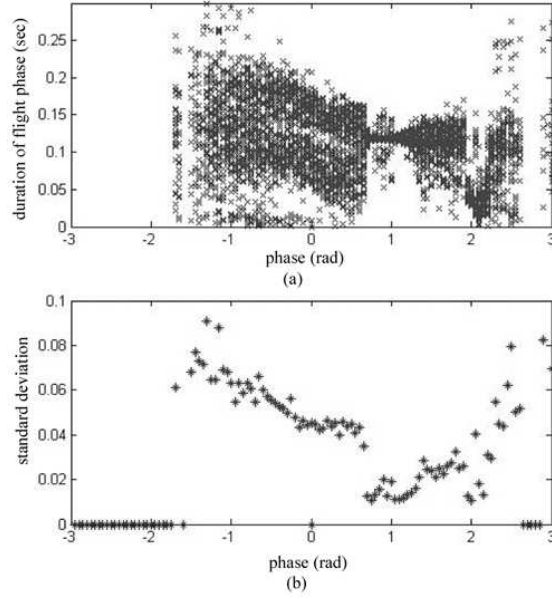


Figure 7-7: Body dynamics during the locomotion experiment measured by a contact detector.(a) distribution of the flight phase durations against the phase parameter, and (b) its standard deviation.

the phase parameter around 1.0 radian, the duration is constant at approximately 0.1 second, which indicates that the locomotion behavior is periodic. By contrast, the locomotion with values ϕ between -1.5 to 0.5 shows a large variance, which can be interpreted that the locomotion is rather chaotic. The stability of locomotion is more clearly shown by calculating the standard deviation (SD) (Figure 7-7(b)), in which the lower the value of SD, the more stable locomotion. Note that the plots of $SD = 0.0$ indicate that the robot could not successfully finish 10-second locomotion experiment, but it fell over.

In a similar way, we have conducted the simulation experiments by changing both parameters of frequency and phase. Figure 7-8(a-0) shows the distribution of SD. In the rest of this paper, we call this two-dimensional diagram “behavior landscape”.

Now we introduce another sensory channel which measures the average forward speed of locomotion. (We assume that the robot has a vision sensor which measures the optic flow, for example.) The average forward speed also contains temporal information which indicates the characteristics of locomotion behavior. For example, the average forward speed is generally faster when the locomotion behavior is periodic. Figure 7-8(b-0) shows the behavior landscape in terms of the average forward speed. The average forward speed is obtained in the same 10-second locomotion experiments in which SD was measured.

It is important to mention that there is a certain “structure” in these behavior landscapes. To show them clearly, we applied some threshold values. With these thresholds, we re-draw the behavior landscape with the white and black patches, which indicate the values of +1.0 and -1.0, respectively, as shown the Figure 7-8(a-1-3 and b-1-3). For example, the figure (a-1) has a white region at the right side of

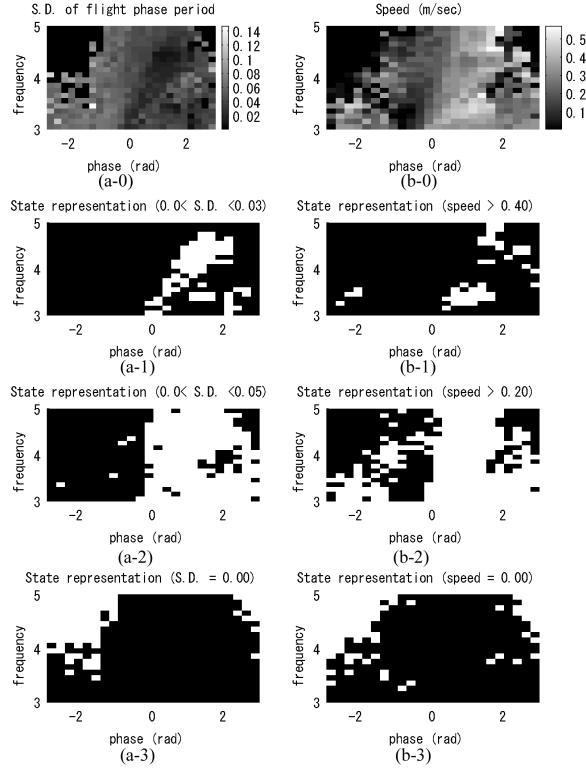


Figure 7-8: Behavior landscape obtained by a ground contact detector (a-0), and the visual velocity detector (b-0). This landscape is then segmented by threshold in (a-1-3) and (b-1-3).

the figure, which indicates the “periodic” locomotion; the figure (a-2) shows a large white region in the right half which corresponds to “relatively stable” locomotion; and the figure (a-3) shows the regions of “unstable” locomotion. In a similar way, the figure (b-1) shows the regions of “fast” locomotion; (b-2) “relatively fast”. Note that all these physically meaningful terms of stability and velocity (the words with double quotations) are from observer’s perspective, and the robot itself does not “know” what these values mean. However, these physically meaningful states can potentially be discretely identifiable owing to the landscape structures originated in the body dynamics.

7.5 Sensing Physical Properties

This section explores how the measurement of body dynamics can be used for sensing. Two case studies will be introduced by using the above-mentioned simulation, in which two physical parameters were changed. In the first series of experiments, we set the body mass of the robot with three different values, and then analyze how the robot could be discriminate these differences through two sensory channels. In the second experiment, the coefficient of friction is examined also with three different

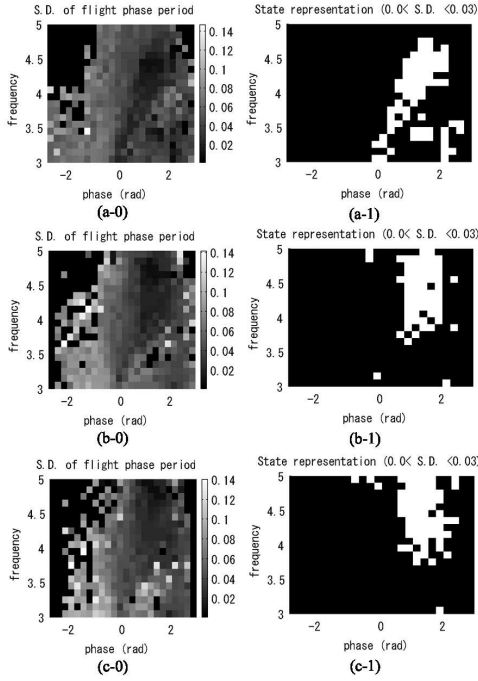


Figure 7-9: The different dynamics observed by the contact detector with respect to the different body mass of (a) 0.5, (b) 1.0 and (c) 1.5 kg. The landscape is then segmented by threshold in (a,b,c-1).

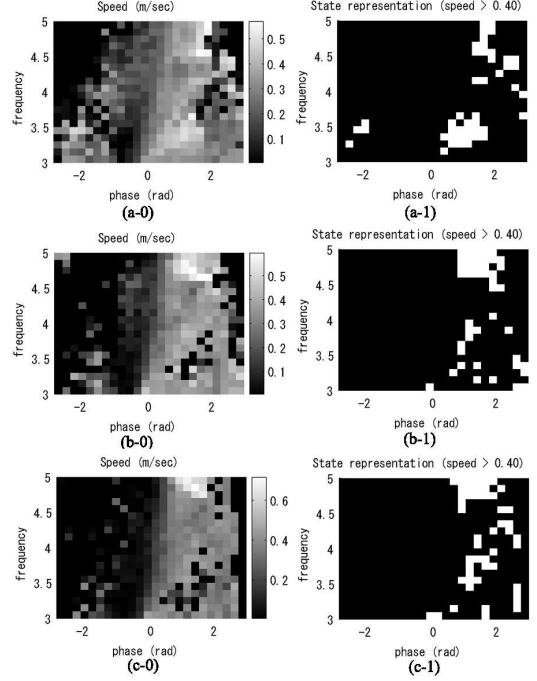


Figure 7-10: The different dynamics observed by the speed detector with respect to the different body mass of (a) 0.5, (b) 1.0 and (c) 1.5 kg. The landscape is then segmented by threshold in (a,b,c-1).

values.

7.5.1 Effect of Body Mass

We conducted the three simulation experiments in the same way as described in the previous section, but with three different body mass of 0.5, 1.0 and 1.5 kg by increasing the weight of the spinal segment. And again, the stability of the behavior is analyzed with respect to SD and average forward speed by varying the motor control parameters. The result obtained by the contact detector is shown in Figure 7-9 and the one by the speed measurement is shown in Figure 7-10. As shown in Figure 7-9, the rough structures of the figures (a,b,c-0) are somewhat similar; the area of “unstable” locomotion is in the upper left corners; the area of “periodic” locomotion is at the upper right regions. To show it more clearly, we again applied a threshold value as shown in Figure 7-9(a,b,c-1). (A value of threshold is heuristically determined.) By setting a threshold, we could see that the stable region moves toward higher frequency as the body mass increases. The average forward speed shows an even clearer tendency; with the light body mass, there are two peaks in the landscape, i.e. the regions at the lower middle and at the upper right, whereas the region of lower middle disappears as the body mass increases.

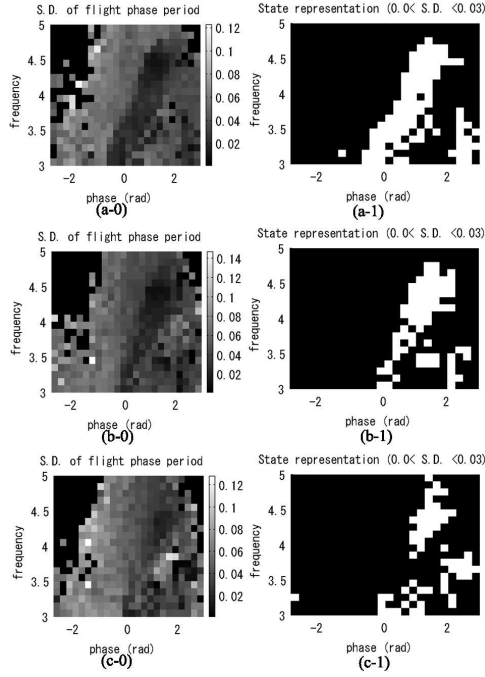


Figure 7-11: The different dynamics observed by the contact detector with respect to the different ground friction of (a) 0.5, (b) 0.65 and (c) 0.8. The landscape is then segmented by threshold in (a,b,c-1).

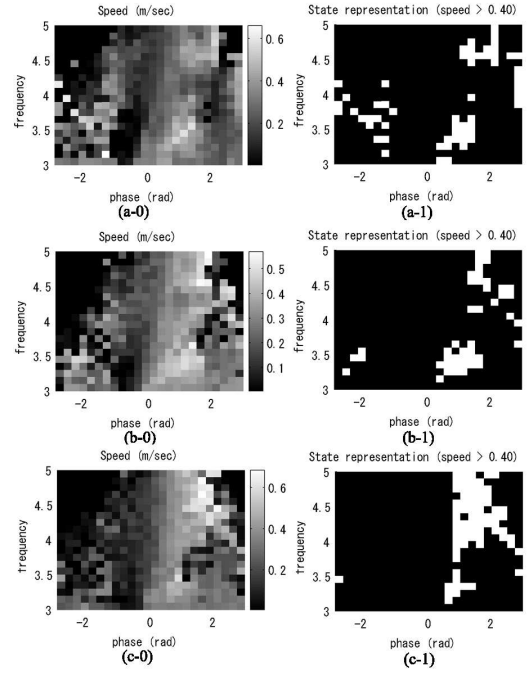


Figure 7-12: The different dynamics observed by the speed detector with respect to the different ground friction of (a) 0.5, (b) 0.65 and (c) 0.8. The landscape is then segmented by threshold in (a,b,c-1).

An important implication from these experiments is that the difference of the body mass can be identified by using two different sensory channels of the contact detector and the vision sensor. This is because the physical differences are reflected in the dynamic behavior of the body, and the foot contact and the forward speed are physically related to the body mass. As more concrete example, with the light body weight, the periodic running behavior is observed by the sensors at the range of middle motor frequency, whereas the sensors indicate more unstable locomotion as the weight increases.

7.5.2 Effect of Ground Friction

The next case study focuses on the difference in the environment, rather than the body of the robot itself. By following the same procedure as the previous experiments, we now examine the behavior landscape with three different friction coefficients in the ground interaction model, 0.5, 0.65, and 0.8. (The body mass is set to 0.5kg.) The distribution of SD is shown in Figure 7-11 and the average forward speed in Figure 7-12.

From the distribution of SD shown in Figure 7-11, the difference in the ground friction can be clearly identified between (a-1) and (c-1); the middle region at low

frequency disappears as the friction coefficient increases. For the average forward speed, on the other hand, there is a large white region at the upper right with the high ground friction (Figure 7-12(c-1)).

This experimental result again shows that both contact detector and visual sensor are able to display the difference in the ground friction. For example, when the ground friction is changed from low to high, the periodic running behavior is no longer possible at the low frequency motor control, which can be detected by a contact detector and a vision sensor.

7.6 Discussion

The experimental results presented in this paper demonstrated potential importance of body dynamics for sensing. This section speculates the implications of the experimental results with respect to the task of object recognition and category learning, which are two fundamental functions for adaptive autonomous systems.

Recognition through body dynamics

From the experimental results shown in this paper, it is shown that the stability of dynamic system-environment interaction can be exploited for the recognition of physical properties in the environment. For example, because the locomotion model has a preferred control parameters in a specific environmental condition, a distinctive behavior pattern is induced in a different environmental condition even with the same control parameters. The substantial change of behavior is then reflected in the sensory channels with discretely identifiable states (i.e. the white regions in Figure 7-11 and 7-12). One of the benefits gained from this approach is that recognition process of the environment can be very simplified; A simple thresholding is sufficient to discriminate the environmental properties. In other words, the interaction derived from body dynamics can “structure” the sensory information for the recognition of the environment.

Another significant benefit of this approach is that the body dynamics plays a role of “interpreter” of physical properties for the sensory system. As shown in this paper, for example, the body mass and the ground friction can be estimated by using a visual sensor, an on-off contact detector, an inertia sensor, a joint angle sensor and a motor torque sensor. The underlying mechanism of this unique characteristic is that, because the environmental properties are reflected in the behavior patterns of the body, the properties can be estimated through the behavior of each component contributing to the whole body dynamics. As a result, many sensory channels can potentially be used for estimating these properties.

Toward category learning

The feature of multi-modal sensing is particularly important for situated systems, i.e. the systems that acquire the information about the environment through their own sensory systems. For a situated system, the sensory information acquired through one sensory channel is not very meaningful. Generally in the conventional robotic

systems, sensory information is interpreted by a human designer and implemented in a control program. For a system which grows through the interaction with the environment, however, grounding is a fundamental issue as pointed out by the so-called “symbol grounding problem” [102, 37, 127]. For the symbol grounding problem, sensory information becomes more “meaningful” by correlating multi-modal sensory information. Because information from each sensory channel is generated by a certain physical interaction, the robot is able to learn the relation between different physical interactions by correlating the respective information. For example, the body mass can actually be measured by a single sensory channel, a simple pressure sensor on the foot. The information extracted from this sensory channel, however, becomes more meaningful if it is combined with information from other sensory channels, e.g. locomotion speed, the force exerted on the leg joints, energy consumption, and motor signals. The robot might be able to “understand” the meaning of the slope angle or of high friction, by correlating sensory patterns from different channels.

From the experimental results of multi-modal sensory information, we could obtain an additional implication in terms of control strategy and category learning. As demonstrated in the experimental results in section 3, no significant differences can be acquired in the sensory information for categorization when the behavior is actively stabilized by tuning the control parameters. However, as shown in Figure 7-11 and 7-12, because the system requires the different control parameters in a different environment for the stable locomotion process, the motor control parameters in isolation can be used for the identification of the environment. This might be the reason that efferent copy plays an important role for the task of categorization in biological systems.

7.7 Summary

This paper presents a few case studies demonstrating the conceptual strategy to exploit body dynamics for sensing. By exploring a dynamic locomotion model of a four-legged robot in simulation and the real world, a number of benefits of this approach are explained in concrete terms. In particular, it is shown that, by exploiting the system-environment interaction derived from body dynamics, a few physical properties can be reflected in the sensory information with a set of discretely identifiable states over multi-modal sensory space. Although we still have to elaborate what are the “good” body dynamics for sensing, the experimental results are highly encouraging toward our further understanding of the relation between morphological properties, body dynamics, control and sensing particularly for object recognition and category learning of embodied autonomous systems.

Chapter 8

Final Discussion

In this thesis, we have discussed conceptual principles of cheap design, behavioral diversity, and cognitive processes through experimental studies, using several real-world robots. Although these principles provide significant insights, they need to be elaborated further with a number of additional case studies. This chapter summarizes the results and contributions of this thesis and speculates about broader perspectives.

8.1 Summary of Results

In Chapter 2, based on the biological knowledge of visual navigation in flying insects, we investigated a computational model of Elementary Motion Detectors (EMDs) and its response to the movement of a robotic platform. The EMD model was then implemented in a control architecture for course stabilization and visual odometry, which are the mechanisms required for goal-directed visual navigation. This control architecture was tested in a two-dimensional simulation environment in order to analyze the feasibility of the navigation model. Sensory morphology and the number of EMD modules were identified to be important parameters to achieve visual navigation in an environment with noise.

In Chapter 3, the control architecture investigated in Chapter 2 was augmented for three-dimensional goal-directed navigation by integrating a reflex which compensates for the vertical movement. An untethered flying robot was used to investigate the control architecture in an unstructured environment. It was shown that three-dimensional goal-directed navigation is possible by using the course stabilization and odometry mechanisms, but the odometry performance was somewhat dependent on the route that the robot traveled. This dependency of the odometry response to the route, however, can be corrected through a learning process, if the sensory morphology is properly taken into account.

Chapter 4 introduced the behavioral diversity of a locomotion robot, Stumpy, which is driven by an inverted pendulum. Even though the robot has only two actuated joints, it is able to exhibit a rich variety of locomotion behaviors with several different gaits and locomotion directions. It was shown how the morphological properties, such as body dimension, weight distribution, and intrinsic stability achieved

by the wide elastic feet, can be exploited for the purpose of locomotion.

The behavioral diversity of Stumpy was explored further in Chapter 5. We have observed several different kinds of behaviors including different locomotion gaits and directions by using a single actuated joint. The influence of ground friction was also investigated, and it was shown that the behavioral diversity of the robot relies significantly on the intrinsic stability in different kinds of behaviors and environments.

In Chapter 6, another type of locomotion system of a four-legged robot, Puppy, was investigated. Although this robot has a more complicated design of the body (which contains 8 actuated and 4 passive elastic joints), rapid legged locomotion was demonstrated without the need of sensory feedback, owing to the intrinsic self-stabilizing character. In addition, the use of the self-stabilization mechanism leads to the computationally simplest control of forward velocity.

And finally in Chapter 7, the influence of dynamic locomotion behavior on cognitive processes was explored by using a four-legged robot simulation. Because dynamic locomotion is relying considerably on body design and environmental constraints, body mass and ground friction were recognized through dynamic locomotion behavior by using a number of different sensory channels including an on-off touch sensor and a visual motion detector. It was shown that the physical properties of body and environment were reflected on the sensory information through the dynamic locomotion behavior. Further speculation suggests that such a “structured” sensory information can simplify the tasks of cognitive processes such as object recognition, symbol grounding, and category learning.

8.2 Evaluation and Perspectives

Although we have discussed the conceptual design principles (i.e. body dynamics, sensory systems, and adaptive control) in Chapter 1, the exploration is still in a premature stage, and therefore needs to be elaborated with many more case studies. In fact, we still do not know how to design and construct “good bodies” for dynamic behavior. For example, Stumpy and Puppy have been designed and constructed with much know-how developed through a number of cycles of trial and error, which remain to be formulated further in dynamics, control engineering and information theoretic terms.

The direct contribution of this is two-fold: On the one hand, the conceptual design principles are explained with a set of concrete experimental work, and on the other, the experimental studies suggest a few potential real-world applications. Because the latter contribution is rather self-explanatory from the technical details outlined in the previous chapters, here we evaluate how the conceptual design principles are related to further issues in the fields of robotics, artificial intelligence, biology, psychology, and neuroscience.

In summary, these further issues can be categorized into the following three directions of research. Firstly, we have shown that the synthetic methodology (i.e. understanding by building robots) is a powerful explanatory tool, with which we can model the mechanisms of interest and test them in the real world for a system-

atic exploration. Especially for biological sciences such as ethology, neuroscience, and biomechanics, it is often difficult to estimate how much biological systems rely on “cheap” mechanisms to achieve adaptive behavior. For example, as discussed in Chapter 1, Behavior Types I and II are particularly difficult to investigate without synthetic studies. Obviously, the cheap mechanisms introduced in the case studies do not explain the entire range of adaptive behavior of complex biological systems, but they provide significant insights which are usually difficult to identify in the investigation of living organisms (refer to section 8.3, for example). Secondly, the case studies explored in this thesis provide additional evidence that the adaptive behavior cannot be fully understood only by investigating the “body” and the “mind” independently. Especially, we have demonstrated that “high-level” cognitive processes can emerge from the “low-level” specifications such as morphology, material properties, and the environment dependency of control (see section 8.4.). And thirdly, the case studies of cheap design and behavioral diversity provide a number of implications for the progress of further challenging topics such as an incremental design strategy. By understanding the underlying “cheap” mechanisms for adaptive behaviors, we are able to obtain additional insights into the evolutionary and ontogenetic developmental processes (see section 8.5).

In the following sections, we will speculate about these issues further based on the achievements laid out in this thesis.

8.3 Body Dynamics in Nature

As explained in Chapter 1, one of the major contributions of this thesis is to demonstrate the behavioral diversity by using Behavior Types II and III. Some of the future work includes how the design principles of body dynamics can be applied for our further understanding of adaptive behaviors in nature.

8.3.1 Cheap Design for Speed and Precision

Since the foundation of behavior-based robotics, one of the main interests in the field of adaptive behavior study has been speed. It has been explored how quickly robots can achieve complicated adaptive behavior (e.g. [42]). The robots presented in this thesis also exhibit rapid behaviors, as shown in dynamic locomotion of Stumpy and Puppy. The navigation mechanism investigated in the case study of the flying robot could potentially be applied also for fast movement, although the behavior of this robot is relatively slow due to its small motors. In general, cheap design makes rapid behavior possible because the systems require less control by exploiting the constraints derived from morphological properties and the ecological niche. However, an open question is how the systems can achieve speed *and* precision? As in nature, some of the biological systems are able to catch a tiny moving fly; juggle 5 balls with two hands; hit a small ball traveling at 150km/h. The case studies in this thesis suggest a few potentially important implications for this open problem.

A self-stabilization mechanism exploiting the morphological properties is a fascinating issue for achieving both speed and precision of behaviors. For example, even though we employed open-loop control without sensory feedback, the dog robot *Puppy* achieved a stable running behavior by exploiting morphological properties. For stable legged locomotion, the interaction of the four legs with the ground has to be precise, as an imprecise touch-down angle of one of the legs, for example, could cause a fatal instability and the robot could fall over. Compared to conventional legged robots which generally make use of precise sensing of, for example, body attitude and leg angles, *Puppy* has no sensor and relies on the self-stabilization mechanism derived from the compliant legs as explained in Chapter 6. Designers of robotic systems often make a significant effort to implement powerful actuators in order to mimic animals' rapid and precise behaviors and their extremely high muscle performance. However, it has been known that the material properties are often exploited to generate some of the rapid and precise behaviors even in biological systems (for examples of arm movement, see [124, 28], and for leg movement, see [2, 74, 40]).

Despite the importance of morphological self-stabilization mechanisms, an additional improvement could be made by utilizing control. So far, it is only partially understood how to apply sensory feedback while exploiting body dynamics. In other words, the question is how the various Behavior Types can be integrated into a system, as investigated in the hand-eye coordination behavior of human (e.g. [124, 117]). It is interesting to explore this line of research in relation to the mechanisms of learning and body schema, since the physical body properties are required for feedforward control. Another approach is the use of informational dynamics which is intrinsic to some of the neural structures, such as central pattern generator models (e.g. [114, 63, 59]). Because of the self-organizing character of these models (such as the entrainment phenomenon), the sensory information could be "loosely" processed without losing the characteristics of exploiting body dynamics as discussed in Chapter 1. A question that arises from this argument seems to be how the balance between body dynamics and informational dynamics would be achieved as discussed in [62].

8.3.2 Body Dynamics of Artificial and Biological Systems

In this thesis, we have focused on how adaptive behaviors can emerge from the interaction between morphology, control, and environment by using the synthetic methodology. This approach also contributes considerably to understanding animals' behavior as shown in the navigation of bees (Chapter 2 and 3, see also [122]). From the case studies shown in this thesis, one of the issues that needs to be discussed is in which level we should abstract animals' adaptive behaviors. For example, all of the legged robots can be biologically plausible in a sense.

In contrast to the conventional two-legged robots, a distinctive approach is shown in Figure 8-1, which demonstrates one of the mechanisms from a recent comparative study of bipedal locomotion in a human and a robot [58]. Although the passive dynamic walking provided a significant impact on the mechanism of walking behavior, it could not explain the complicated behavior of the knee joint, which generally has three-peak cycles of angular movement. This is important for three purposes: At

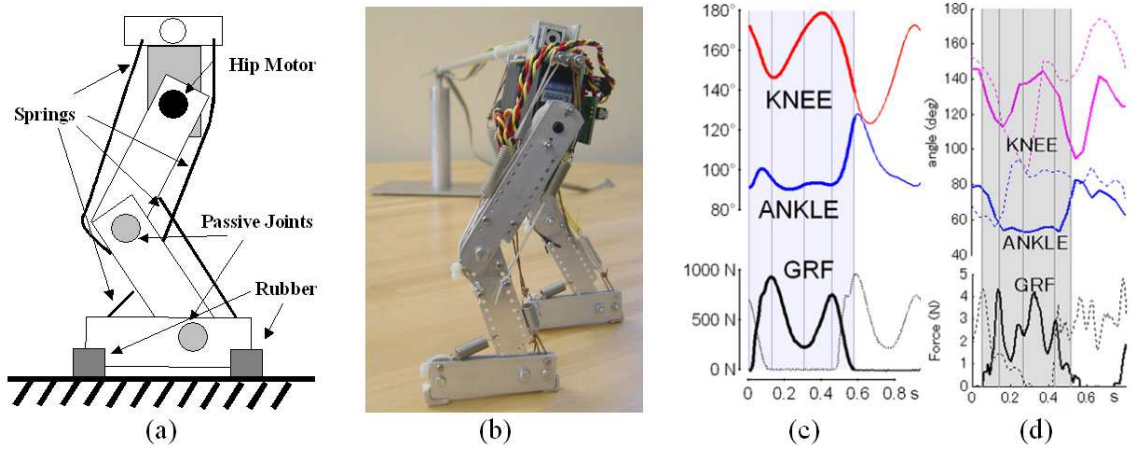


Figure 8-1: (a) Schematics of the robot design, (b) Photograph of the robot with the supporting rotational bar, (c) Knee and ankle angular trajectories and ground reaction force of human locomotion, and (d) Those from the robot experiment.

the beginning of the stance phase (the left region in the figure), the angle of the knee joint goes down (flex) to avoid impact, then it goes up (extend) to support the body. Finally it decreases (flex) again to achieve ground clearance during the swing phase. Because the passive dynamic walking does not explain this leg operation during walking behavior, it is still believed that a lot of control is involved in the walking behavior of humans. However, the newly developed model which consists of passive knees and ankle joints and an elastic tendon system show that, by exploiting the interaction between the actuated joint, passive joints and the ground reaction force, we found it possible to achieve a biologically plausible walking behavior with Behavior Type II. An implication from this example is that the knee movement can be generated by the intrinsic body dynamics derived from the specific morphological properties.

As shown in this case study, one of the notable implications of this thesis is the fact that a different level of abstraction in adaptive behaviors in nature (i.e. body dynamics) is introduced. Throughout this thesis, by considering Behavior Type II and III, we have been able to develop and test a set of novel models that have not been explored for the comprehensive understanding of adaptive behaviors in nature so far. The investigation at the abstraction level of body dynamics will lead to further investigations of prosthetic applications and the “mutual adaptation” of biological and artificial systems [125].

8.4 From Locomotion to Cognition

Inspired by long-distance navigation of bees, the flying robot experiments demonstrated that a form of memory can actually be very simple for the purpose of navigation: The optical flow can be used for the measurement of traveling distance and course stabilization, with which the flying robot is able to learn how to reach the tar-

get locations smoothly. One of the implications from this case study suggests that the cognitive processes such as the structure of memory, cannot be viewed in isolation, but it is important to consider the cognitive processes in relation to the behavior and the active interaction with the environment.

Another case study, shown in Chapter 7, demonstrated how behaviors and the interactions with the environment can be related to the problem of “symbol grounding”. This case study illustrated how the symbols could be grounded through a dynamic interaction with the environment. In particular, the intrinsic body dynamics is an interesting property for constructing discrete sensory states. Moreover, it is important to note that these sensory states are physically grounded by exploiting the discrete behavior patterns such as locomotion gaits of the legged system.

There are, at least, three potential research directions. Firstly, it is important to consider scalability of the principle of body dynamics for sensing. In Chapter 7, we investigated how movement of the whole body can be influenced by the physical properties in the environment. The concept of body dynamics for sensing is, however, also applicable locally. For example, whiskers of rodents and skin of human fingers have intrinsic dynamics optimized for sensing, and these topics have been investigated in robotic platforms (e.g. [43, 68]). It is highly interesting to explore how local and global body dynamics can explain the higher levels of complexity in cognitive processes. Secondly, the relation between body dynamics and sensory-motor coordination has to be considered in terms of informational structures. As discussed in Chapter 7, informational structures in sensory input can be generated through dynamic interactions with the environment, while it has also been previously shown that sensory information can be structured through sensory-motor coordination [101, 83, 71]. It is an important issue how these two mechanisms are related to each other, and how the quality and complexity of informational structures can be enhanced by using both mechanisms. And thirdly, processing of structured sensory information has to be explored further. Particularly, as discussed in Chapter 1, it is still an open question how the multi-modal sensory information generated through body dynamics can be correlated to generate “meaningful” discrete states.

8.5 Embodied Incremental Development

We have built a number of robots during this thesis project (Figures 8-3, 8-4, 8-5, 8-6). Some of them function, others do not. Yet every one of them was a necessary step to develop the concepts and ideas described in this thesis. In other words, the robots that we are interested in are by no means complete at the beginning, but have to be built on the basis of previous developments. Interestingly, through the development of all these robots, similar kinds of technology result in diversification and optimization: On the one hand we have many different species such as flying, running, brachiating, and swimming robots, on the other hand, we have the step-by-step optimization as shown in the series of flying robots, Stumpy, and the dog robots. This was actually one form of evolutionary process. Owing to this series of developmental processes, there are a number of implications that provide additional

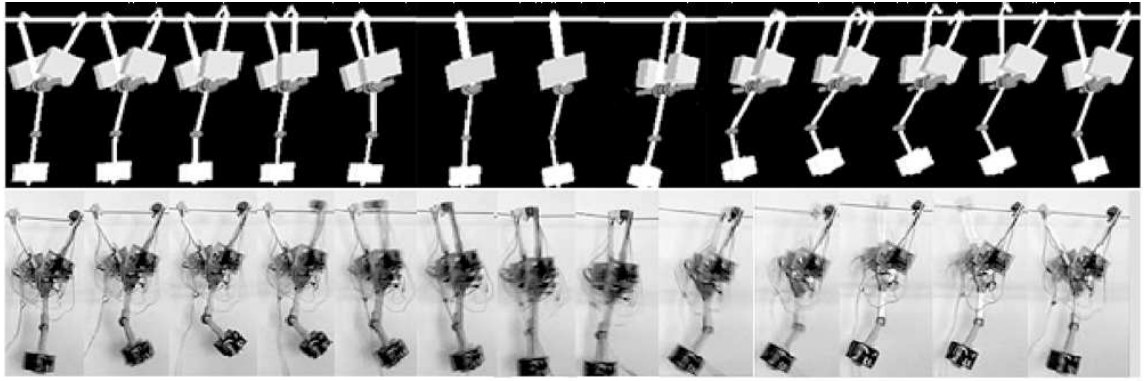


Figure 8-2: From simulation to the real world. Although the overall behavior looks similar in simulation and the real world, the control architectures of these two systems are very much different due to the simplified model of physics in simulation (e.g. the bar does not bend, and there is no friction at the passive joint)[32].

insights into the mechanisms of the incremental developmental strategy, which is potentially important for understanding the origin of adaptive behavior as discussed in Chapter 1.

8.5.1 Simulation and the Real World

A question often addressed in this line of research is why we do not use simulation to design and develop such complicated robots, instead of the “hands-on evolution”. Although we have tried simulation-based rapid prototyping (see Figure 8-2 and [32]), we found that there are a few fundamental reasons why we often cannot use a computer simulation.

One of the most significant questions of adaptive behavior in biological systems is how animals adapt to new kinds of environments and, as a result, extend their ecological niche by means of evolutionary and developmental processes. However, the physical interaction models in computer simulation are always restricted to explore such adaptation phenomena due to the boundary conditions and the approximation of the models. For example, typically the models of friction, material properties, and fluid dynamics can be only applicable within a certain range.

Secondly, in order to explore the adaptation mechanisms, the systems of interest have to be investigated in an environment with a certain degree of complexity. For example, the learning of long-distance visual navigation of bees cannot be studied in a extremely simple environment, because no visual motion can be detected. It is quite often more complicated to program a certain degree of complexity into the environment than building a real-world robot. Therefore, it is important to use the world as its own model, rather than attempt to create a model of the world for the “embodied incremental development”.

8.5.2 Design Principles for Incremental Development

Nature often makes use of similar components, and as a result, bodies are composed of repetitive structure. For example, most animal bodies contain repetitive structures of skeleton, muscles, sensory systems, cells and tissues. As another example, many design modules employ very similar mechanisms throughout different species. One of the fundamental questions in the study of incremental development of adaptive systems is the underlying mechanisms of evolutionary and ontogenetic developmental processes [29, 86, 72, 25]. In particular, what are the mechanisms that generates a form of modular and hierarchical structure that leads to adaptive functions and behaviors? Some of the mechanisms have been explained, for example, in the context of genetic regulatory networks e.g. [8, 5], and in the concept of “freezing and freeing” joint movement in a complex musculoskeletal system e.g. [6, 69].

A series of robots that were developed during this project contain such repetitive structures: For example, the visual system of flying robots comprises of a number of motion detector modules; most of the locomotion robots use similar actuation modules, for example. From this perspective, there are a few important principles for the evolutionary and developmental design strategies that we could learn from the case studies presented in this thesis. Here we discuss three conceptual implications.

Firstly, a modular structure is intrinsically robust against unstructured environment due to its redundancy. In Chapter 3, for example, the flying robot uses thousands of the same motion detector modules running in parallel. Although the experiment was conducted in some unstructured environments, and some of the motion detectors could not measure the proper optical flow, there were many more that worked properly. On average, therefore, it functions in a relatively robust manner. More generally, redundancy derived from a modular structure can increase robustness of the desired functions. It is important to note that, although a single module is sufficient to perform one kind of behavior, the redundancy results in behavioral diversity, which leads to the second implication.

Namely, because of their morphological properties, the sensors can often play more than one role. For example, the flying robot uses the same kind of elementary motion detector modules for detecting rotational, horizontal, and vertical movement depending on its sensory morphology. From the viewpoint of incremental development, therefore, redundant structures provide a possibility to emerge the behavioral diversity. Even if the modules are the same, they provide different functions because of the physical constraints such as morphology.

And thirdly, repetitive structure are important to preserve the previously developed ecological balance. A developmental process can change (remove, add or modify) only some parts of the system, and it should avoid large changes as well as starting up a completely new mechanism from scratch. In other words, a completely new device or mechanism should not be added suddenly because it might destroy the balance, or interdependencies, of the entire system. Quite often this aspect of the natural developmental process is ignored when building artificial systems. As another example, the system should be able to preserve previously developed “behaviors”, i.e. body dynamics and a type of system-environment interaction. For example, as discussed

in chapter 6, rapid legged locomotion is relying on the intrinsic body dynamics, which is determined by body weight distribution, motor torque, body dimensions, and environmental factors. If a heavy device in a part were added all at once, or if the actuators were substantially changed, the resonance frequency of the whole body would be varied, and the rapid locomotion might no longer be possible.

Although the implications explained here suggest only a few potential underlying mechanisms, further exploration of cheap design and behavioral diversity will provide clues to understand the hierarchical structures and the modularity for incremental developmental processes.

8.6 Conclusion

The concept of cheap design provided a significant paradigm shift for designing and understanding artificial systems. Compared to the conventional design methodology, the most salient feature of cheap design is that behaviors and functions of the systems are dependent on the physical properties derived from the body and the environment. Although it is generally more complicated to develop systems by following the principle of cheap design, it is the fundamental issue for a comprehensive understanding of adaptive behavior and cognitive processes. By using the synthetic methodology, this thesis explored two types of behaviors (i.e. Behavior Type II and III), which provided a set of in-depth implications for our understanding of behavioral diversity and cognitive processes in autonomous adaptive systems. Through the case studies presented in this thesis, the following conceptual principles have been demonstrated.

Body dynamics Because behavior is a result of system-environment interactions, it cannot be viewed in the framework of control and symbol processing only, but the morphological properties are essential. We have explored how body dynamics is related to behavioral diversity in terms of multiple attractor states and self-stabilization mechanisms.

Body dynamics for sensing Because the behavior of an embodied system is dependent on system-environment interactions, physical properties of the environment can be estimated by sensing the behavior of the system. By following this approach, the system is able to acquire (a) multi-modal sensory information through body dynamics and (b) discrete structures in a continuous sensory state.

Control for behavioral diversity By exploiting sensory-motor coordination, sensor morphology, and spatio-temporal patterns of sensory information, a system is able to achieve stable behavior processes and rich behavioral diversity. When the design of a system takes these points into account, a form of goal-directed behavior can be achieved by simple control.

The hands-on evolution over 30 individual robots made it possible to develop the conceptual studies of adaptive systems presented in this thesis. A unique aspect

of building robots is that we could provide concrete case studies of modeling, testing, and applications. This methodology also helps to communicate among various scientific disciplines such as biology, psychology, neuroscience, artificial intelligence, robotics, and other engineering sciences. Although we are still at the beginning of our exploration, investigations using real-world robots are highly expected to provide additional insights into complex organisms in nature.



Figure 8-3: Flying robots: Melissa I, Melissa II, and 10 flying robots built for the Science Fair at the Zurich Main Station (From left to right).



Figure 8-4: Stumpy robots: Stumpy I, Stumpy II, Stumpy III, Stumpy IV, and Mini-Stumpy.

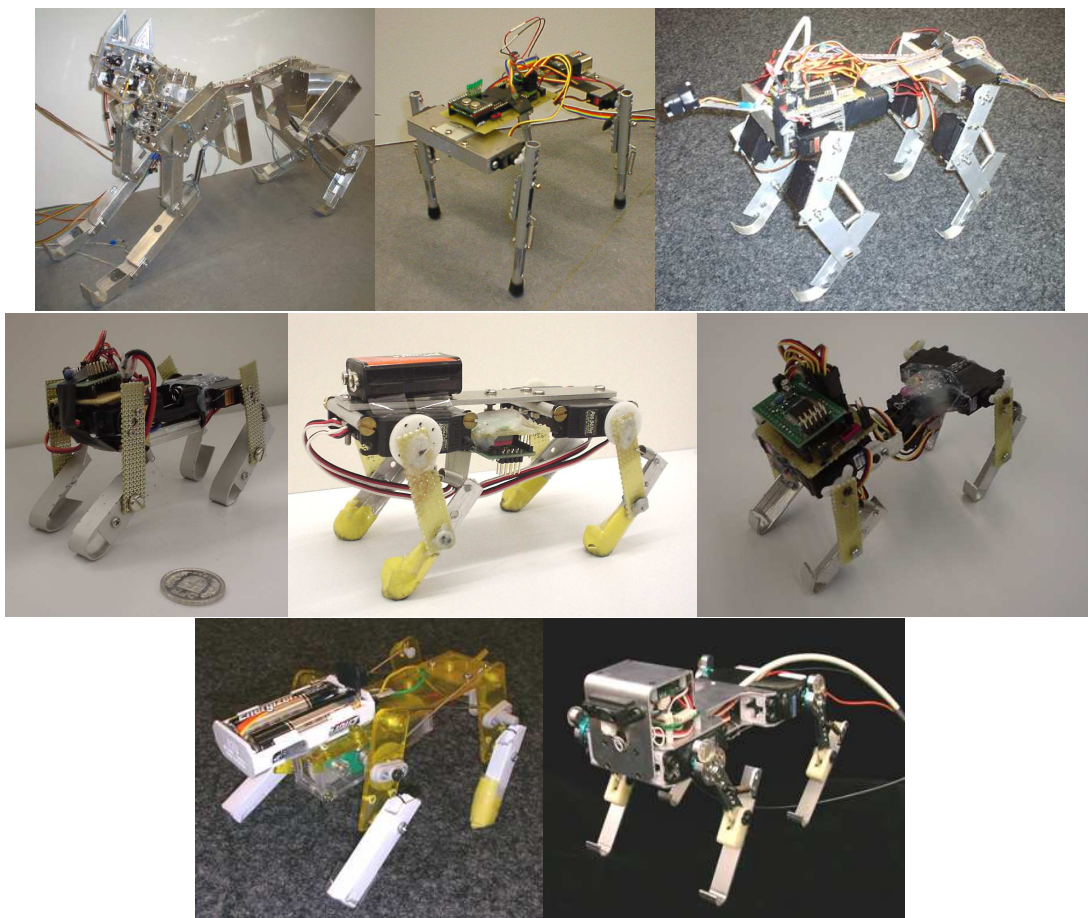


Figure 8-5: Dog robots: Geoff, AILab-scout, Puppy, Mini-Dog I, Mini-Dog II, Mini-Dog6M, Mini-Dog1M, and Mini-DogExpo.

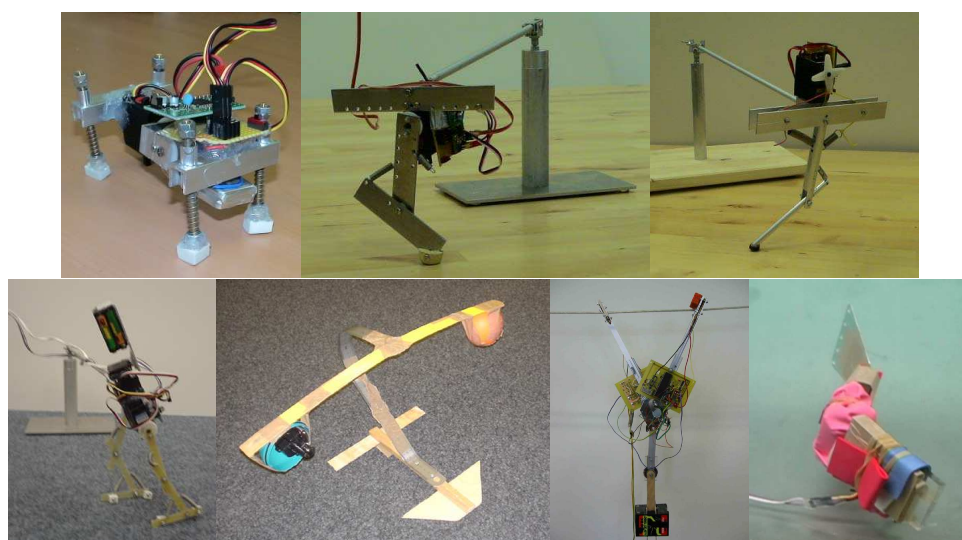


Figure 8-6: Other robots: StumpDog, Monop0, Monop1, Biped, Dumbo, Monkey, and The Fish Robot called Wanda.

Bibliography

- [1] Alexander, R. McN.(1984). Elastic energy stores in running vertebrates, *Amer. Zool.*, 24, 85-94.
- [2] Alexander, R. McN. (1990). Three uses for springs in legged locomotion, *The International Journal of Robotic Research*, 9, No. 2, 53-61.
- [3] Amidi O., Kanade T., and Fujita K., (1998). A visual odometer for autonomous helicopter flight,” *Intelligent Autonomous Systems, Y. Kakazu et al. (Eds.), IOS Press*, 123-130.
- [4] Ashby, W. R. (1956). Introduction to cybernetics, Chapman and Hall, London.
- [5] Banzhaf, W. (2004). On evolutionary design, embodiment, and artificial regulatory networks, Embodied artificial intelligence, Iida et al. (Eds), LNCS/AI Vol. 3139, Springer, 284-292.
- [6] Bernstein, N. (1967). The coordination and regulation of movements. Oxford: Pergamon.
- [7] Blickhan, R., Wagner, H., and Seyfarth, A. (2003). Brain or muscles?, *Rec. Res. Devel. Biomechanics*, 1, 215-245.
- [8] Bongard, J.C. (2002). Evolving modular genetic regulatory networks. In *Proc. IEEE 2002 Congress on Evolutionary Computation (CEC2002)*. MIT Press, 305-311.
- [9] Borst, A., and Egelhaaf, M. (1993). Detecting visual motion: Theory and models, *Visual Motion and its Role in the Stabilization of Gaze*, (Eds.) Miles, F.A. and Wallman, J., Elsevier Science, 3-27.
- [10] Brooks, R. A. (1989). A robot that walks: Emergent behaviors from a carefully evolved network. *Neural Computation* 1(2), 253-262.
- [11] Brooks, R. A. (1991). Intelligence without reason, *Proceedings of the 12th International Joint Conference on Artificial Intelligence (IJCAI-91)*, Morgan Kaufmann publishers Inc.: San Mateo, CA, USA, 569-595.
- [12] Brooks, R. A. (1991) Intelligence without representation. *Artificial Intelligence*, 47: 139-160.

- [13] Brooks, R. A. and Stein L. A. (1994). Building brains for bodies. *Autonomous Robots*, 1(1):7-25.
- [14] Buehler, M., Battaglia, R., Cocosco, A., Hawker, G., Sarkis, J. and Yamazaki, K. (1998). Scout: A simple quadruped that walks, climbs and runs In: *Proc. Int. Conf on Robotics and Automation*, 1707-1712.
- [15] Cavagna, G. A., Heglind, N. C. and Taylor, C. R.: Mechanical work in terrestrial locomotion: Two basic mechanisms for minimizing energy expenditure, *American Journal of Physiology* 233, 243-261, 1977.
- [16] Chahl, J. S., Srinivasan, M. V., (1997). Reflective surfaces for panoramic imaging, *Applied Optics*, vol. 36, No. 31, 8275-8285.
- [17] Cham, J. G., Bailey, S. A., Clark, J. E., Full, R. J. and Cutkosky, M. R.: Fast and robust: hexapedal robots via shape deposition manufacturing, *The International Journal of Robotics Research*, 21, Issue 10, 869-882, 2002.
- [18] Clancey, W. J. (1989). The frame of reference problem in cognitive modeling. In *Proceedings The Eleventh Annual Conference of the Cognitive Science Society*, 107-114, Hillsdale, New Jersey. Lawrence Erlbaum.
- [19] Clancey, W. (1991). The frame of reference problem in the design of intelligent machines: In K. vanLehn, (Ed.), *Architectures for intelligence: The twentysecond Carnegie symposium on cognition*.(pp. 357-424). Hillsdale, NJ: Lawrence Erlbaum Associates.
- [20] Collins, S. H., Wisse, M., and Ruina, A. (2001). A three-dimentional passive-dynamic walking robot with two legs and knees. *International Journal of Robotics Research* 20, 607-615.
- [21] Collins, S., Ruina, A., Tedrake, R., and Wisse, M. (2005). Efficient bipedal robots based on passive dynamic walkers, *Science Magazine*, Vol. 307, 1082-1085.
- [22] Cruse, H., Bartling, C. H., Brunn, D. E., Dean, J., Dreifert, M., Kindermann, T., and Schmitz, J. (1995). Walking: A complex behavior controlled by simple systems. *Adaptive Behavior* 3(4), 385-418.
- [23] Dennett, D. (1987). Cognitive wheels: The frame problem in artificial intelligence, in Pylyshyn, Z.W. (ed.), *The Robot's Dilemma: The Frame Problem in Artificial Intelligence*, Norwood, NJ: Ablex.
- [24] Dickinson, M.H., C.T. Farley, R.J. Full, M.A.R. Koehl, R. Kram, and S. Lehman. (2000). How animals move: An integrative view. *Science* 288:100-106.
- [25] Edelman, G. M. (1988). *Neural darwinism: The theory of neuronal group selection*. Basic Books, New York.

- [26] Fagg, A. H., Lewis, J. F., and Bekey, G. A., (1993). The use autonomous flying vehicle: An experiment in real-time behavior-based control, In Proceedings of the IEEE/RSJ International Conference on Intelligent Robots and Systems, 1173-1180.
- [27] Fend, M.: Whisker-based texture discrimination on a mobile robot. To appear in Proceedings of the Eighth European Conference on Artificial Life (ECAL), 2005.
- [28] Flanagan, J. R., Wing, A. W., Haggard, P. (Eds.) (1998). Hand and brain : The neurophysiology and psychology of hand movements, Academic Press.
- [29] Floreano, D., Mondada, F., Perez-Urbe, A., and Roggen, D. (2004). Evolution of embodied intelligence, Embodied artificial intelligence, Iida et al. (Eds), LNCS/AI Vol. 3139, Springer, 293-311.
- [30] Franceschini N., Pichon J. M., Blanes, C., (1992). From insect vision to robot vision, *Phil. Trans. R. Soc. Lond. B*, 337, 283-294.
- [31] Franceschini, N., Riehle, A., Nestour, A., (1989). Directionally selective motion detection by insect neurons, Facets of Vision, Stavenga/Hardie(Eds.), Springer-Verlag, 360-390.
- [32] Frutiger, D., Bongard, J. and Iida, F. (2002). Iterative product engineering: Evolutionary robot design, The Fifth International Conference on Climbing and Walking Robots (CLAWAR'02), 619-626.
- [33] Fukuoka, Y., Kimura, H., and Cohen, A. H. (2003). Adaptive dynamic walking of a quadruped robot on irregular terrain based on biological concepts, *Int. Journal of Robotics Research*, Vol.22, No.3-4, 187-202.
- [34] Full, R.J. and Koditschek, D. E. (1999). Templates and anchors - Neuromechanical hypotheses of legged locomotion on land. *J. exp Bio.* 202, 3325-3332.
- [35] Furst, S., and Dickmanns, E. D., (1998). A vision based navigation system for autonomous aircraft, Intelligent Autonomous Systems, Y. Kakazu et al. (Eds.), IOS Press, 765-774.
- [36] Gould, J. L., Gould, C. G., (1988). The honey bee, Scientific American Library, New York.
- [37] Harnad, S. (1990). The symbol grounding problem, *Physica D*, 42: 335-346.
- [38] Harrison, R. R., Koch, C., (1998). A neuromorphic visual motion sensor for real-world robots, Workshop on Defining the Future of Biomimetic Robotics, IROS'98.
- [39] R. Hayashi and S. Tsujio (2001). High performance jumping movements by pendulum-type jumping machines In *Proc. IEEE/RSJ Int. conf. on Intelligent Robots and Systems* 722-727.
- [40] Herr, H. M., McMahon, T. A. (2000). A trotting horse model, *The International Journal of Robotics Research*, 19, No. 6, 566-581.

- [41] Hirose, S. (1993). *Biologically Inspired Robots — Snake-like Locomotors and Manipulators*, Oxford University Press.
- [42] Holland, O. (2004). The future of embodied artificial intelligence: Machine consciousness?, *Embodied artificial intelligence*, Iida et al. (Eds), LNCS/AI Vol. 3139, Springer, 37-53.
- [43] Hosoda, K. (2004). Robot finger design for developmental tactile interaction - Anthropomorphic robotic soft fingertip with randomly distributed receptors, Iida et al. (Ed.), *Embodied Artificial Intelligence*, Springer, Vol.3139, 219-230.
- [44] Huber, S. A., and Bulthoff, H. H. (1997). Modeling obstacle avoidance behavior of flies using an adaptive autonomous agent, *Proceedings of 7th International Conference on Artificial Neural Networks, ICANN '97*, W.Gerstner et al. (Eds.), 709-714.
- [45] Huber S. A., Franz M. O., Bulthoff H. H., (1999). On robots and flies: Modeling the visual orientation behavior of flies, " *Robotics and Autonomous Systems 29, Elsevier*, 227-242.
- [46] Hyon, S., Kmijo, S., Mita, T.: 'Kenken' - A Biologically Inspired One-Legged Running Robot *J. of the Robotics Society of Japan*, Vol. 20, No. 4, 453-462, 2002.
- [47] Iida, F., and Lambrinos, D., (2000). Navigation in an autonomous flying robot by using a biologically inspired visual odometer, *Sensor Fusion and Decentralized Control in Robotic System III*, Photonics East, Proceeding of SPIE, vol. 4196, 86-97.
- [48] Iida, F., Dravid, R., and Paul, C., (2002). Design and control of a pendulum driven hopping robot, *Proc. of the IEEE/RSJ International Conference on Intelligent Robots and Systems (IROS 02)*, 2141-2146.
- [49] Iida, F. (2001). Goal-directed navigation of an autonomous flying robot using biologically inspired cheap vision. *Proceedings of the 32nd ISR (International Symposium on Robotics)*, 1404-1409.
- [50] Iida, F. (2002). Biologically inspired visual odometer for navigation of a flying robot. *Proc. of Intelligent Autonomous Systems 7*, 142-149.
- [51] Iida, F. (2003). Exploiting friction for a hopping robot. *Proc. of Adaptive Motion of Animals and Machines*.
- [52] Iida, F. and Pfeifer, R. (2004). "Cheap" rapid locomotion of a quadruped robot: Self-stabilization of bounding gait, *Intelligent Autonomous Systems 8, F. Groen et al. (Eds.)*, IOS Press: Amsterdam The Netherlands, 642-649.
- [53] Iida, F. and Pfeifer, R. (2004). Self-stabilization and behavioral diversity of embodied adaptive locomotion. *Embodied artificial intelligence*, Iida et al. (Eds), LNCS/AI Vol. 3139, 119-128.

- [54] Iida, F., Pfeifer, R., Steels, L., Kuniyoshi, Y. (Eds.) (2004). Embodied artificial intelligence. Lecture Notes in Computer Science, Vol. 3139, Springer, ISBN: 3-540-22484-X.
- [55] Iida, F. (2005). Cheap design approach to adaptive behavior: Walking and sensing through body dynamics, International Symposium on Adaptive Motion of Animals and Machines 2005.
- [56] Iida, F., Gomez, G. J., and Pfeifer, R. (2005). Exploiting body dynamics for controlling a running quadruped robot. Proceedings of the 12th Int. Conf. on Advanced Robotics (ICAR05). July18th-20th, Seattle, U.S.A., 229-235.
- [57] Iida, F. and Pfeifer, R. (2005). Structuring sensory information through body dynamics, IROS05 Workshop on Morphology, Control and Passive Dynamics.
- [58] Iida, F., Minekawa, Y., Rummel, J. and Seyfarth, A. (2005). Toward a human-like biped robot with compliant legs, *Intelligent Autonomous Systems 9*, (in press).
- [59] Ijspeert, A.J. (2001). A connectionist central pattern generator for the aquatic and terrestrial gaits of a simulated salamander. *Biological Cybernetics*, 84(5):331-348.
- [60] Ioi, K., Igarashi H. and Murakami, A. (2001). Design of a gravitational wheeled type robot In *Proc. International Symposium on Robotics* 175-179.
- [61] Ishiguro, A., Ishimaru, K., Hayakawa, K., and Kawakatsu, T. (2003). Toward a "well-balanced" design: A robotic case study -How should control and body dynamics be coupled?-, in *Proc. of The 2nd International Symposium on Adaptive Motion of Animal and Machines*.
- [62] Ishiguro, A., and Kawakatsu, T. (2004.) How should control and body systems be coupled? A robotic case study, Embodied artificial intelligence, Iida et al. (Eds), LNCS/AI Vol. 3139, Springer, 107 - 118.
- [63] Kimura, H., Fukuoka, Y., Hada, Y., Takase, K. (2002). Three-dimensional adaptive dynamic walking of a quadruped - rolling motion feedback to CPGs controlling pitching motion -, *Proc. of the 2002 IEEE International Conference on Robotics and Automation*, 2228-2233.
- [64] Kubow, T. M., Full, R. J. (1999). The role of the mechanical system in control: a hypothesis of self-stabilization in hexapedal runners, *Phil. Trans. R. Soc. Lond. B*, 354, 849-861.
- [65] Kuniyoshi, Y., Yorozu, Y., Inaba, M., and Inoue, H. (2003). From visuo-motor self learning to early imitation -a neural architecture for humanoid learning. International Conference of Robotics and Automation 2003, 3132-3139.

- [66] Kuniyoshi, Y., Yorozu, Y., Ohmura Y., Terada, K., Otani, T., Nagakubo, A., Yamamoto T. (2004). From humanoid embodiment to theory of mind, Embodied artificial intelligence, Iida et al. (Eds), LNCS/AI Vol. 3139, Springer, 202 - 218.
- [67] Lichtensteiger, L., and Pfeifer, R. (2002). An optimal sensor morphology improves adaptability of neural network controllers, In: Jose R. Dorronsoro (Ed.): Artificial Neural Networks - ICANN 2002, International Conference, Lecture Notes in Computer Science, LNCS 2415, Springer, Heidelberg. 850-855.
- [68] Lungarella, M., Hafner, V. V., Pfeifer, R., Yokoi, H. (2002). An artificial whisker sensor for robotics, Proceedings of the IEEE/RSJ International Conference on Intelligent Robots and Systems (IROS), 2931-2936.
- [69] Lungarella, M. and Berthouze, L. (2002). On the interplay between morphological, neural and environmental dynamics: A robotic case-study. Adaptive Behavior, 10(3-4):223-241.
- [70] Lungarella, M., Metta, G., Pfeifer, R., and Sandini G. (2003). Developmental robotics: a survey, Connection Science 15, 4, 151-190.
- [71] Lungarella, M., Pegors, T., Bulwinkle, D. and Sporns, O.: Methods for quantifying the informational structure of sensory and motor data. Neuroinformatics (to appear).
- [72] Mayr, E. (1982). The growth of biological thought, Harvard University Press.
- [73] McGeer, T. (1990). Passive dynamic walking. *International Journal of Robotics Research* 9, 62-82.
- [74] McMahon, T. A., (1984). Muscles, reflexes, and locomotion, Princeton University Press.
- [75] McMahon, T. A., Cheng, G. C. (1990). The Mechanics of Running: How Does Stiffness Couple with Speed?, *J. Biomechanics*, Vol. 23, Suppl. 1, 65-78.
- [76] Metta, G., Sandini, G., and Konczak, J. (2003). Early integration of vision and manipulation, Adaptive Behavior, 11(2): 109-128.
- [77] Mura F., Franceschini N. (1994). Visual control of altitude and speed in a flying agent, *Proceedings of 3rd international conference on Simulation of Adaptive Behavior: From Animal to Animats III*.
- [78] Murphy, K. and Raibert, M. (1985). Trotting and bounding in a planar two-legged model, In *Fifth Symposium on Theory and Practice of Robots and Manipulators*, A. Morecki, G. Bianchi, K. Kedzior (eds) Cambridge: MIT Press, 411-420.
- [79] Netter, T., and Franceschini, N. (1999). Towards nap-of-the-earth flight using optical flow, Proceedings of ECAL99, 334-338.

- [80] Netter T., and Franceschini N., (2002). A Robotic aircraft that follows terrain using a neuromorphic eye, " *Proceedings of the 2002 IEEE/RSJ Intl. Conference on Intelligent Robots and Systems*, 29-134
- [81] Neumann T. R., Bulthoff H. H. (2001). Insect inspired visual control of translatory flight, Kelemen, J. and Posik P. (Eds) ECAL2001 LNAI2159 Springer Verlag , 627-636
- [82] Nolfi S., Floreano D. (2000). Evolutionary robotics: The biology, intelligence, and technology of self-organizing machines. Cambridge, MA: MIT Press.
- [83] Nolfi, S. (2002). Power and limit of reactive agents. *Neurocomputing* 49, 119-145.
- [84] Paul, C. and Bongard, J. (2001). The road less travelled: Morphology in the optimization of biped robot In Proc. IEEE/RSJ International Conference on Intelligent Robots and Systems, 226-232.
- [85] Paul, C., Dravid, R., Iida, F. (2002). Control of lateral bounding for a pendulum driven hopping robot. *Proc. of 5th International Conference on Climbing and Waling Robots (CLAWAR 2002)*, 333-340.
- [86] Pfeifer, R. and Iida, F. (2004). Embodied artificial intelligence: Trends and challenges. Embodied artificial intelligence, Iida et al. (Eds), LNCS/AI Vol. 3139, Springer, 1-26.
- [87] Pfeifer, R., Iida, F., and Bongard, J. (2005). New robotics: Design principles for intelligent systems. *Artificial Life*, January 2005, vol. 11, no. 1-2, 99-120.
- [88] Pfeifer, R. and Lambrinos, D. (2000). Cheap Vision - Exploiting Ecological Niche and Morphology, Theory and practice of informatics: SOFSEM 2000, 27th Conference on Current Trends in Theory and Practice of Informatics, Milovy, Czech Republic; Vaclav Hlavac, et al. (Eds.), pp. 202-226.
- [89] Pfeifer, R. and Scheier, C. (1999). Understanding Intelligence. *The MIT Press*.
- [90] Playter, R. R. (1994), Passive dynamics in the control of gymnastic maneuvers , *Ph.D Thesis* Department of Aeronautical and Astronautical Engineering, Massachusetts Institute of Technology, Cambridge, Massachusetts.
- [91] Poulakakis, I., Smith, J. A. and Buehler, M. (2003). On the dynamics of bounding and extensions towards the half-bound and the gallop gaits, In: *Proc. of the 2nd Int. Symp. on Adaptive Motion of Animals and Machines*.
- [92] Pylyshyn, Z.W. (Eds.) (1987). The robot's dilemma: The frame problem in Artificial Intelligence, Norwood, NJ: Ablex.
- [93] Raibert, M. H. and Brown, H. B. (1984). Experiments in balance with a 2D one-legged hopping machine, In *Journal of Dynamic Systems, Measurement and Control* Vol. 106: 75-81.

- [94] Raibert, M. H., Brown, H. B. and Chepponis, M. (1984). Experiments in balance with a 3D one-legged hopping machine, In *International Journal of Robotics Research*, Vol 3:2, 75-92.
- [95] Raibert, M. H. (1985). Four legged-running with one legged algorithms. In *Second International Symposium on Robotics Research*, H. Hanafusa, H. Inoue (eds.) Cambridge: MIT Press, 311-315.
- [96] Raibert, M. H. (1986). *Legged robots that balance*. MIT Press, Cambridge, Massachusetts.
- [97] Reichardt W. (1969). Movement perception in insects, In *W. Reichardt (Eds.), Processing of optical data by organisms and machines*, New York: Academic, 465-493.
- [98] Ringrose, R. (1997). Self-stabilizing running In *PhD Thesis* Computer Science Dept, Massachusetts Institute of Technology.
- [99] Rossel, S., (1993). "Navigation by bees using polarized skylight," *Comparative Biochemistry and Physiology (A)* 104, 695-708.
- [100] Santos-Victor, J., Sandini, G., Curotto, F., Garibaldi, S., (1993). Divergent stereo for robot navigation: Learning from bees," *CVPR93*, 434-439.
- [101] Scheier, C., Pfeifer, R. and Kuniyoshi, Y. (1998). Embedded neural networks: exploiting constraints. *Neural Networks* 11 (7-8), 1551-1569.
- [102] Searle, J. (1980). Minds, brains and programs. *Behavioral and Brain Sciences*, 3: 417-457.
- [103] Seyfarth, A., Geyer, H., Guenther, M., Blickhan, R. (2002). A movement criterion for running, *Journal of Biomechanics*, 35, 649-655.
- [104] Simon, H.A. (1969). The sciences of the artificial. Cambridge, Mass.: MIT Press.
- [105] Spenceberg, D. and Kirchner, F.: Learning spatial categories on the basis of proprioceptive data, In *Proceedings of the 3rd International Symposium on Adaptive Motion in Animals and Machines*, 2005.
- [106] Srinivasan, M. V., Lehrer, M., Kirchner, W. H., and Zhang, S. W., (1991). Range perception through apparent image speed in freely-flying honeybees, *Visual Neuroscience*, 6, 519-535.
- [107] Srinivasan, M. V., Zhang, S. W., Lehrer, M., Collett, T. S., (1996). Honeybee navigation en route to the goal: Visual flight control and odometry, In *Navigation* (ed. R. Wehner, M. Lehrer and W. Harvey). *Journal of experimental Biology*. 199, 155-162.

- [108] Srinivasan, M. V., Zhang, S. W., and Bidwell, N., (1997). Visually mediated odometry in honeybees, *Journal of Experimental Biology*, 200, 2513-2522.
- [109] Srinivasan, M. V., Chahl, J. S., and Zhang, S. W., (1997). Robot navigation by visual dead-reckoning: inspiration from insects, *International Journal of Pattern Recognition and Artificial Intelligence*, 11(1), 35-47.
- [110] Srinivasan M. V., Poteser M., Kral K., (1999). Motion detection in insect orientation and navigation, *Vision Research* 39, 2749-2766.
- [111] Srinivasan M. V., Chahl, J.S., Weber, K., Venkatesh, S., Nagle, M.G., Zhang, S.W., (1999). Robot navigation inspired by principles of insect vision, *Robotics and Autonomous Systems* 26, 203-216.
- [112] Srinivasan M. V., Zhang S., Altwein M., and Tautz J., (2000). Honeybee navigation: Nature and calibration of the "odometer", *Science*, vol. 287, 851-853.
- [113] Srinivasan M. V., Zhang S. W., Chahl J. S., Barth E., and Venkatesh S., (2000). How honeybees make grazing landings on flat surfaces, *Biol. Cybern.* 83, 171-183.
- [114] Taga, G., Yamaguchi, Y., Shimizu, H. (1991). Self-organized control of bipedal locomotion by neural oscillators in unpredictable environment, *Biol Cybern*, 65, 147-159.
- [115] Tedrake, R., Zhang, T.W. and Seung, H.S. (2004). Stochastic policy gradient reinforcement learning on a simple 3D biped. Proc. of the 10th Int. Conf. on Intelligent Robots and Systems, 3333-3334.
- [116] Thompson, D. W. (1942). On growth and form. *Dover book: New York, NY*.
- [117] van Beers, R. J., Baraduc, P., and Wolpert, D. M. (2002). Role of uncertainty in sensorimotor control, *Phil. Trans. R. Soc. Lond. B* 357, 1137-1145.
- [118] van der Zwaan, S., Bernardino, A., Santos-Victor, J. (2002). Visual station keeping for floating robots in unstructured environments, *Robotics and Autonomous Systems* 39, 145-155.
- [119] Vogel, S. (1998). Cats' paws and catapults. *W. W. Norton & Company: London*.
- [120] von Frisch, K. (1949). Die Polarization des Himmelslichtes als orientierender Faktor bei den Tanzen der Bienen, *Experimentia*, 5, 142-148.
- [121] Vukobratovic, M. and Stokic, D. (1975). Dynamic Control of Unstable Locomotion Robots, *Mathematical Biosciences*, 24, 129-157.
- [122] Webb, B., and Consi, R. C. (Eds.) (2001). Biorobotics, AAAI Press.
- [123] Wisse, M. and van Frankenhuyzen, J. (2003). Design and construction of MIKE: A 2D autonomous biped based on passive dynamic walking. *Proceedings of International Symposium of Adaptive Motion and Animals and Machines (AMAM03)*

- [124] Wolpert, D.M., Miall, R. C., Kawato, M. (1998). Internal models in cerebellum, Trends in Cognitive Sciences, Vol. 2, No. 9, 338-347.
- [125] Yokoi, H., Arieta, A. H., Katoh, R., Yu, W., Watanabe, I., Maruishi M. (2004). Mutual adaptation in a prosthetics application, Embodied artificial intelligence, Iida et al. (Eds), LNCS/AI Vol. 3139, Springer, 146-159.
- [126] Yoshikawa, Y., Tsuji, Y., Hosoda, K., and Asada, M. (2004). Is it my body? - body extraction from uninterpreted sensory data based on the invariance of multiple sensory attributes -, In Proc. of the 2004 IEEE/RSJ International Conference on Intelligent Robots and Systems , 2325-2330.
- [127] Ziemke, T. (1999). Rethinking grounding, In Understanding representation in the cognitive sciences - Does representation need reality?, Riegler, A., et al.(Eds.), Kluwer Academic Publishers.

Publications contributing to this thesis

- Iida, F. and Lambrinos, D. (2000). Navigation in an autonomous flying robot by using a biologically inspired visual odometer, Sensor Fusion and Decentralized Control in Robotic System III, Photonics East, Proceeding of SPIE, vol. 4196, 86-97.
- Iida, F. (2001). Goal-directed navigation of an autonomous flying robot using biologically inspired cheap vision. Proceedings of the 32nd ISR (International Symposium on Robotics), 1404-1409.
- Iida, F. (2002). Biologically inspired visual odometer for navigation of a flying robot. Proc. of Intelligent Autonomous Systems 7, 142-149.
- Iida, F., Dravid, R. and Paul, C. (2002). Design and control of a pendulum driven hopping robot, Proceedings of International Conference on Intelligent Robots and Systems 2002 (IROS 02), 2141-2146.
- Iida, F. (2003). Exploiting Friction for the locomotion of a hopping robot, The 2nd International Symposium on Adaptive Motion of Animals and Machines (AMAM03).
- Iida F. (2003). Biologically Inspired Visual Odometer for Navigation of a Flying Robot, Robotics and Autonomous Systems, Vol 44/3-4, 201-208.
- Iida F. and Pfeifer R. (2004). “Cheap” rapid locomotion of a quadruped robot: Self-stabilization of bounding gait, Intelligent Autonomous Systems 8, F. Groen et al. (Eds.), IOS Press: Amsterdam, the Netherland, 642-649.
- Iida, F. and Pfeifer, R. (2004). Self-stabilization and behavioral diversity of embodied adaptive locomotion. Embodied artificial intelligence, Iida et al. (Eds), LNCS/AI Vol. 3139, 119-128.
- Iida, F. (2005). Cheap design approach to adaptive behavior: Walking and sensing through body dynamics, International Symposium on Adaptive Motion of Animals and Machines 2005.
- Iida, F. and Pfeifer, R. (2005). Structuring sensory information through body dynamics, IROS05 Workshop on Morphology, Control and Passive Dynamics.

Other publications

- Paul, C., Dravid, R. and Iida, F. (2002). Control of lateral bounding for a pendulum driven hopping Robot, Proc. of 5th International Conference on Climbing and Waling Robots (CLAWAR 2002), 333-340.
- Frutiger, D., Bongard, J. and Iida, F. (2002). Iterative product engineering: Evolutionary robot design, The Fifth International Conference on Climbing and Walking Robots (CLAWAR'02), 619-626.
- Iida, F., Pfeifer, R., Steels, L., Kuniyoshi, Y. (Eds.) (2004). Embodied artificial intelligence, LNCS/AI Vol. 3139, Springer.
- Pfeifer, R. and Iida, F. (2004). Embodied artificial intelligence: Trends and challenges. Embodied artificial intelligence, Iida et al. (Eds), LNCS/AI Vol. 3139, Springer, 1-26.
- Pfeifer, R. and Iida, F. (2005). Morphological computation: Connecting body, brain and environment. Japanese Scientific Monthly, Vol. 58, No. 2, 48-54.
- Pfeifer, R., Iida, F., and Bongard, J. (2005). New robotics: Design principles for intelligent systems. Artificial Life, January 2005, vol. 11, no. 1-2, 99-120.
- Hamburger, V., Berns, K, Iida, F. (2005). Standing up with motor primitives, International Conference on Climbing and Walking Robots (CLAWAR'05).
- Iida, F., Gomez, G. J., and Pfeifer, R. (2005). Exploiting body dynamics for controlling a running quadruped robot. Proceedings of the 12th Int. Conf. on Advanced Robotics (ICAR05). July18th-20th, Seattle, U.S.A., 229-235.
- Ziegler, M., Iida, F., and Pfeifer, R. (2005). “Cheap” underwater locomotion: Morphological properties and behavioral diversity, IROS05 Workshop on Morphology, Control and Passive Dynamics.
- Iida, F., Minekawa, Y., Rummel, J. and Seyfarth, A. (2005). Toward a human-like biped robot with compliant legs, *Intelligent Autonomous Systems 9*, (in press).

Curriculum Vitae

Last name: Iida
First name: Fumiya
Date of birth: May 4, 1974 in Tokyo, Japan
Nationality: Japan

Education

1993.04. - 1997.03 Undergraduate study of mechanical engineering at Science University of Tokyo, Japan

1997.03. Bachelor of Engineering, Science University of Tokyo, Japan

1997.04. - 1999.03 Graduate study of mechanical engineering at Science University of Tokyo, Japan

Master of Engineering, Science University of Tokyo, Japan
Title: Communicative Interaction between Human and Face Robot
Advisor: Prof. Dr. Fumio Hara

1999.04. - 2005.09. PhD candidate and research assistant at Artificial Intelligence Laboratory, Department of Informatics, University of Zurich, Switzerland

2004.04. - 2005.09. Research assistant at Locomotion Laboratory, Institute of Sports Science, University of Jena, Germany

PhD Dissertation, University of Zurich, Switzerland
Title: Cheap Design and Behavioral Diversity of Autonomous Adaptive Robots
Advisors: Prof. Dr. Rolf Pfeifer and Prof. Dr. Hiroshi Yokoi